EMBRY-RIDDLE
Aeronautical University™
SCHOLARLY COMMONS

5-2016

Mechanical and Electrical Characterization of Hybrid Carbon Nanotube Sheet-Graphene Nanocomposites for Sensing Applications

Jiukun Li

MECHANICAL AND ELECTRICAL CHARACTERIZATION OF HYBRID CARBON

NANOTUBE SHEET - GRAPHENE NANOCOMPOSITES FOR SENSING

APPLICATIONS

A Thesis

Submitted to the Faculty

of

Embry-Riddle Aeronautical University

by

Jiukun Li

In Partial Fulfillment of the

Requirements for the Degree

of

Master of Science in Aerospace Engineering

May 2016

Embry-Riddle Aeronautical University

Daytona Beach, Florida

MECHANICAL AND ELECTRICAL CHARACTERIZATION OF HYBRID CARBON NANOTUBE SHEET - GRAPHENE NANOCOMPOSITES FOR SENSING APPLICATIONS

By

Jiukun Li

A Thesis, prepared under the direction of the candidate's committee chairman, Dr. Sirish Namilae, Department of Aerospace Engineering, has been approved by the members of the thesis committee. It was submitted to the School of Graduate Studies and Research and was accepted in partial fulfillment of the requirements for the degree of Master of Science in Aerospace Engineering.

THESIS COMMITTEE

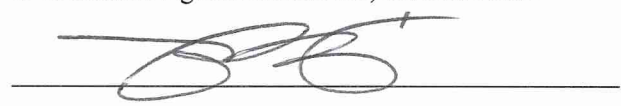Chairman, Dr. Sirish Namilae

Member, Dr. Daewon Kim

Member, Dr. Marwan Al-Haik

Department Chair, Dr. Anastasios Lyrintzis
or Graduate Program Coordinator, Dr. Eric Perell

Date 29 Apr 2016

Dean of College of Engineering, Dr. Maj Mirmirani

Date 4/29/2016

Vice Chancellor, Academic Support, Dr. Christopher Grant

Date 4/29/16

ACKNOWLEDGMENTS

TABLE OF CONTENTS

LIST OF TABLES

LIST OF FIGURES

SYMBOLS

R	resistance
I	current
ΔV	voltage drop
ρ	resistivity
w	width of nanocomposites
t	thickness of nanocomposites
l	length of nanocomposites
σ_m	conductivity of nanocomposites
L	number of fillers to form on conducting path
S	number of conducting networks
R_m	resistance between two adjacent conducting particles
R_c	resistance of one conducting particle
J	tunneling current
m	mass of electron
e	charge of electron
h	Plank's constant
V	applied voltage
s	thickness of insulating distance between conducting fillers
s_o	original average distance between conducting fillers
s'	average distance modified by additional fillers and strain
So'	original average distance modified by additional fillers
a^2	effective cross-sectional area
φ	height of the potential barrier for insulating area
R/R_o	resistivity change
ε	strain
D	diameter of particles
d	diameter of additional fillers
θ	CNT volume fraction
θ'	volume fraction of additional fillers

n	number of distances between CNTs
n'	number of distances covered by additional fillers
A	surface area of nanocomposites

ABSTRACT

The unique mechanical and electrical properties of carbon nanotubes and graphitic structures have drawn extensive attention from researchers over the past two decades. The electro-mechanical behavior of these structures and their composites, in which electrical resistance changes when mechanical deformation is applied facilitates their use in sensing applications.

In this work, carbon nanotube sheet – epoxy nanocomposites with the matrix modified with various contents of coarse and fine graphene nanoplatelets are fabricated. The addition of a secondary filler results in improvements of both electrical and mechanical properties. In addition, with the inclusion of the second filler, change in resistivity with mechanical deformation (manifested by gauge factor) is significantly enhanced. Nanocomposite with 5 wt. % coarse graphene platelets achieved the most effective resistivity-strain behavior and largest gauge factor. Similar trend in variation of gauge factor variation was observed for fine graphene nanoplatelet – nanotube sheet nanocomposites. An analytical model for explaining these observations, incorporating strain and the effect of second filler, is developed.

Sensors fabricated using these hybrid nanocomposites can be potentially used in damage sensing of aerospace carbon-fiber composites.

1. Introduction

1.1 Background

Carbon fiber reinforced composites are used as structural materials of choice in wide range of fields, especially in aerospace engineering, due to their light weight and relatively high mechanical strength. Compared to conventional aerospace materials, composites possess attractive characteristics, such as light weight, corrosion resistance and high resistance to fatigue damage. Due to their advanced properties and economic savings, composites have been widely used in military and civil aircraft, such as Lockheed Martin F-22, Northrop Grumman B-2, Airbus 380, and Boeing 787. Many of these commercial and military airplanes have more than 50% of their structure made of composites.

New developments in areas like structural health monitoring and damage sensing can improve the overall usage and performance of composite structures. Because of the laminate structure of composites, flaws and damages that occur in composites include delaminations, wrinkles, porosity etc., which are very different from defects in metallic structures. Therefore, there is a need for developing new methods of damage sensing and detection.

Carbon nanotubes (CNTs), as novel materials, have attracted thousands of researchers to develop applications based on their unique mechanical, electrical, and electro-chemical properties. The high mechanical strength and unique electrical behavior, low density and compatibility with common composite matrix materials, are some of the properties that make them attractive for developing sensors, especially for aerospace

composite structures where weight saving is a major consideration.

An alternative way of using CNTs is to form a thin membrane where free standing CNTs are interwoven by van der Waals force utilizing method of chemical vapor deposition. This membrane is often referred to as CNT sheet or buckypaper (F. L. De Volder, H. Tawfick, H. Baughman, & Hart, 2013). The electrical and mechanical behavior of buckypaper depends largely on CNT-CNT interactions (Erik T Thostenson and Tsu-Wei Chou, 2003). This thesis investigates the mechanical and electrical behavior of CNT sheet based nanocomposites with the intention of developing a method for damage detection in conventional carbon fiber reinforced composites.

This thesis attempts to explore and understand the microscale mechanisms of electrical and mechanical properties of buckypaper nanocomposites. Neat epoxy and epoxy mixtures with fine graphene nanoplatelets and coarse graphene platelets of different weight fractions are employed to infiltrate neat buckypaper. Effective improvement in stiffness and strength is found in the two filler nanocomposites compared to neat buckypaper nanocomposites. In addition, resistivity also changes to a greater extent with the application of strain with the addition of second filler. These properties have the potential to be applied on the surface or imbedded in the middle of carbon fiber reinforced composites for applications in damage detection of aircraft structures. Additional applications are in the area of composite repair, wherein the nanocomposite sensors can be used to study the effectiveness of repair.

1.2 Motivation

Carbon fiber composites are in general lighter than metallic materials. Despite the

fact that aluminum alloy costs $2/lb while Graphite/Epoxy costs $40/lb, composites are still widely used in aerospace applications due to their high performance in reduction of weight, achieving relative high strength and modulus. Weight savings is very important for economics, every single pound in weight saving results in huge savings in operational costs in aeronautics and astronautics (Hoskin & Baker, 1986). High specific strengths and specific moduli for most of the composites are two main factors that composites is widely used in aerospace industry. Figure 1.1and Figure 1.2 show the specific strength and specific stiffness for common materials used in aerospace industry.
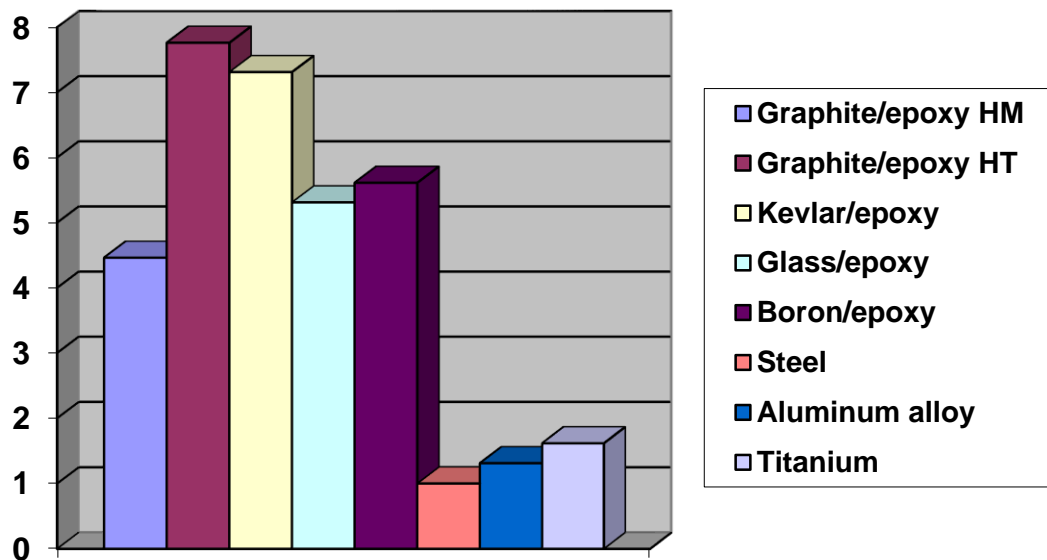
Figure 1.1 Relative specific strength (Jones, 1999)
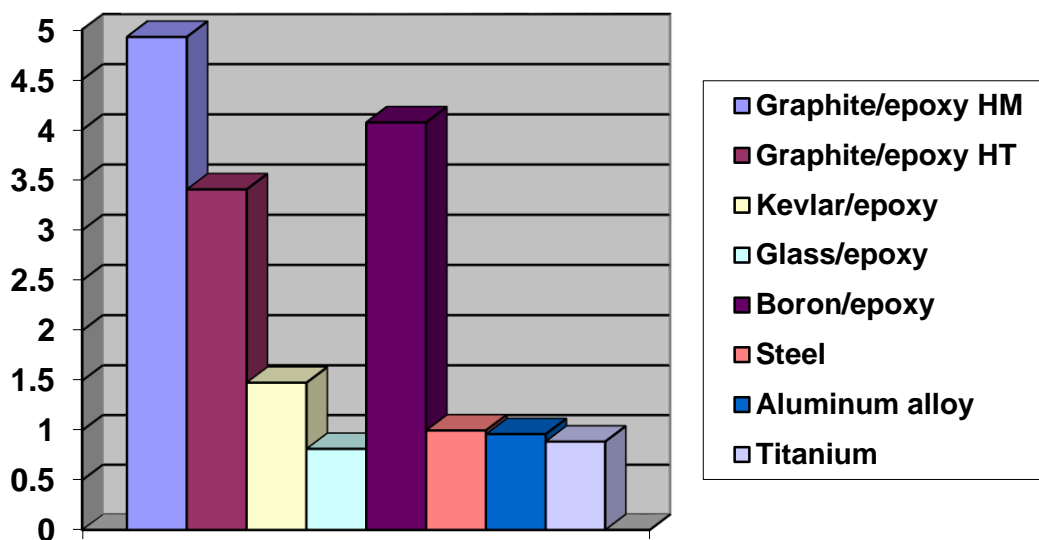
Figure 1.2. Relative specific modulus (Jones, 1999)

While the weight savings have led to the ubiquitous use of composites in aerospace applications, there are several areas that need further attention. For example, composites often fail by the growth of delaminations and debonding between plies. There are other common defects like wrinkles and porosity. Effective non-destructive and structural health monitoring techniques are required for increasing the usage of composites in aerospace applications.

Non-destructive composite testing methods such as thermography, acoustography, acousto-ultrasonics, air-coupled ultrasound and radiography need expensive setups and professional workers with adequate training. A nanocomposite sensor, can potentially monitor the damage or delamination in composite structures in aerospace and other applications. Use of epoxy matrix for these nanocomposites enables easy integration into carbon fiber composite structures. The development of damage detection sensor is the primary motivation for this work. Additionally, this thesis aims to understand the basic

mechanisms in electro-mechanical behavior of nanocomposites that can be generalized to other materials systems.

1.3 Problem statement and research objectives

The primary motivation is to develop a damage detection sensor and methodology for composite structures using carbon nanotube based nanocomposites. This thesis explores and understand the micro-scale mechanisms of electrical and mechanical properties of hybrid nanotube sheet- graphene platelet nanocomposites through experiments and analytical model. This research uses experiments of mechanical deformation and simultaneous electrical measurements to achieve this objective. An analytical model is developed to explain the results of the experiments. The specific research objectives are as follows:

a) Design and fabricate nanocomposites suitable for strain sensing with different combinations of Buckypaper and graphene platelet fillers including:

1. Buckypaper infiltrated with pure epoxy

2. Buckypaper infiltrated with epoxy modified using fine graphene nanoplatelets of varying contents, 1 %, 2 %, 5 %, 10 %, and 20 % by weight, respectively.

3. Buckypaper infiltrated with epoxy mixture in which 1 %, 2 %, 5 %, 10 % and 15 % of coarse graphene platelets are mixed, separately.

b) Tensile deformation and simultaneous resistivity measurement of the nanocomposites. The results of the tests are displacement-force and resistivity-time curves obtained through LabVIEW software.

c) Microstructural characterization of the hybrid nanocomposite and fracture surfaces using Scanning Electron Microscopy.

d) Analyze and explore the improvement in buckypaper nanocomposites with incorporation of epoxy mixture prepared with different percentage of fine graphene nanoplatelets or coarse graphene platelets and the electro-mechanical property for every sample.

e) Develop suitable models to explain the decrease of electrical resistivity and change of electrical resistivity with applied strain.

f) Suggest applications in damage detection of carbon fiber composites.

By determining the electrical resistivity change of every sample with strain application by tensile machine, this thesis gains basic understanding of their electro-mechanical properties and reveal the potential for damage sensing. This will allow to determine if these nanocomposite sensors can be used for damage sensing in aircraft structures.

2. **Literature review**

2.1 Composites

A composite material is the combination of two or more materials differing in composition or form on a macroscale, where components are still identifiable after combination. The constituents retain their identities in the composite; that is, they do not dissolve or otherwise merge completely into each other, although they act in concert. Normally, the components can be physically identified and exhibit an interface between one another. There are four commonly accepted types of composite materials, which are fibrous composites that consist of continuous or chopped fibers in a matrix, laminated composites materials that consist of layers of various materials, particulate composites materials that are composed of particles in a matrix, and combinations of some or all of the above (Hoskin & Baker, 1986). The most commonly used type of composite in aircraft structures, is fiber-reinforced laminated composite. This is the combination of fibrous and laminated composites. Another category of composites are nanocomposites where in the reinforcing element is at nanoscale, e.g. nanoparticles or nanotubes.

This thesis studies the electrical and mechanical behavior of nanocomposite with the intention of using them for damage detection in carbon fiber reinforced composites.

2.2 Graphene and carbon nanotubes

A whole new world of nanotechnology has been brought about by the discovery of graphitic nanostructures starting with fullerenes and carbon nanotubes. Smalley et al (Kroto, Heath, O'Brien, Curl, & Smalley, 1985) discovered a new form of carbon known

as Fullerene C_{60}. This carbon structure named for Buckminister Fuller has a football like

cage structure with atoms on hexagonal and pentagonal faces. Three related types of

graphitic nanoparticles, which are multi-walled nanotube (MWNT), single-walled

nanotube (SWNT) and carbon nanofiber (CNF) discovered by Iijima in 1991(Iijima,

1991), Bethune and colleagues in 1993 (Bethune et al., 1993), E. Hammel et al. in 2004

(Hammel et al., 2004), respectively. The structure of these different nanoparticles are

shown in Figure 2.1 (Yeh, 2007).
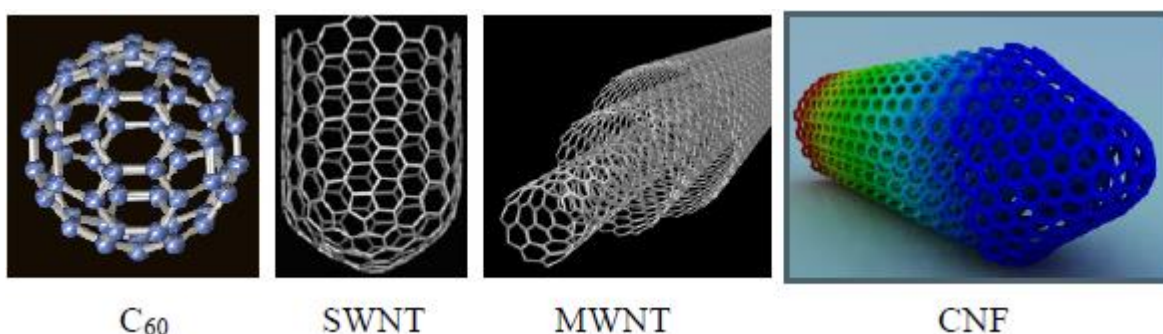
Figure 2.1. Structure of carbon nanoparticles (Yeh, 2007)

2.2.1 Structure of graphene and carbon nanotubes

There are two styles of covalent bonds between carbon atoms, which are

categorized as sp^2 and sp^3. Graphite is formed with sp^2 bonds, while diamond is

constituted with the sp^3 bonds, which is shown in Figure 2.2. The sp^2 bond is extremely

strong within a plane in graphitic structures. The bonds between layers of graphite are

based on van Der Waals interactions and have much lower strength. This makes graphite

weaker than diamond.

A graphene sheet is a 2-dimensional hexagonal lattice sheet formed by carbon

atom on each vertex in atomic scale, shown as in Figure 2.3. A perfect hexagon is

formed when six carbon atoms are connected by six sp^2 bonds. A graphene sheet is then

formed to be a honeycomb-like structure when more bonds gather together. The graphene

structure, with its extraordinary mechanical and electrical properties is the basic structural

unit for other allotropes, such as graphite, charcoal, CNTs and Fullerenes and usually

considered to be an unlimited aromatic molecule. It is about 207 times stronger than steel

and is an effective thermal and electrical conductor (Moisala, Li, Kinloch, & Windle,

2006). The unique properties of CNTs have drawn attention of large number of

researchers and scientists (Koratkar, 2013).
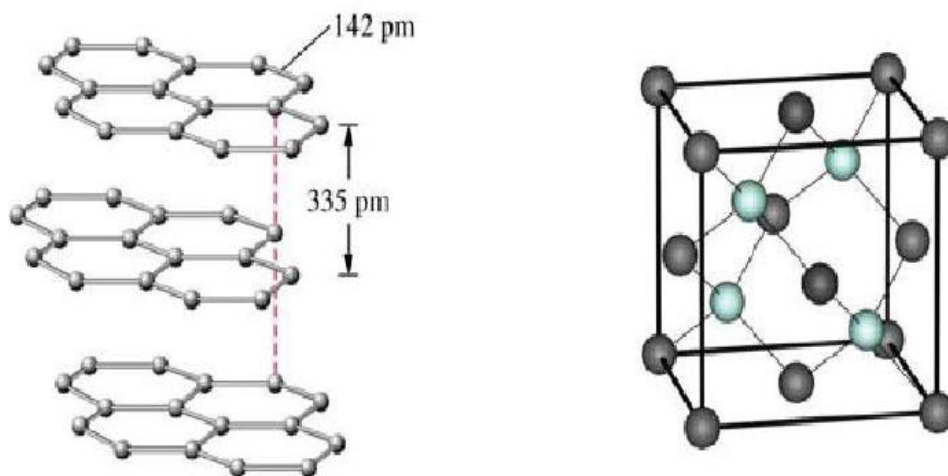
Figure 2.2 Structures of graphite and diamond (Kan, 2013)
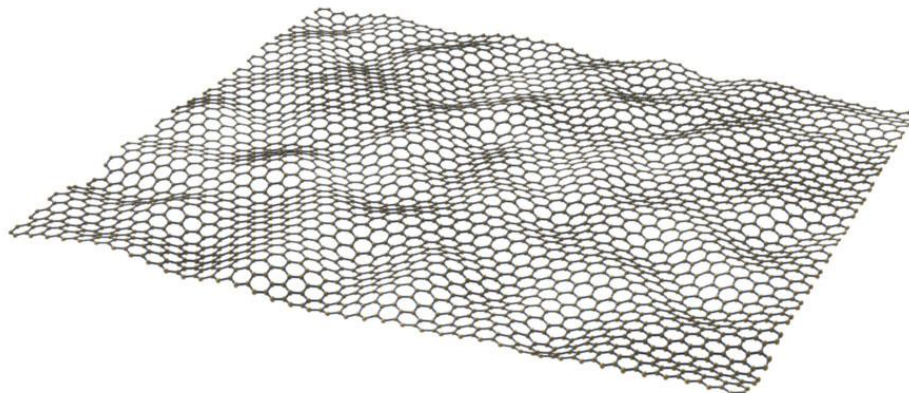
Figure 2.3 Schematic of graphene sheet (Yeh, 2007)

The structure of CNT is formed when a graphene sheet is rolled up to form a cylinder, which is axial symmetrical along the axis of the tube. These rolled up process is shown in Figure 2.4. When there is only one single layer of graphene is rolled up, the resulting cylinder is called single walled nanotube (SWNT). Typical diameters of SWNT range from 0.6 nm to 1.0 nm and densities from 1.33 g/cm^3 to 1.4 g/cm^3 (Treacy, Ebbesen, & Gibson, 1996). Multi-wall nanotube (MWNT) has a similar structure but with two or more graphene layers rolled into cylindrical form. The inner diameter of MWNT has a range from 1.5 nm to 15 nm while the outer diameter ranges from 2.5 nm to 30 nm (Wong, Sheehan, & Lieber, 1997).
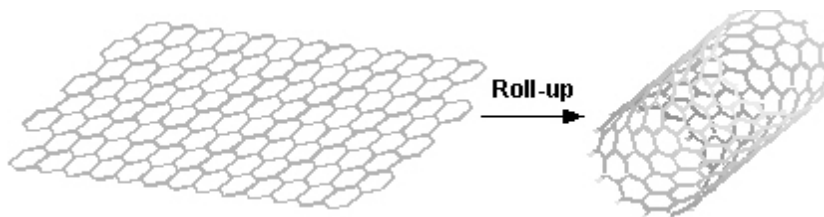
Figure 2.4 Schematic diagram of a graphene sheet rolling up to a SWNT (Yeh, 2007)

Figure 2.5 Schematic diagram of a SWNT and a MWNT (Yeh, 2007)

Due to this unique molecule structure, SWCNTs and MWCNTs are found to be ultra-strong, super-light and exhibit metallic and/or semi-conducting properties. The strong sp^2 bonds in these structures are responsible for their high strength and toughness. Good current carrying properties and thermal conductivity are also benefits of the tubular structure which enables ballistic electron and phonon transfer (Baughman, Zakhidov, & de Heer, 2002).

2.2.2 Mechanical and electrical properties of carbon nanotubes

In terms of mechanical properties, a SWCNT is among the strongest and stiffest materials. Many experimental investigations and theoretical calculations determine that the Young's modulus of carbon nanotubes is about 1.2TPa and their strength is in the range of 50-200 GPa (Ma, Siddiqui, Marom, & Kim, 2010). This is approximately one hundred times higher than steel. Compared to conventional materials, they have low

density of 1.2-1.4 g/cm^3, which is an order of magnitude lower than that of steel (Bethune et al., 1993). With high Young's modulus and light weight, materials made by CNTs have motivated proposals for their use in many structural and functional applications. Besides, CNTs have a significantly high aspect ratio and recently much longer nanotube ropes have been produced with a length of around 15 centimeters (Erik T Thostenson and Tsu-Wei Chou, 2003) while the diameter for SWCNT is only 0.6-1 nm (50 nm for MWNT).

Besides the outstanding mechanical properties, CNTs also have high electrical properties. They have 1000 times current transfer ability than copper wire (Salvetat et al., 1999). In addition, they can exhibit either metallic or semiconductor characteristics based on their chirality. Also, experimental investigations indicate that CNTs exhibit high strain dependence on conductivity (Yin et al., 2011). Strain application on individual CNT using atomic force microscope led to large difference in electrical conductivity (Maune & Bockrath, 2006). The intrinsic strain dependence on resistive properties of CNTs can be used to make the individual CNTs as the nanoscale sensing element (Saito, Fujita, Dresselhaus, & Dresselhaus, 1992).

Apart from their well-known characteristics of mechanical and electrical properties, CNT have superior thermal properties. CNTs maintain thermal stability up to 2800^0C and 750^0C in vacuum and air respectively. Their thermal conductivity is twice that of diamond (Berber, Kwon, & Tománek, 2000). Another attractive property of CNTs is their high surface area. CNTs are treated as the potential reinforcement material for high-performance structural and multifunctional composites in the future, where a single tube can approach surface area of as high as $1300m^2/g$ two orders of magnitude higher

than in conventional fibers.

2.2.3 Mechanical and electrical properties of carbon nanotube composites

Due to the excellent mechanical, electrical, and thermal properties, CNTs are treated as the ideal reinforcements for high performance materials. Difficulties associated with homogenous alignment and effective load transfer between CNTs and the matrix, are two main factors that limit the performance of reinforcement. The microscopic strength of individual CNTs is not able to be transferred to scaled-up macroscopic CNTs network. Thus, a number of approaches are developed by researchers to improve the alignment, reduce waviness and improve interface adhesion.

In order to improve the alignment, to transfer load and to reduce waviness in CNTs network, methods including twisting, stretching, magnetic field process, and chemical bonding of networks are utilized. By using a drawing and stretching approach, the ultimate strength of the composite is improved by 50 %, 150 %, and 190 % corresponding to the stretch ratio of 2 %, 4 % and 7 %, relatively (Pham et al., 2008a). A twisting method is employed to result in a tensile strength of 8.8 GPa and Young's modulus of 357 GPa in a sample gauging 1 mm (Liu et al., 2010). Also, by a combination of twisting and condensing methods which is called continuous spinning method is used. A high tensile strength of 1 GPa and modulus of 120 GPa is achieved by using method of wet spinning (Behabtu et al., 2013). Similarly, using a stretch winding process resulted in a high volume fraction nanocomposites with a tensile strength of 3.8 GPa and modulus of 293 GPa (X. Wang, 2013). One research project used a mechanical stretching method to apply on fabricated CNT sheet, arriving a tensile strength of roughly 2.1 GPa and

modulus of 169 GPa (Cheng et al., 2009). Mechanical stretching turns out to be the most effective methods to attempt high strength and Young's modulus for the process to be scaled up, compared to other methods that only manufactured very small samples.

The conductivity of CNTs is also improved according to many researches. High electrical conductivity is measured by two- and four point probe on 25-mm single filament and displayed as 2.9 ± 0.3 MS/m which is a resistivity of 35 ± 3 microohm*cm at the room temperature (X. Wang, 2013). It is also shown that the resistivity is increased to 5 ±0.5 MS/m which is a resistivity of 22 ± 4 microohm*cm averagely, while best to 17.5 microohm*cm by doping iodine which is a known and stable CNT dopant. These CNTs remain stable after being placed in laboratory condition for over 1 year and a thermal cycling to 200˚C in air for 24 hours (Behabtu et al., 2013). Also, the electrical properties of SWCNT/polymer nanocomposites are remarkable reinforced by magnetic field processing (Choi et al., 2003).

Apart from dispersing CNTs in polymer, CNTs are employed to grow on carbon and glass fiber, fabricating hybrid nanocomposites with improved mechanical, electrical and thermal properties of the reinforcement (M Al-Haik et al., 2010) (Marwan Al-Haik et al., 2009).

2.3.4 Electro-mechanical behavior of CNT composites

A dramatic and convertible correlation is discovered between mechanical deformation and electrical resistance of CNTs about a decade ago (Tombler et al., 2000). This makes the usage of CNT nanocomposites possible in applications such as strain sensor and actuators. Several publications talk about applications of various

nanocomposites for strain sensing e.g., parylen-C/CNTs (Y.-T. Huang, Huang, Hsu, Chao, & Vu, 2012), polyelectrolyte/CNTs(Kenneth J. Loh, Kim, Lynch, Kam, & Kotov, 2007), poly(L-lactide)/CNTs (Xu et al., 2010) and polysaccharide/CNTs (Mittal, 2011). Both linear and non-linear responses of electrical resistance was observed resulting from application of mechanical strain on the nanocomposites, where individual CNTs are directly dispersed in the matrix (I. Kang, Schulz, Kim, Shanov, & Shi, 2006a) (Thostenson & Chou, 2006) (Zhang, Sakalkar, & Koratkar, 2007) (Böger, Wichmann, Meyer, & Schulte, 2008) (K.J. Loh, Kim, Lynch, Kam, & Kotov, 2007) (C. Li, Thostenson, & Chou, 2008). Many different polymers are used to fabricate nanocomposites for strain sensing and actuator applications such as polyvinylidene fluorid (Park, Gu, Wang, Kwon, & DeVries, 2013) and poly (ionic liquid) (Gendron et al., 2015). These actuators operate at lower voltage compared to traditional smart material actuators (Mukai et al., 2009).

The resistance change with applied deformation of CNT nanocomposites is predicted to be a result of interactions between CNTs instead of intrinsic property of individual CNTs (J. H. Kang et al., 2009). This increases the role of matrix material and fabrication procedure.

The electro-mechanical behavior of CNT composites has been utilized for other sensing applications such as gas identification (S. Kim, 2006) and cardiac and neurophysiological recording (Gerwig et al., 2012), temperature dependent sensors (Mohiuddin & Hoa, 2011) etc.

2.3 Carbon nanotube sheet or buckypaper

Because of the mass production of carbon nanotubes it is now possible to make carbon nanotube sheets in large sizes (few meters square) (F. L. De Volder et al., 2013). These CNT sheets or buckypaper consist of entangled carbon nanotube networks forming into a thin macroscopic membrane with the assistance of van der Waals interactions at the junction of nanotubes (Chapartegui et al., 2012). They have been fabricated using single-walled and multi-walled nanotubes both aligned and with random orientations and have been used to make composites with various polymeric matrices (Chang et al., 2013a) (Q. Wu, Zhang, Liang, & Wang, 2008). Researchers have demonstrated many applications of nanotube sheet composites including actuators (Chang et al., 2013a), sensors (Papa, Gaillard, Gonzalez, & Chatterjee, 2014) and artificial muscles (Vohrer, Kolaric, Haque, Roth, & Detlaff-Weglikowska, 2004).

2.3.1 Structures and properties

As it is mentioned before, an alternative approach for fabricating CNT composites is using CNT sheet, also called buckypaper. These are self-supporting entangled CNTs formed into a thin macroscopic membrane with assistance of van der Waals interactions at the junction of tubes (Chapartegui et al., 2012). Scanning Electron Microscope (SEM) micrograph of buckypaper with a magnification of 1000 is shown in Figure 2.6. Buckypaper is commonly fabricated by a suspension and filtration process (Ahmadalinezhad, Wu, & Chen, 2011).
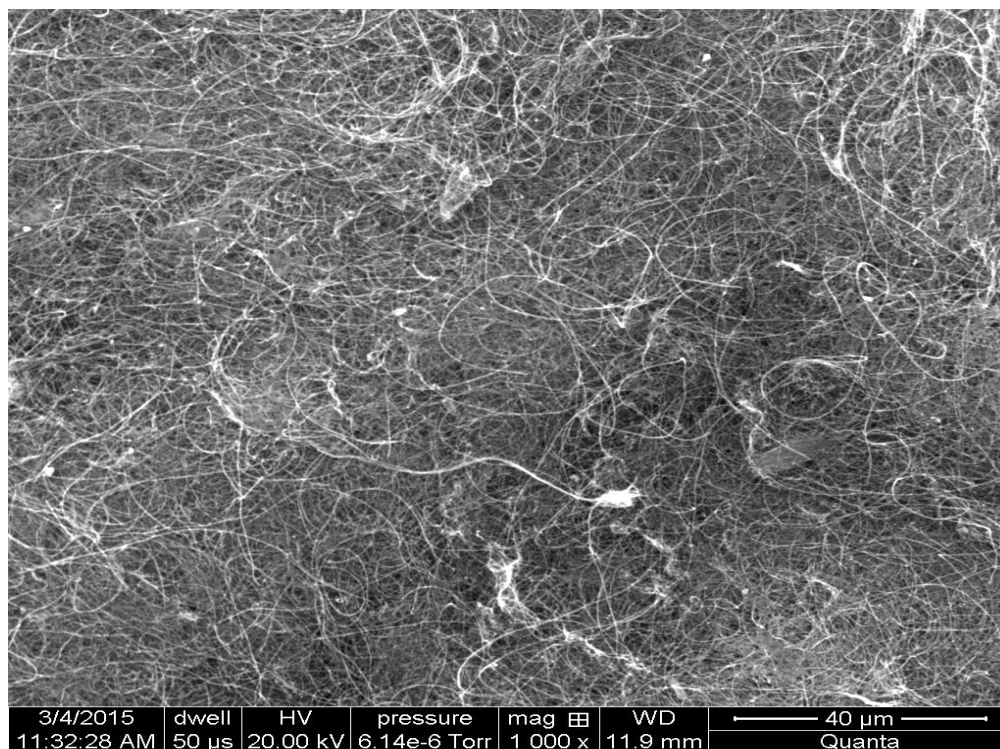
Figure 2.6 SEM micrograph of buckypaper

Due to the manufacturing process, surfaces on both sides of buckypaper are different which are named neat surface and matt surface, separately. The neat surface is more glossy and smooth, while the other one has more wrinkles as shown in Figure 2.7 and Figure 2.8.

| 3/4/2015 | dwell | HV | pressure | mag ⊞ | WD | — 400 µm — |
| 11:30:43 AM | 50 µs | 20.00 kV | 7.08e-6 Torr | 100 x | 12.1 mm | Quanta |
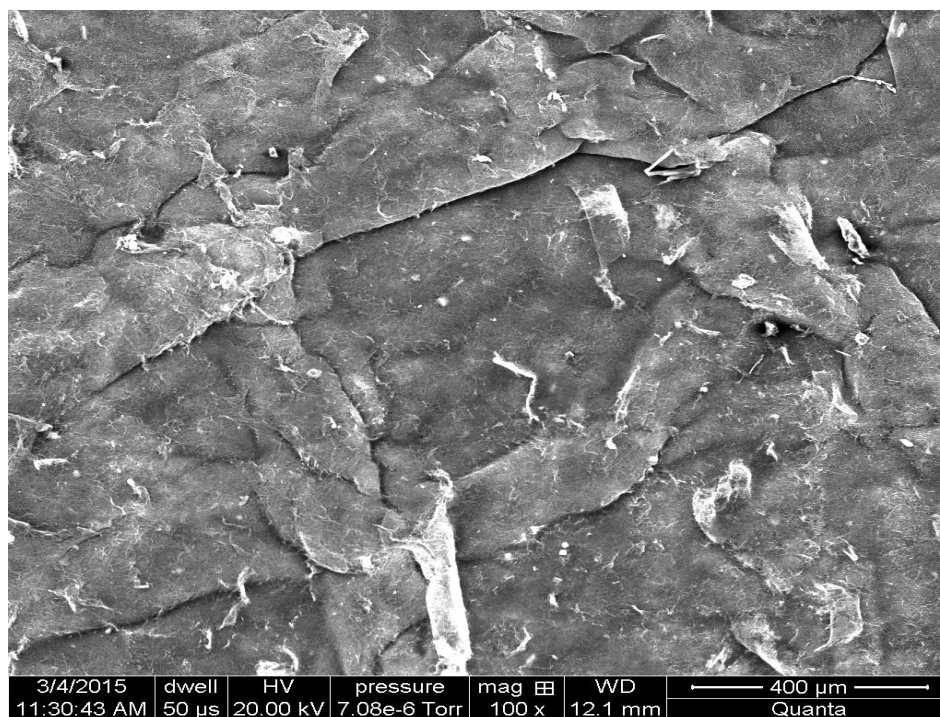
Figure 2.7 Neat surface of buckypaper

| 3/4/2015 | dwell | HV | pressure | mag ⊞ | WD | — 400 µm — |
| 11:53:47 AM | 50 µs | 20.00 kV | 1.08e-5 Torr | 100 x | 11.4 mm | Quanta |
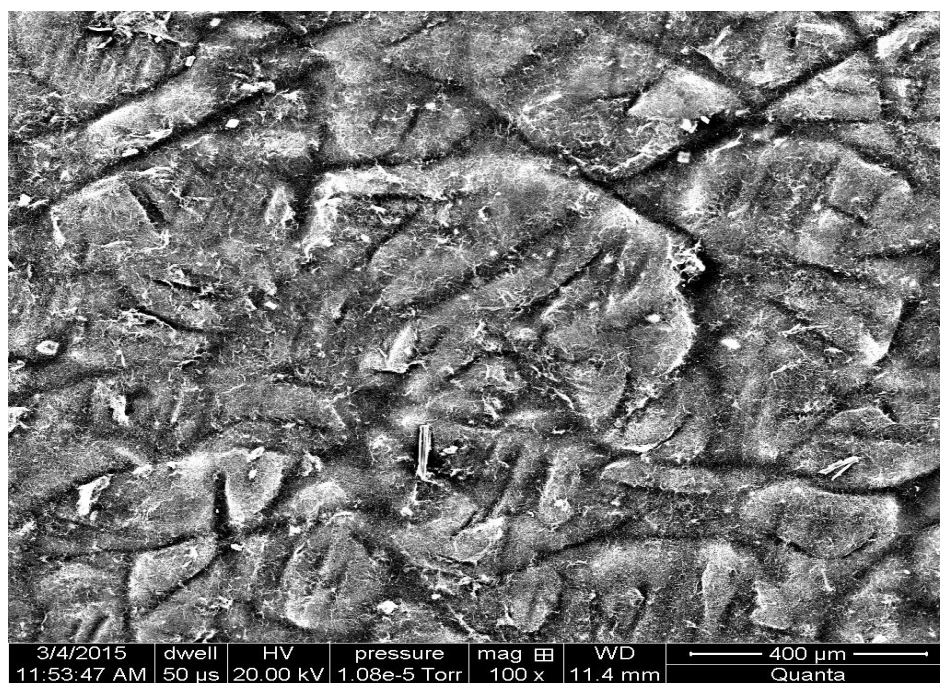
Figure 2.8 Matt surface of buckypaper

As thin membranes with a thickness of 10 – 50 microns, buckypaper is classified as smart nanomaterials owing to their mechanical, electrochemical, and electromagnetic properties.

Buckypaper with aligned CNTs are fabricated to pursue higher electrical conductivity, field emission, and mechanical properties. The CNTs have been aligned with assistance of magnetic (Correa-Duarte et al., 2005) and electric fields (Chen, Saito, Yamada, & Matsushige, 2001), shear flow and mechanical stretching (Fan & Advani, 2005) in various investigations. Both aligned buckypaper and randomly oriented buckypaper based nanocomposites are as shown in Figure 2.9 (Behabtu et al., 2013) (Bin, Kitanaka, Zhu, & Matsuo, 2003) (Xin & Woolley, 2004) (Ismach & Joselevich, 2006).
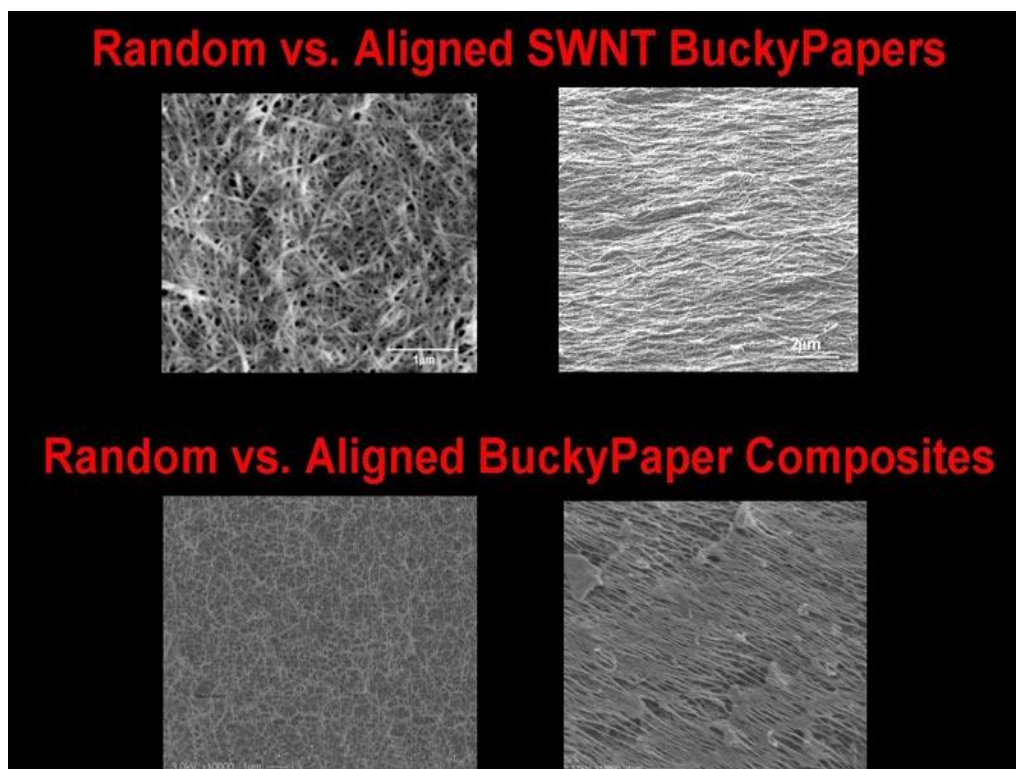
Figure 2.9 Buckypaper and aligned buckypaper (Yeh, 2007)

2.3.2 Advantages and limitations of buckypaper

Both SWCNT and MWCNT buckypapers of size up to several square meters are manufactured by CNT suspension and vacuum filtration process (F. L. De Volder et al., 2013). High concentration of CNTs is found in buckypaper nanocomposites. Buckypaper based nanocomposites can avoid agglomeration, achieving uniform dispersion compared to CNT dispersed composites (Chapartegui et al., 2012). Buckypaper nanocomposites also exhibits higher sensitivity of electrical properties when subject to deformation (Wichmann, Buschhorn, Gehrmann, & Schulte, 2009) (Park, M., 2008). Owing to the isotropic property of buckypaper, it is capable of sensing in different directions compared to most of traditional sensor which has only capability of one direction (Z. Wang, Liang, Wang, Zhang, & Kramer, 2004). Furthermore, with success of manufacturing of square-meter sixed buckypaper, desirable sizes and formats can be easily obtained.

However, application of buckypaper in practice is still limited by challenge of infiltration by high viscosity resin without of assistance of solvents and sonication. The waviness of CNTs is intrinsically produced during the fabrication of CNT sheets. This plays a role in reducing the stiffness of buckypaper and their composites (Robert M., 1999). Weak van der Waals interactions are the primary binding forces between nanotubes and this further contributes to the lowering of mechanical and electrical properties of buckypaper composites (Pham et al., 2008b). Nanotube ropes have very low bending rigidity, and thus readily form into porous composites of entangled, randomly oriented ropes and nanoscale impurities (Díez-Pascual, Guan, Simard, & Gómez-Fatou, 2012b). Some of these impurities can be removed by acid treatment and dispersion of the nanotubes is commonly achieved using a surfactant (Y. Geng, Liu, Li, Shi, & Kim,

2008). Despite of such promising results, the fundamental mechanisms of conductivity and electro-mechanical behavior need to be understood to utilize these materials to their fullest potential.

2.3.3 Buckypaper infiltration

One of the main tasks of current research is to develop a fabrication method for polymer-based CNTs composite. However, to manufacture CNTs reinforced composites with high CNT concentration and good alignment remains a great challenge since CNTs tend to form agglomerates (Z. Wang et al., 2004). By using buckypaper where CNTs are entangled and arranged in random alignment, a part of the critical issue can be overcome. High CNT concentration and good load transferring is usually observed in buckypaper nanocomposites. Many matrix materials such as epoxy, polyether ether ketone and poly (phenylene sulfide) etc. have been used for these composites (Mohiuddin & Van Hoa, 2011) (Díez-Pascual, Guan, Simard, & Gómez-Fatou, 2012a).

However, there are some additional issues that appear to limit the final property of the nanocomposites such as infiltration difficulties. This has been a subject of many investigations (Aldalbahi & Panhuis, 2012). Epoxy and benzoxazine resin have been used to infiltrate buckypaper with the aid of vacuum system and related curing cycle. Different temperatures are applied to create desirable curing cycles. Elastic modulus of 1.6 GPa and 1.8 GPa are found in buckypaper / epoxy and buckypaper / benzoxazine composites (Chapartegui et al., 2013). Another method uses compression pressing. To decrease the high viscosity of the mixture which is up to 2700 at room temperature, acetone was utilized to dilute the epoxy resin. Resin of Epon 862 is applied to soak the impregnated

buckypaper for whole night with a hot press molding process (Z. Wang et al., 2004).

A method of layer-by-layer assembly is applied to produce buckypaper /liquid crystalline polymer (Parmax) composites as shown in (Chang et al., 2013a). According to scanning electron microscope images, no distinct interfaces between layers are observed because of the full infiltration of polymer into buckypaper with the application of high pressure and temperature. In this buckypaper /Parmax nanocomposites with a MWCNT content of 6.23 wt. % , the tensile strength and Young's modulus are tested to be 390 MPa and 33 GPa respectively, which were substantially improved comparing to neat liquid crystalline polymer. Remarkable improvement of electrical conductivity of the composites is shown to be 100 S/cm (from approximately 10^{-3} S/cm of neat Parmax). Buckypaper infiltrated with three kinds of polymers have been employed as a sensors attached to a dog-bone shaped epoxy matrix tensile specimen. (Rein, Breuer, & Wagner, 2011).
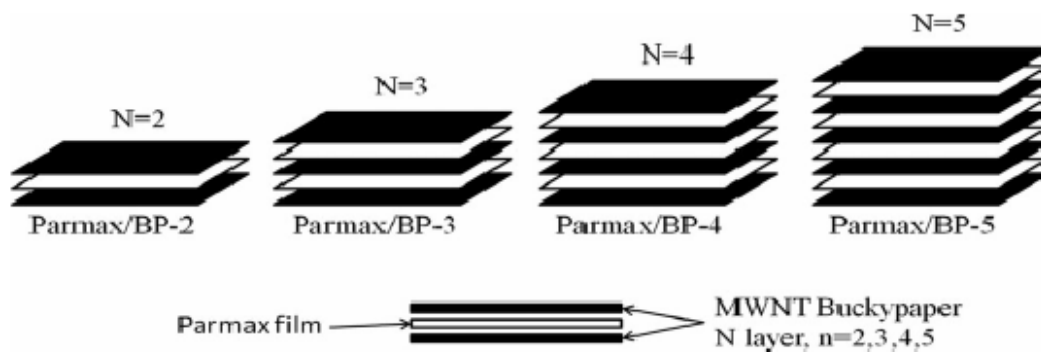
Figure 2.10 Schematic diagram of preparation of laminate structure Parmax/ buckypaper composites (Chang et al., 2013b)

Many other polymers are also utilized to fabricate nanocomposites such as

buckypaper /Nafion (Chapartegui et al., 2013), poly (phenylene sulphide)/ buckypaper, poly (ether ether ketone)/ buckypaper, and polymerization of cyclic butylene terephthalate (pCBT)/Buckypaper (Z. Li, Downes, & Liang, 2015) etc. These are used for applications such as sensors (Y.-T. Huang et al., 2012)(Rein, Breuer, & Wagner, 2011), actuators (Chang et al., 2013a) (Cottinet et al., 2012), artificial muscles (Vohrer et al., 2004) as well as cold field emission (Knapp, Schleussner, & Wüest, 2008), etc.

Matrix materials other than polymers have also been used to fabricate nanocomposites with buckypaper reinforcement. Two clay/ buckypaper hybrid sheets containing 0.05 wt. % and 0.2 wt. % of Cloisite NA+ clay are fabricated through a high-pressure filtration process (Q. Wu et al., 2008). It is found that the clay/ buckypaper composites survive under a relative high external radiant heat flux and significantly reduce the heat release rate.

This thesis also develops an analytical model to explain our experimental observations. The next section describes recent research in this area.

2.4 Analytical models of electrical behavior of nanocomposites

Several researchers have developed an electrical model to mathematically describe electrical behavior of the nanocomposites under direct current. A direct current is the unidirectional flow of electric charge, which can flow through conductors, semiconductors, insulators, and composites. The contribution of conductivity in the nanocomposites partially depends on polymer and discrete fillers, therefore it may not be continuous or linear. There is a critical filler concentration which is called percolation threshold, at which electrical conductivity is increased by several orders of magnitude.

The electrical conductivity of the nanomaterial rapidly increases leading the composite to go from an insulator to semiconductor and conductor with increase in filler loading. This is because fillers dispersed in polymers do not form a continuous and linear conductive path, rather it is discrete and nonlinear (X. Zhao et al., 2009).

One of the model by Kirkpatrick (Sahini & Sahimi, 1994) (Kirkpatrick, 1973a) (Zallen, 2008) is to predict the direct current electrical conductivity based on the likelihood of contact between fillers within the composites, which is defined as a power law equation

$$\sigma_m = \frac{1}{\rho_m} = A(\phi - V_{bc})^b$$

(2.1)

Where σ_m is the conductivity of the composite, A is the conductivity of the filler, ϕ is the volume fraction of filler, V_{bc} is the volume fraction of percolation threshold, and b is the critical exponent which can be obtained by experiments. The percolation threshold is the minimum volume fraction of the filler to form a continuous path of particles to transport electrical charge when both sides of the nanomaterial is electrically polarized by a direct current source.

The relationship between the conductivity and volume fraction of the nanomaterial is shown as in Figure 2.11 (Vargas-Bernal, Herrera-Pérez, Calixto-Olalde, & Tecpoyotl-Torres, 2013a). As illustrated in the figure, the conductivity of the composite is very close to the insulating polymer, and then the electrical conductivity undergoes a drastic increase with the formation of percolation threshold and consolidation of continuous conductive network. Finally, the maximum electrical conductivity is achieved when a completely network is formed.
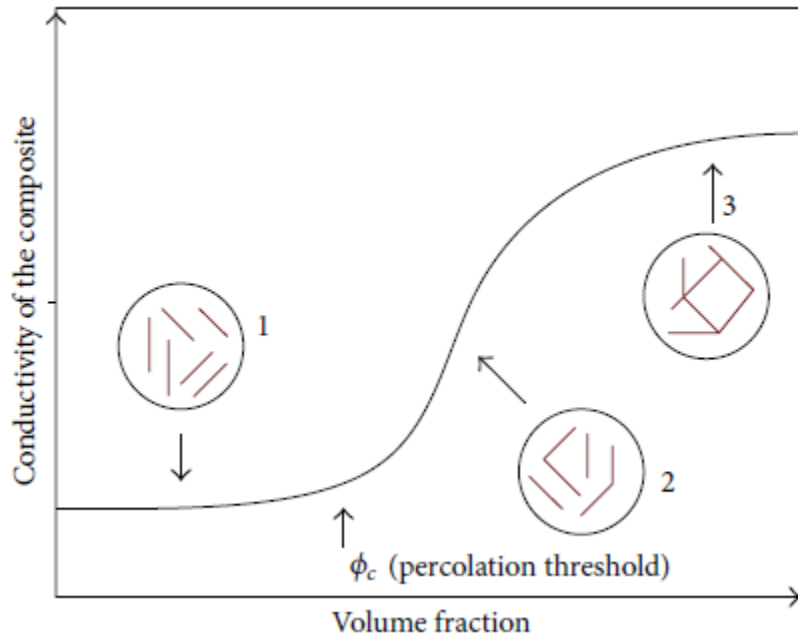
Figure 2.11 Dependence of electrical conductivity on filler volume fraction (Vargas-Bernal, Herrera-Pérez, Calixto-Olalde, & Tecpoyotl-Torres, 2013b)

One more electrical model is developed by McLachlan et al. (McLachlan et al., 2005a) (McLachlan, 2000) (McLachlan, Blaszkiewicz, & Newnham, 1990a), it statistically proposes the direct current electrical conductivity of the nanocomposites based on the effective medium theory by means of the equation

$$\frac{(1-\emptyset)(\rho_m^{\frac{1}{p}}-\rho_f^{\frac{1}{p}})}{\rho_m^{\frac{1}{p}}+((1-P_c)/P_c)\rho_f^{\frac{1}{p}}} + \frac{\emptyset(\rho_m^{\frac{1}{p}}-r_f^{\frac{1}{p}})}{\rho_m^{\frac{1}{p}}+((1-P_c)/P_c)r_l^{\frac{1}{p}}} = 0 \qquad (2.2)$$

Where $\emptyset$ is the volume fraction of the filler, ρ_c is the resistivity of the filler, r_l is the resistivity of the polymer or matrix, P_c is the percolation threshold of filler, and P is a characteristic value experimentally obtained.

Based on the "S" shape of dependence of electrical conductivity on filler volume

fraction, a sigmoidal function (Rawlings, Pantula, & Dickey, 1998) (Barrett, 1995) is employed to predict electrically conductive behavior of nanomaterials. Generically, the sigmoidal function is defined as

$$S(t) = \frac{a}{1+e^{(-bt+c)}} \qquad (2.3)$$

This function is modified for the prediction of direct current electrical conductivity of nanocomposites

$$\sigma_m = \sigma_p + \frac{SF-\sigma_P}{1+\exp[-(\varphi-PCP)/\omega]} \qquad (2.4)$$

Where σ_m is the conductivity of the nanocomposites, SF is the conductivity of the filler, σ_p is the conductivity of the polymer, ϕ is the volume fraction of the filler, PCP is the volume fraction in the midpoint of the percolation threshold, and ω is the range with of the percolation. Thus, the conductivity σ is now independent variable, and the constants can be defined as $a = SF - \sigma_P$, and $c = PCP/\omega$.

The model suggested by Mamunya et al. (Mamunya, Davidenko, & Lebedev, 1996) (Mamunya, Davydenko, Pissis, & Lebedev, 2002) and (Keith, King, & Johnson, 2008), is based on surface energy of the polymer and filler as well as the aspect ratio of the filler. Additionally, the presence of clusters of connected particles is also considered to effect the electrical conductivity of composites. The relationship between the electrical conductivity of the composite and the volume fraction of the filler are defined as

$$\log(\sigma_m) = \log(SC) + (log(SF) - LOG(\sigma_C))(\frac{\phi-\phi_C}{F-\phi_C})^k \qquad (2.5)$$

Where:

$$k = \frac{k\emptyset_c}{(\emptyset - \emptyset_C)^{0.75}} \qquad (2.6)$$

$$K = A - B\gamma_{pf} \qquad (2.7)$$

$$\gamma_{pf} = \gamma_p + \gamma_f - 2(\gamma_p \gamma_f)^{0.5} \qquad (2.8)$$

$$F = \frac{5}{\frac{75}{10+AR} + AR} \qquad (2.9)$$

σ_m is the conductivity of the composite, SC is the conductivity of the nanocomposite at percolation threshold, SF is the conductivity of nanocomposite with maximum packaging fraction, $\emptyset$ and $\emptyset_C$ are the volume fraction and percolation threshold, respectively. γ_{pf}, γ_p, and γ_f are the interfacial tension between polymer and filler, surface energy of the polymer, and surface energy of the filler, separately. AR is the aspect ratio of the filler. A and B are critical constants which can be experimentally obtained. There are several other models that utilize numerical techniques like Monte Carlo method and finite element approaches for studying the electrical conductivity of nanocomposites (Haggenmueller, Guthy, Lukes, Fischer, & Winey, 2007).

The extensive research in the area of electro mechanical behavior of carbon nanotube based composites points to the immense potential of these structures for multiple applications.

3. Experimental procedure

This chapter is organized into two main sections, first dealing with fabrication of nanocomposites and second on mechanical and electrical testing of nanocomposites.

3.1 Fabrication of nanocomposites

CNTs in form of buckypaper are treated with great promise for fabricating high-performance multifunctional nanocomposites. One of the limitations is with respect handling of buckypaper. Buckypaper is brittle and susceptible to fracture. To employ the electro-mechanical properties of buckypaper into the application of strain sensing, buckypaper must be infiltrated with epoxy to obtain desirable strength and stiffness. This has been the standard practice since buckypaper was first manufactured by Smalley's group (Bahr et al., 2001).

Among various existing fabrication processes, including controlled growth, filtration-based deposition, and direct deposition, a vacuum-assisting-filtration-process has most favorable features for scaling-up (Lee et al., 2013). With the advantages of a lower energy consumption, a faster producing cycle, and a modifiable open process, the filtration based manufacturing process has proven to be a successful example of the industrialized production system (Jamshidian, Tehrany, Imran, Jacquot, & Desobry, 2010). However, the filtration based manufacturing process yields inconsistent final products even under the best laboratory circumstances, and several defects are observed in the final products. Buckypapers turn out to be hard separated from the filtration membranes and brittle under shear force (Tibbetts, Lake, Strong, & Rice, 2007). The surface becomes wrinkled and warped. Micro-cracks appear on the buckypaper upon

dehydrating process as shown in Figure 3.1 (Kan, 2013).

Figure 3.1 An example of micro-cracked buckypaper (Kan, 2013)

There are two possible ways to enhance the mechanical performance of buckypaper. One can either functionalize the CNTs, or add binding materials. The easiest way to enhance buckypaper's mechanical properties is to add binding materials through the CNT network, since functionalization introduces defects to CNTs which would reduce their mechanical properties (Namilae & Chandra, 2005).

This study uses epoxy resin as the matrix material. Neat epoxy and epoxy modified with second phase fillers, fine graphene nanoplatelets and coarse graphene platelets are utilized to prepare the nanocomposites. Tensile deformation and simultaneous electrical resistivity measurements are then performed on these samples as described in following sections.

3.1.1 Materials

The multiwall carbon nanotube sheet (buckypaper) consisting of 100 % free

standing nanotubes was procured form Nano Tech Labs. The product specifications

mention area density of 21.7 g/m^2 and surface electrical resistivity of 1.5 Ω/ m^2. The

electrical resistivity was independently verified through experimentation.

The coarse graphene platelets used as the additional filler were prepared by finely

chopping low resistance (2.8 *10-2 Ω/ m2) graphene sheet supplied by Graphene

Supermarket. The suppliers report that this sheet (6 inch x 6 inch) is made out of multiple

layers of nanoscale fine graphene nanoplatelets adhesively bonded together. The size of

the laser chopped powder varied between 300 -1000 μm. The fine graphene nanoplatelets

used in the experiments are carboxyl-functionalized fine graphene nanoplatelets, also

supplied by Graphene Supermarket. Scanning electron microscope micrographs indicate

that these fine graphene nanoplatelets are much smaller than coarse graphene platelets

and typical size of a flake is in the range of 0.5 - 3 μm as shown in Figure 3.2.
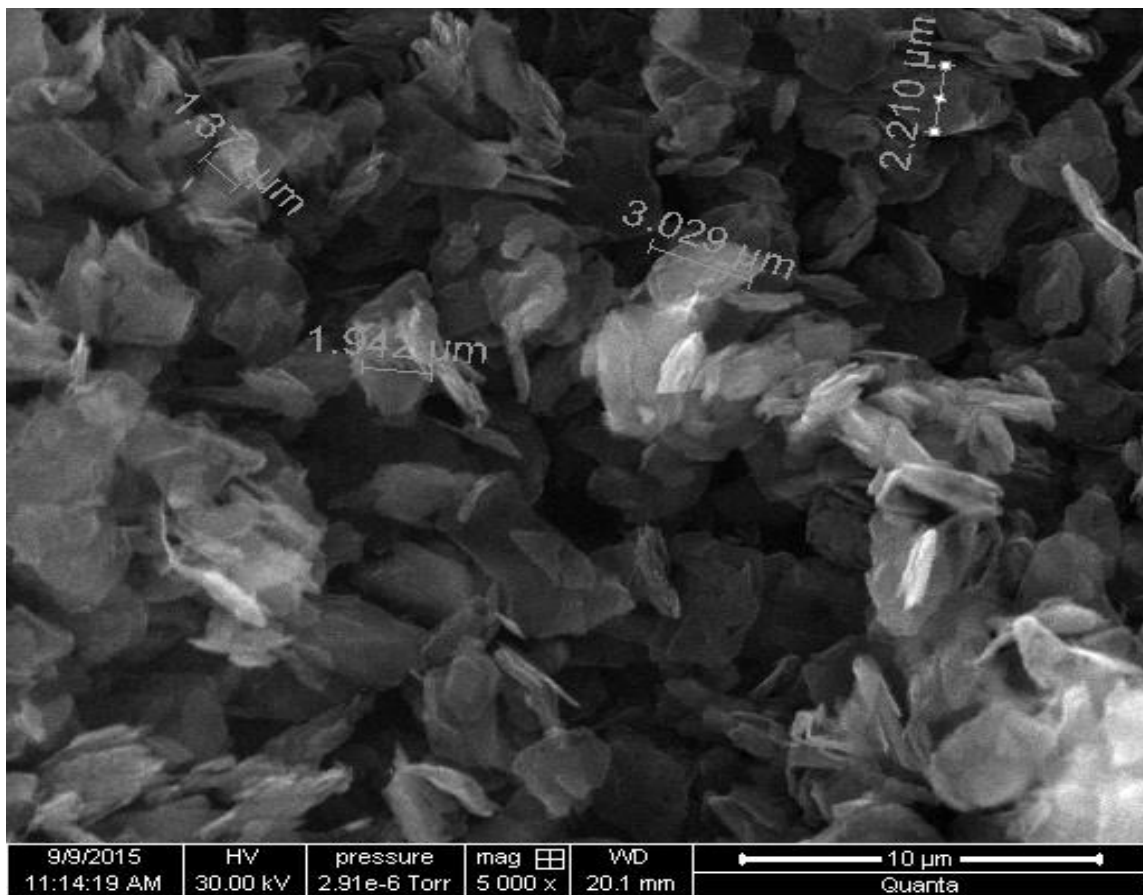
Figure 3.2 SEM micrograph of fine graphene nanoplatelets

The epoxy resin in this study is combined West System # 105 Epoxy Resin with West System # 206 Slow Hardener with a 20 minute working time and a ratio of 5:1. The epoxy resin is a light amber, low-viscosity liquid epoxy resin specifically formulated to functions of wetting out, bonding with glass fiber, carbon fiber and other materials. The slow hardener is also formulated as a low-viscosity curing agent, while extending working and cure time at higher temperatures. Another silver epoxy resin, supplied by MG Chemicals high conductivity and adhesive properties is used to attach electrodes to nanocomposites. This epoxy paste has a 1:1 mix ratio and 4-hour working time.

3.1.2 Infiltration of buckypaper sheet

The CNT sheet is cut into 6.35* 1.27 *10^{-2} m strip samples using a laser blade. Copper plates gauging 32 with dimension of 1.27* 1.27 *10^{-2} m are attached to both sides of the CNT sheet using by conductive silver- epoxy paste. The copper plates are used for conductivity measurement acting as electrodes. These CNT sheets are placed on a peel-ply on a flat aluminum mold as shown in Figure 3.3.
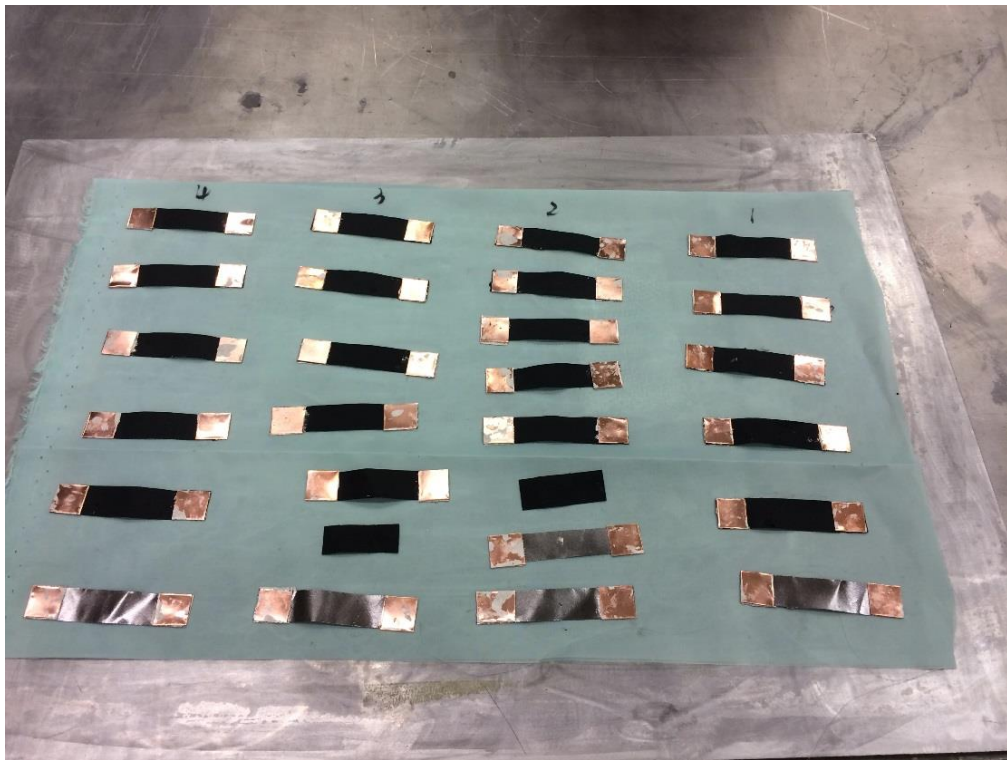
Figure 3.3 Buckypaper strips bonded with copper plate

The second filler particles (fine graphene nanoplatelets or coarse graphene platelets) are mixed into the epoxy resin evenly without hardener as shown in Figure 3.4. The reason particles are mixed into resin is that working time is increased before the mixture solidifies with the addition of hardener.
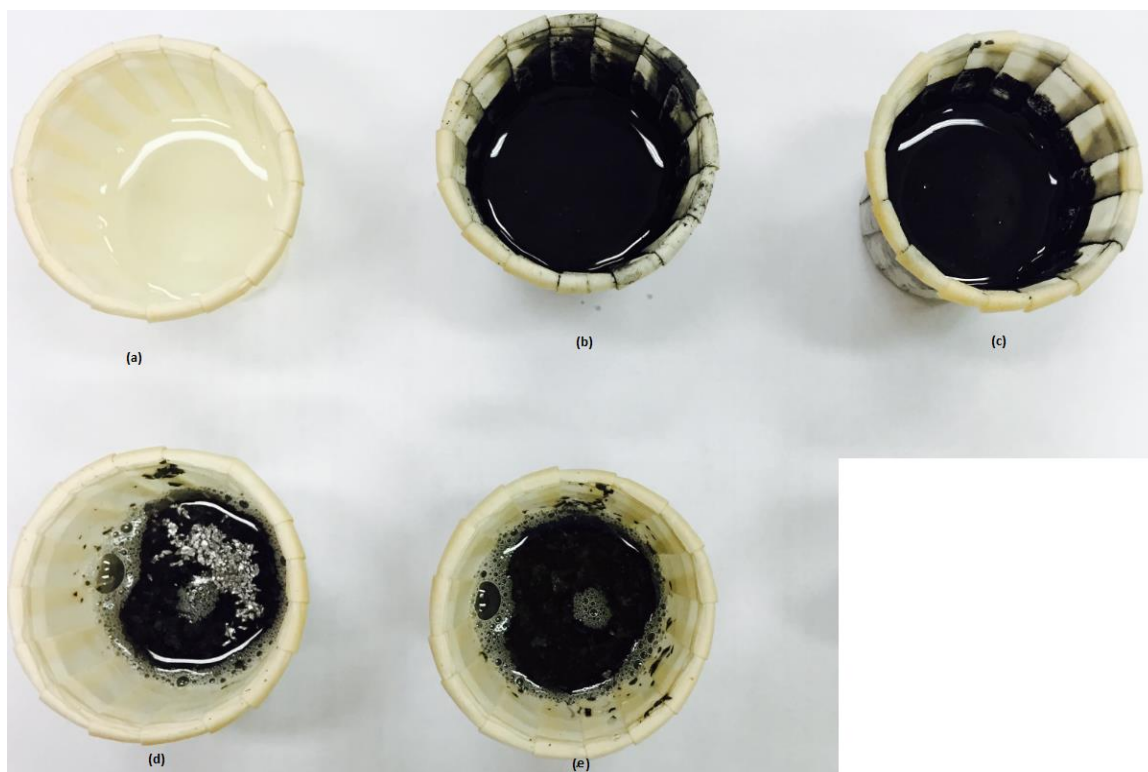
Figure 3.4 Epoxy resin and epoxy resin mixture. (a) Pure epoxy resin; (b) Epoxy resin mixed with 10 wt. % of fine graphene nanoplatelets; (c) Epoxy resin mixed 20 wt. % fine graphene nanoplatelets; (d) Epoxy resin mixed with 5 wt. % coarse graphene platelets; (f) Epoxy mixed with 15 wt. % coarse graphene platelets.

Several of these epoxy mixtures are prepared with varying quantities of the second filler. Separate mixtures are made with resin and hardener in 1:5 volume ratio with (a) 1 wt %, (b) 2 wt %, (c) 5 wt. %, (d) 10 wt % and (e) 15 wt. % coarse graphene platelets as well as with (a) 1 wt %, (b) 2 wt %, (c) 5 wt. %, (d) 10 wt % and (e) 15 wt. % of fine graphene nanoplatelets. The weight of fillers added is calculated before to ensure the particles have the right weight ratio in the eventual liquid mixture.

The evenly mixed resin-filler mix is then applied to both surfaces of the samples. It is then covered with another piece of peel-ply and breather film to remove the excess matrix. This setup is sealed under vacuum and a pressure of 88.05 kPa is provided by the

vacuum system to assist the breathing film to absorb extra epoxy. The samples are peeled after curing the resin for 12 hours at room temperature. The vacuum bag assisting infiltration process is demonstrated as schematic shown in Figure 3.5
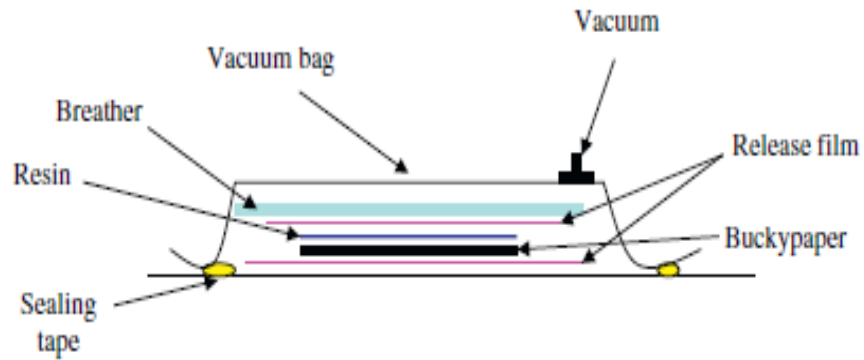
Figure 3.5 Schematic setup for the infiltration process for fabricating nanocomposites

Samples are then peeled off from the peel ply. The copper wires are soldered to the plates on either side to facilitate stable resistance measurement. The final products which are ready to test are shown in Figure 3.6, Figure 3.7, Figure 3.8, Figure 3.9, and Figure 3.10.
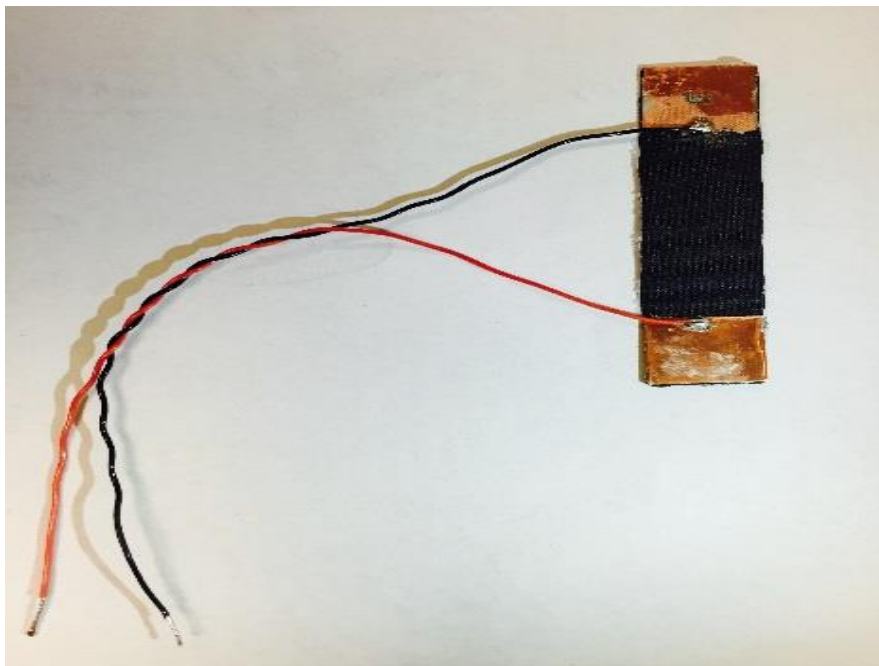
Figure 3.6 A sample infiltrated with pure epoxy resin
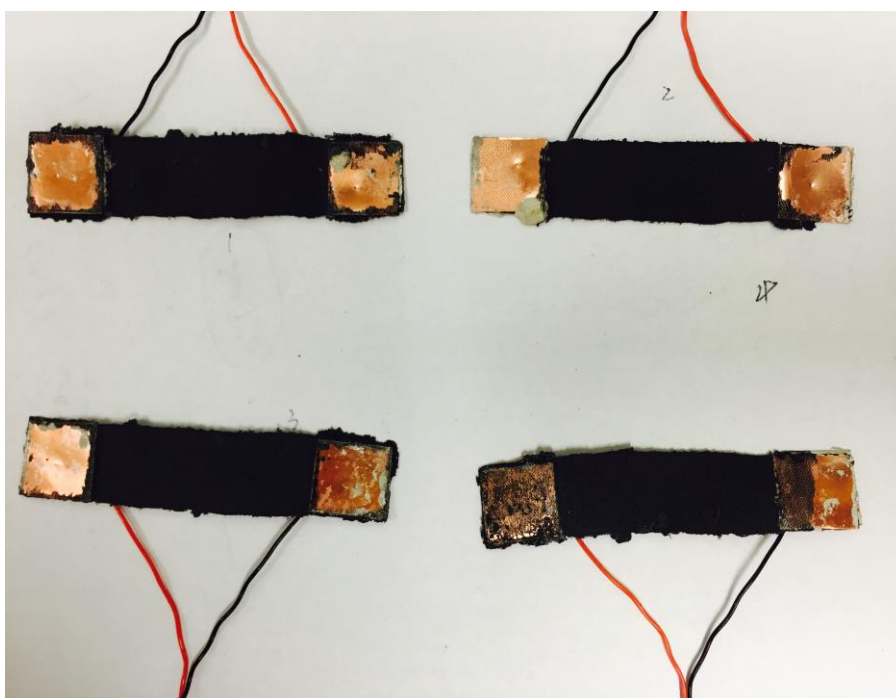
Figure 3.7 Buckypaper nanocomposites infiltrated with 10 wt. % fine graphene nanoplatelets
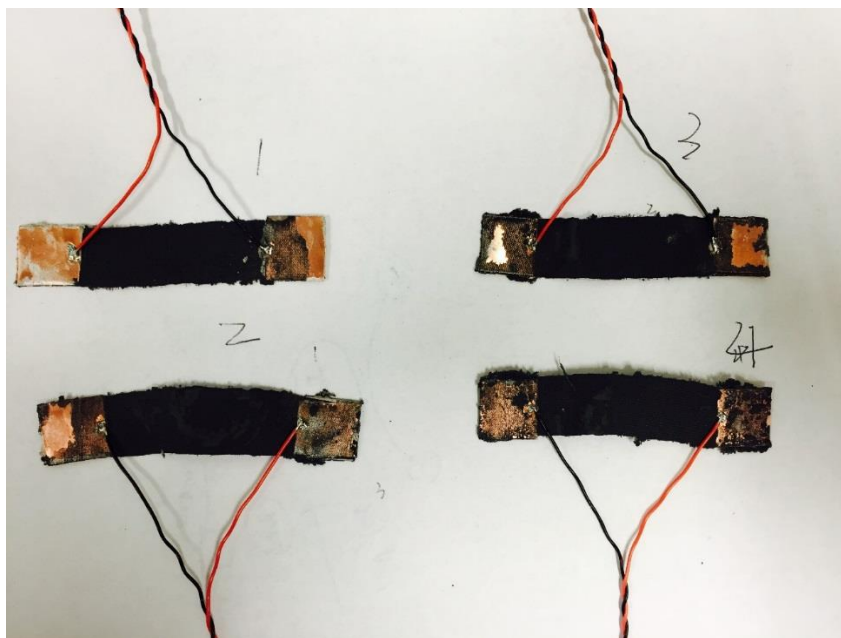
Figure 3.8 Buckypaper nanocomposites infiltrated with 20 wt. % fine graphene nanoplatelets
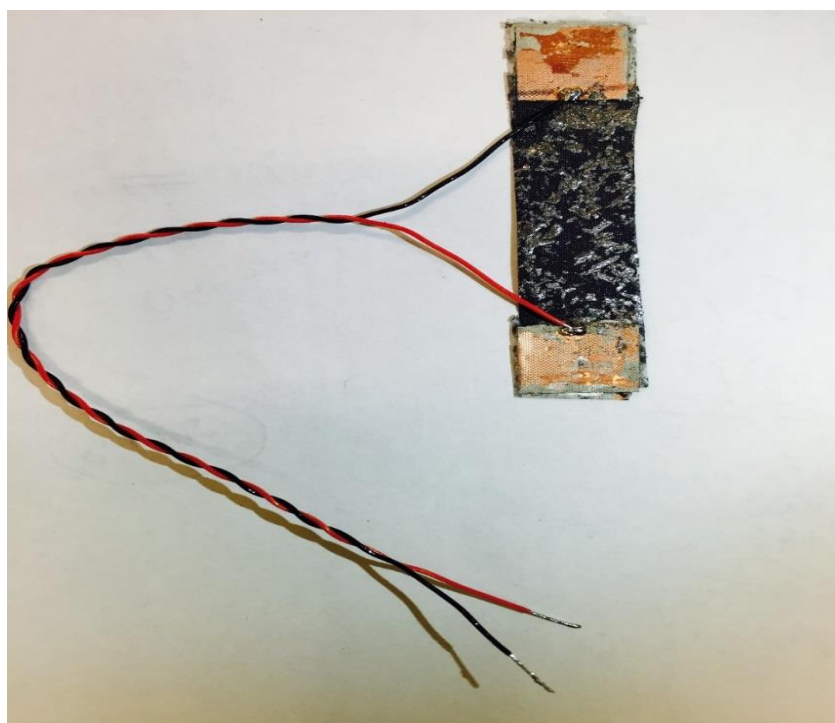
Figure 3.9 Buckypaper nanocomposites infiltrated with 5 wt. % coarse graphene platelets
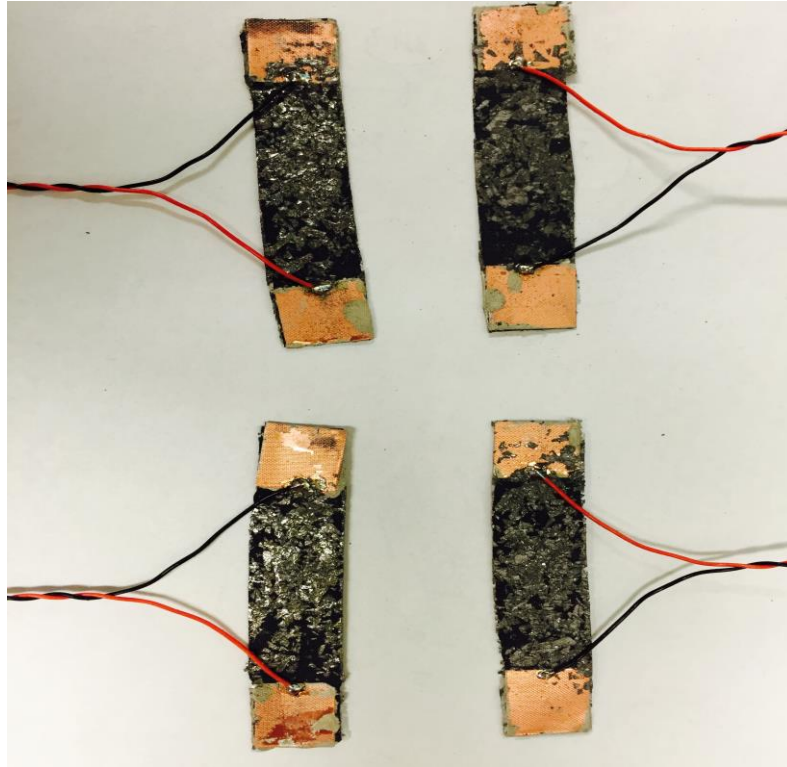
Figure 3.10 Buckypaper nanocomposites infiltrated with 15 wt. % coarse graphene
platelets

3.2 Electrical and mechanical measurement of nanocomposites

The resistance of nanocomposites samples with and without application of

mechanical load is obtained by four point probe testing method according to IEEE and

ASTM standard test methods ("Standard Test Method for D-C Resistance or

Conductance of Moderately Conductive Materials," 2004) ("IEEE Standard Test

Methods for Measurement of Electrical Properties of Carbon Nanotubes," 2005)

("Standard Test Methods for DC Resistance or Conductance of Insulating Materials,"

2005) . This measuring technique is designed to use separate pairs of current-carrying and

voltage-sensing electrodes to make more accurate measurements than two-terminal

sensing method which is simpler and more common. This four point testing method is

specially designed to measure sheet resistance of thin films. Therefore, this method is utilized to measure resistance of sheet samples.

This method works by forcing a current through the sheet and measuring voltage using a four-wire Kelvin-connection scheme. The resistance of the sample is calculated using Ohm's Law by passing a controlled current (of 0.5 Amperes) and recording a voltage drop (ΔV) which is shown in Figure 3.11. The changing resistance can be calculated by the LabVIEW recorded voltage drop using Ohm's law

$$R = \frac{\Delta V}{I}$$
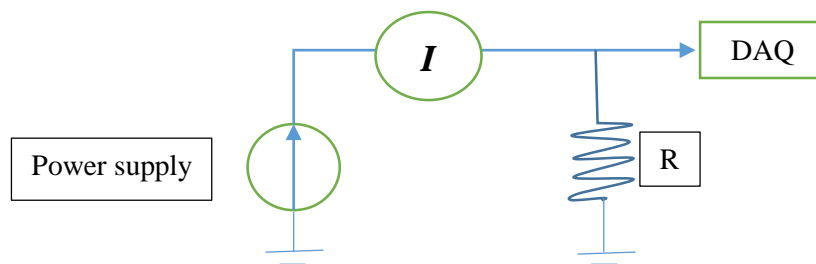
Figure 3.11 Schematic setup for voltage drop test

A simple LabVIEW code is used to monitor the drop of voltage with a data acquisition system. The LabVIEW code is provided in Figure 3.12. The attached copper plates on both sides of the sample are clamped to the grips of CS-225 Digital Force Tester with a machine accuracy better than 1%. A cyclic and breaking condition are preprogrammed in the digital multi-model force and displacement tester. Displacement and force are automatically stored in the computer attached to the tensile testing machine.
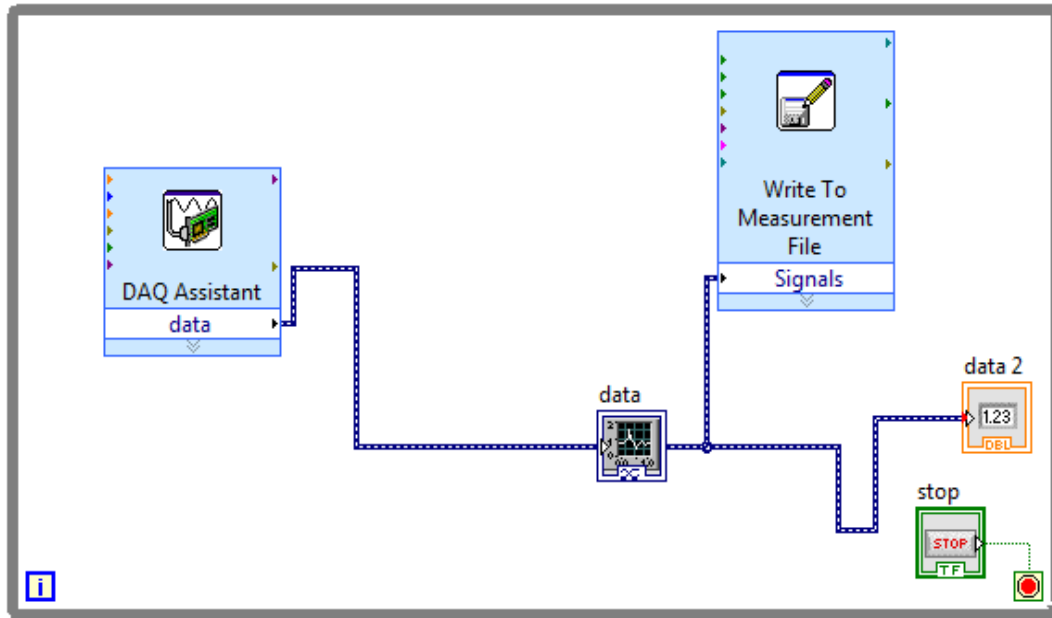
Figure 3.12 LabVIEW code for voltage drop monitoring
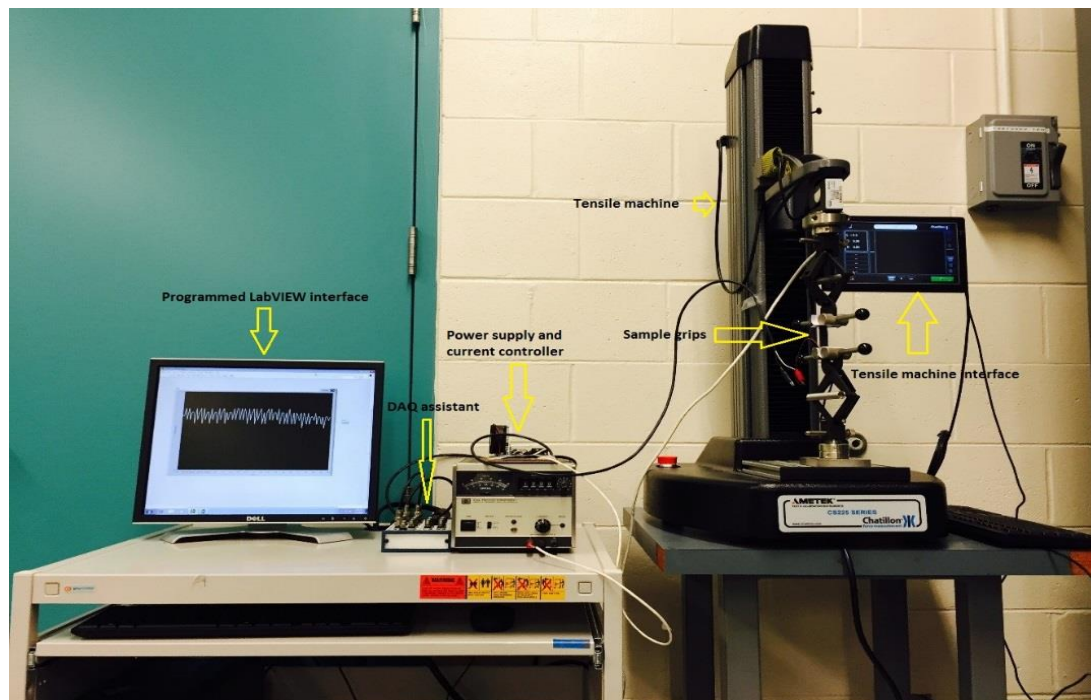
Figure 3.13 Experimental set-up for tensile test

The wires on the sample are connected to the power source as well as the data acquiring system (DAQ) as shown in Figure 3.11. The DAQ is connected to the computer, with LabVIEW. A current of certain value is applied to the samples. LabVIEW code monitors the voltage at two sides of the samples simultaneously. The measured voltage is the voltage drop resulting from the resistance of the nanocomposites. The drop voltage is unstable at the beginning when current start to flow through the samples and then stabilizes to a constant value. The tensile displacement is applied at a speed of 1cm/s after the voltage is stabilized. LabVIEW measures the drop in voltage while the nanocomposites sample is deformed. The force-displacement-time data due to the deformation is recorded in the computer connected to the tensile testing machine.

4. **Mechanical properties of hybrid nanocomposites**

Results of mechanical properties and stress-strain plots of the hybrid nanocomposites are later presented in this chapter.

4.1 Mechanical properties of buckypaper nanocomposites

The mechanical properties of buckypaper, with van der Waals bonds between CNTs, are much lower than those for single CNT. Because of the weak Van der Waals Force in buckypaper, the stress can't be effectively transferred between CNTs. Measured Young's moduli of this porous fibrous material reach maximum value of 2 GPa (Yeh, 2007), which is approximately 0.2 % of the modulus of SWCNT.

Methods to improve mechanical properties of buckypaper in order to use these materials in real-world structural applications have been developed. Buckypaper with aligned CNTs generally have a higher Young's Modulus and tensile strength (C. Huang, Chen, Reneker, Lai, & Hou, 2006). In addition, various polymers are employed to infiltrate buckypaper to reinforce stress transport among CNTs. A tensile strength of approximately 600 MPa and a Young's Modulus of 96 GPa are achieved by fabricating nanocomposites of buckypaper/pCBT (Z. Li et al., 2015). By incorporated CNT sheets with several layers of liquid crystal polymer (LCP) matrix, a Young's modulus of around 33 GPa and a tensile strength of 387 MPa are reported (Chang et al., 2013a). Dispersing CNT sheet in biopolymer s-carrageenan (IC), Young's modulus and tensile strength are reported to be 2.6 GPa and 40 MPa, respectively (Aldalbahi & Panhuis, 2012). More published results for Young's Modulus and tensile strength of buckypaper/polymer

nanocomposites are shown in Table 4.1. However, these improved moduli are far from

the potential that individual CNT properties offer.

Table 4.1 Young's Modulus and Tensile Strength of buckypaper/polymer nanocomposites

Young's modulus (GPa)	Tensile strength (Mpa)	Average tube diameter (nm)	Average rope diameter(nm)	Reference
8	30	0.8	10~50	(Sreekumar et al., 2003)
6.9	57	0.8	10~50	(Coleman et al., 2003)
2.3	6.29	0.8	10~50	(Baughman et al., 1999)
1.1	17.7	0.8		(Pham et al., 2008a)
4	32.3	0.8		' '
1.5	13.5	1.36		' '
2.7	33.2	1.36		' '

4.2 Experimental results of mechanical properties

In the current investigation, the Young's Modulus of buckypaper based

nanocomposites is 149.15 MPa, and tensile strength is 7.28 MPa. The stress-strain plot of

neat buckypaper nanocomposite is shown in Figure 4.1. Compared to values reported in

the literature, Young's Modulus and tensile strength achieved in our experiments are

lower. Considering the final application, this study utilized an epoxy resin capable of

tolerating higher strain. Consequently, the matrix has lower Young's Modulus and

Tensile Strength. The stiffness and failure stress of the pure epoxy however are

reinforced by fabricating the nanocomposite.
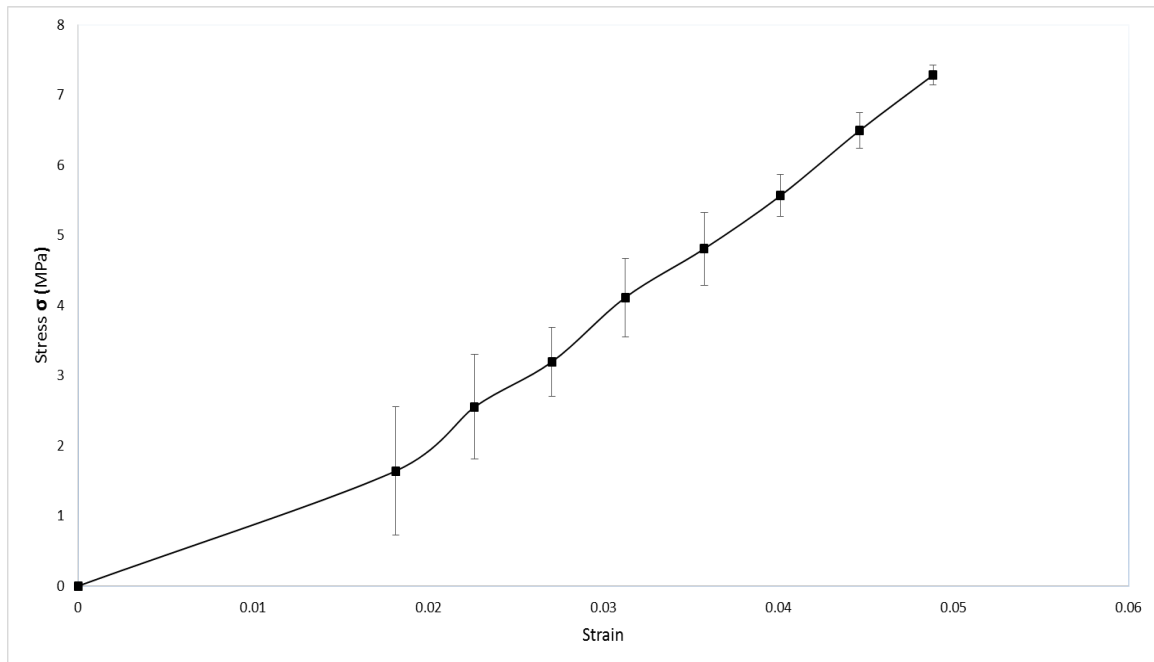
Figure 4.1 Stress-strain plot of neat buckypaper nanocomposites

The mechanical properties of nanocomposites increase with the addition of coarse graphene filler. Figure 4.2 shows the stress-strain plot of nanocomposite with 5 wt. % coarse graphene platelets. The variation in Young's Modulus and failure stress of the nanocomposite strips with addition of second filler are presented in Figure 4.4 and Figure 4.5. Addition of the coarse graphene platelets to epoxy mixture and CNT sheet increases the stiffness and strength of the nanocomposites.
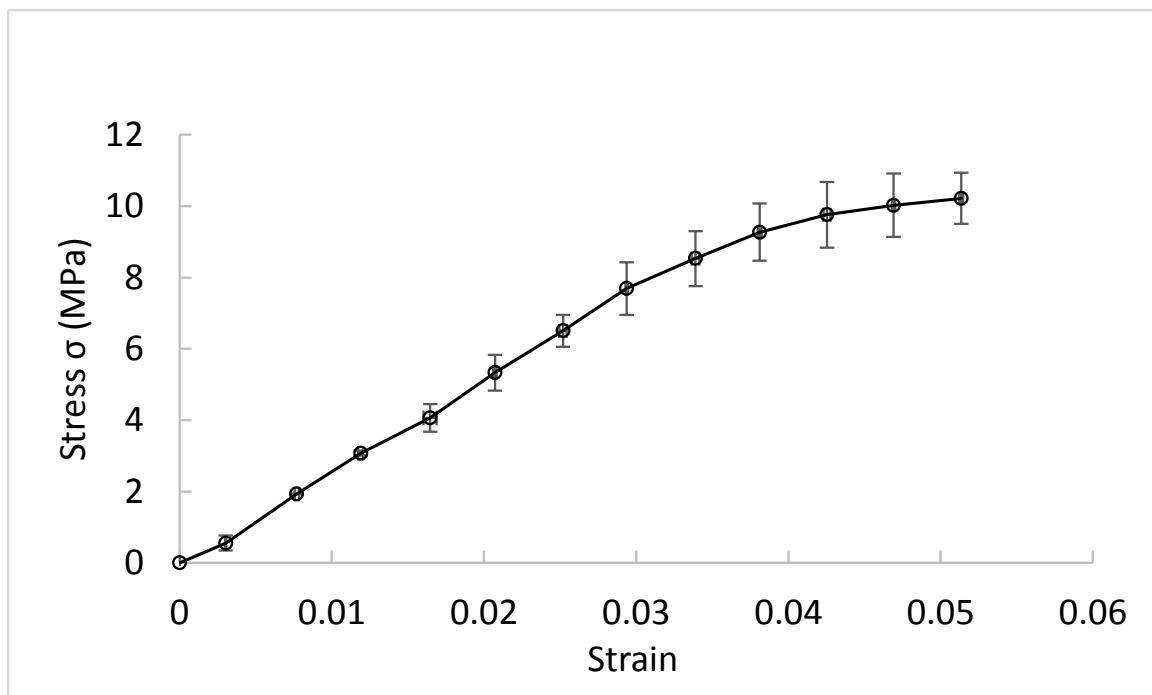
Figure 4.2 Stress-strain plot of nanocomposites with coarse graphene platelets (5 wt. %)

The Young's modulus and failure strength increases rapidly at low wt. % of the second filler. Further increase in properties with increase in coarse graphene platelets is at a lower rate. SEM micrographs indicate that CNTs come into direct contact with coarse graphene filler as shown in Figure 4.3. Bigger fillers which are smooth platelets directly contact with stick like CNTs.

12/9/2015	dwell	WD	mag □	HV	mode	⊢—— 10 µm ——⊣
1:54:58 PM	600 ns	10.5 mm	8 000 x	3.00 kV	SE	Quanta
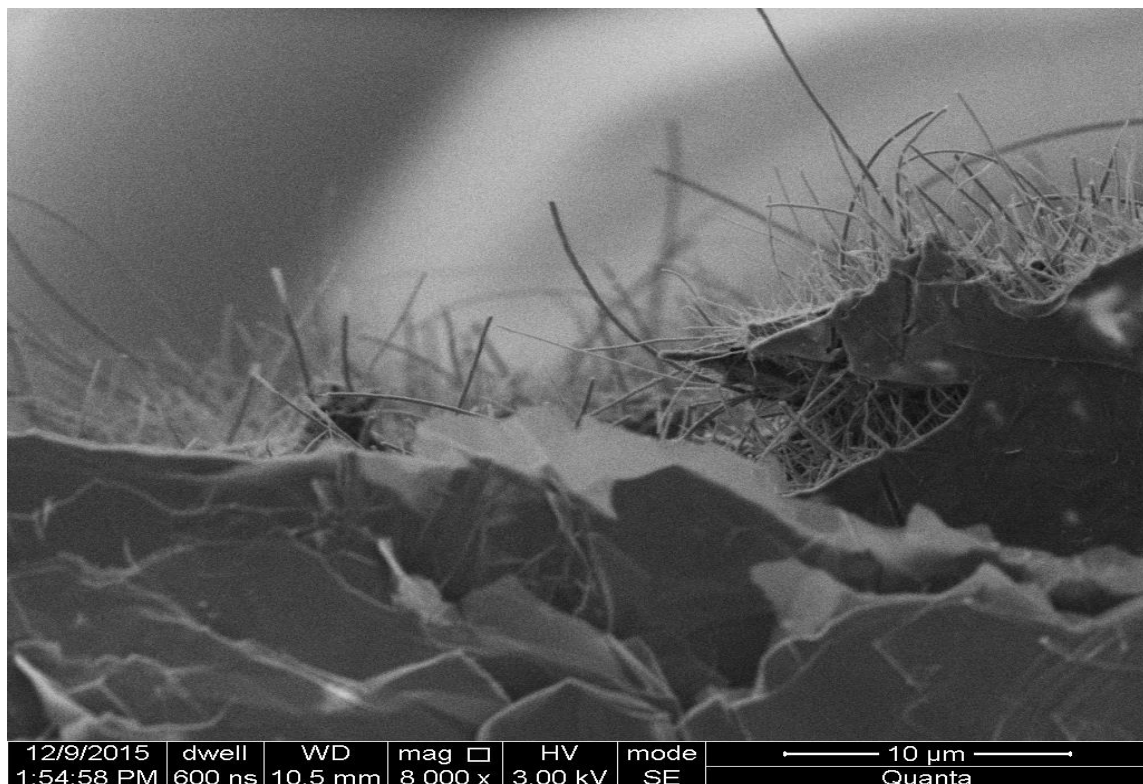
Figure 4.3 Tension fracture cross section of nanocomposites

When at lower weight percentage, nanocomposites is effectively reinforced because coarse graphene fillers can interact with CNTs at a higher rate. In other words, load is effectively transferred to the coarse graphene platelets. However, with increase of filler loading, less fillers can interact with the matrix or CNTs. Therefore, further increase of mechanical properties are at a lower rate.

Overall, as shown in Figure 4.4 and Figure 4.5, the Young's modulus and failure strength increases from 149.15 ± 0.8 MPa and 7.28 ± 0.4 MPa to 395.58 ±1.2 MPa and 16.12 ±0.6 MPa respectively with a 15 wt. % coarse graphene platelet addition. Even with a 5 wt. % modification of epoxy matrix the Young's modulus and tensile strength reach 257.36 ± 1.2 MPa and 10.28 ± 0.5 MPa respectively.
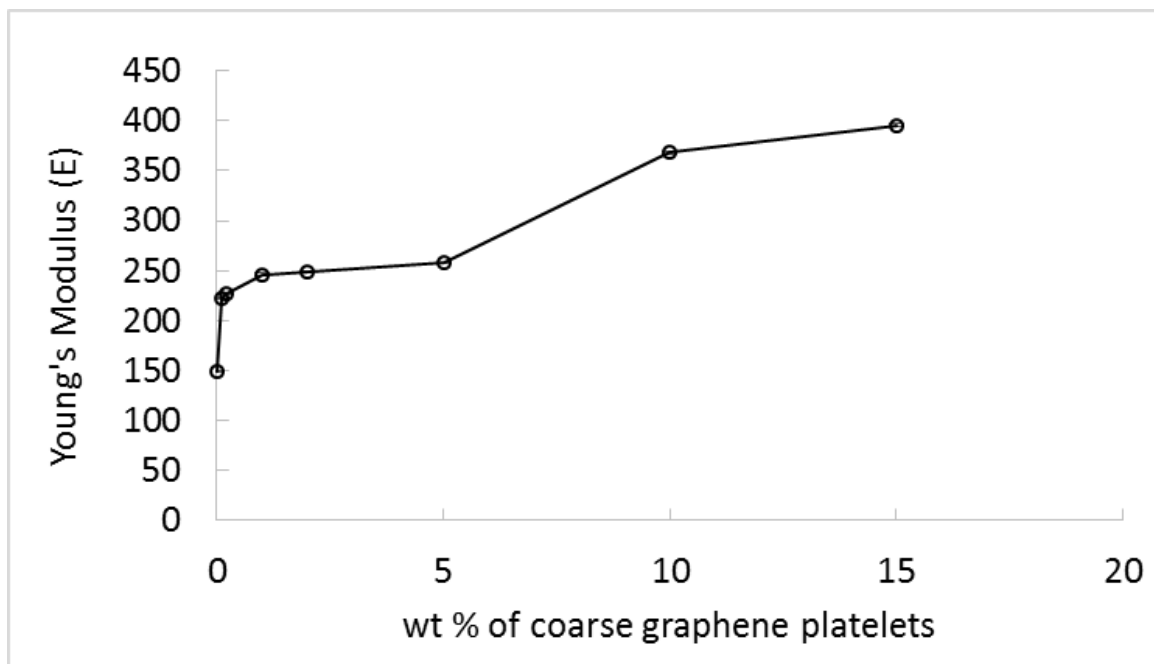
Figure 4.4 Young's Modulus of nanocomposites with coarse graphene platelets
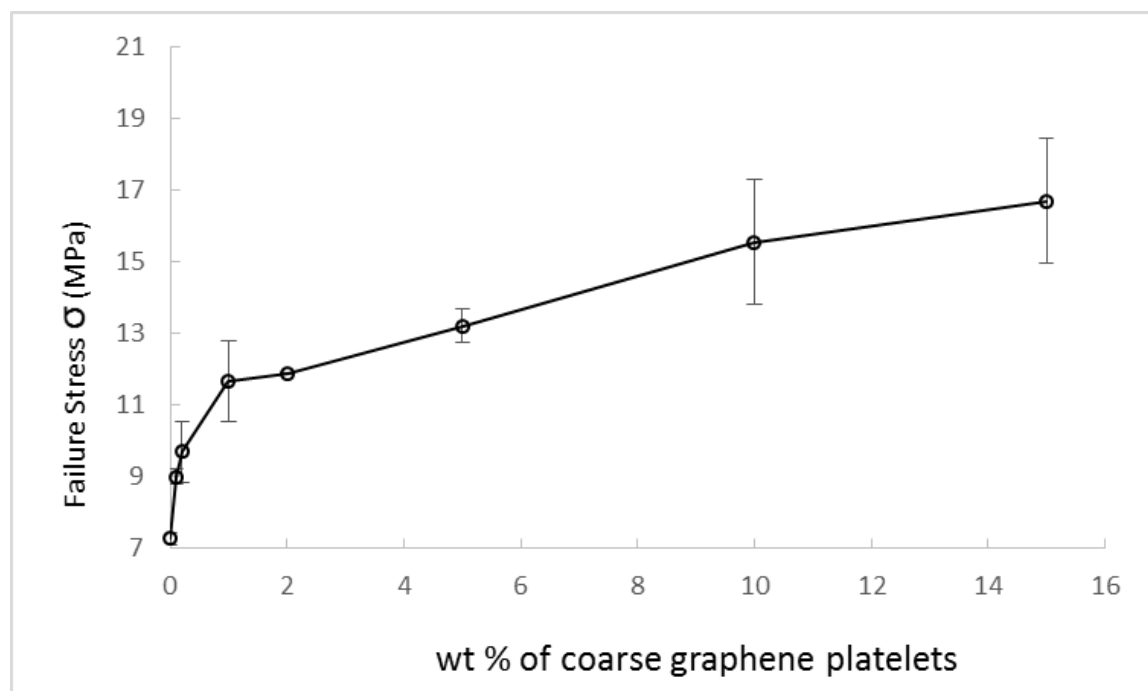
Figure 4.5 Failure stress for various content of coarse graphene platelets based nanocomposites

A similar reinforcement of mechanical properties occurs to nanocomposites with

additional fine graphene nanoplatelets as shown in Figure 4.6 and Figure 4.7. The increase in Young's modulus and tensile strength are both smaller than results gained using coarse graphene platelets. One of the reasons for lower increase may be the agglomeration. Sonication was not performed during fabrication of these specimen. Young's modulus increases from 114.5 MPa to 141.2 MPa when the content of fine graphene nanoplatelets increases from 0 to 20 wt. %, while 8.9 MPa to 10.5 MPa for stress. Figure 4.8, shows the micrographs comparing the two nanocomposites.

There is weaker reinforcement of mechanical properties by fine graphene nanoplatelets, compared to coarse graphene platelets. However, since smaller fillers have more contact surface for reinforcement, graphene nanoplatelets are supposed to have stronger enhancement of mechanical properties. This might be because fine graphene nanoplatelets agglomerate during fabricating process. Thus, fine graphene nanoplatelets have less chance to contact with surface of nanocomposites, and to function as reinforcement.

There has been significant research effort over the past decade in using CNTs as fibers for structural composites. While the CNTs by themselves have excellent strength, stiffness, the predicted mechanical properties have not yet been realized in nanotube composites. This is because of microstructural problems related to fiber–matrix interfacial strength, dispersion of nanotubes within composite and alignment of nanotubes in the loading direction. There have been efforts to improve all three aspects, by approaches like functionalization (Namilae & Chandra, 2005), use of surfactants (S. W. Kim et al., 2012) and magnetic or mechanical alignment (Rein, Breuer, & Wagner, 2011b). Present effort represents another way to improve the mechanical properties by

addition of second filler.
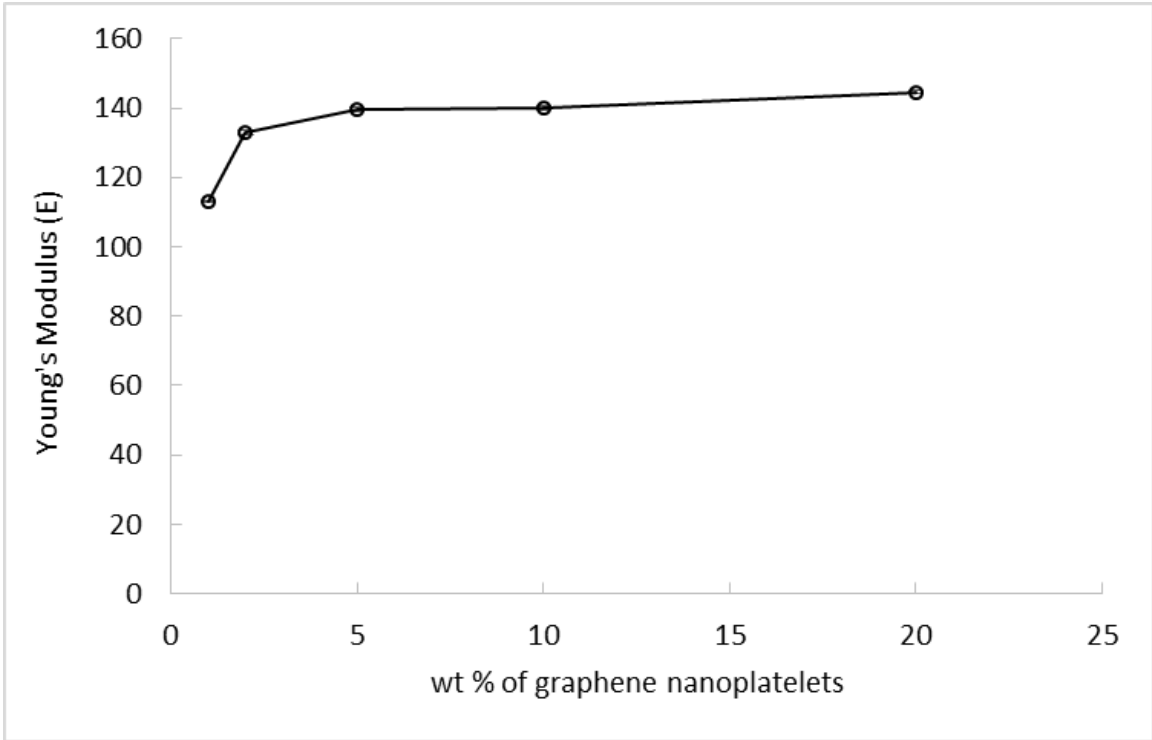
Figure 4.6 Young's Modulus of fine graphene nanoplatelets based nanocomposites
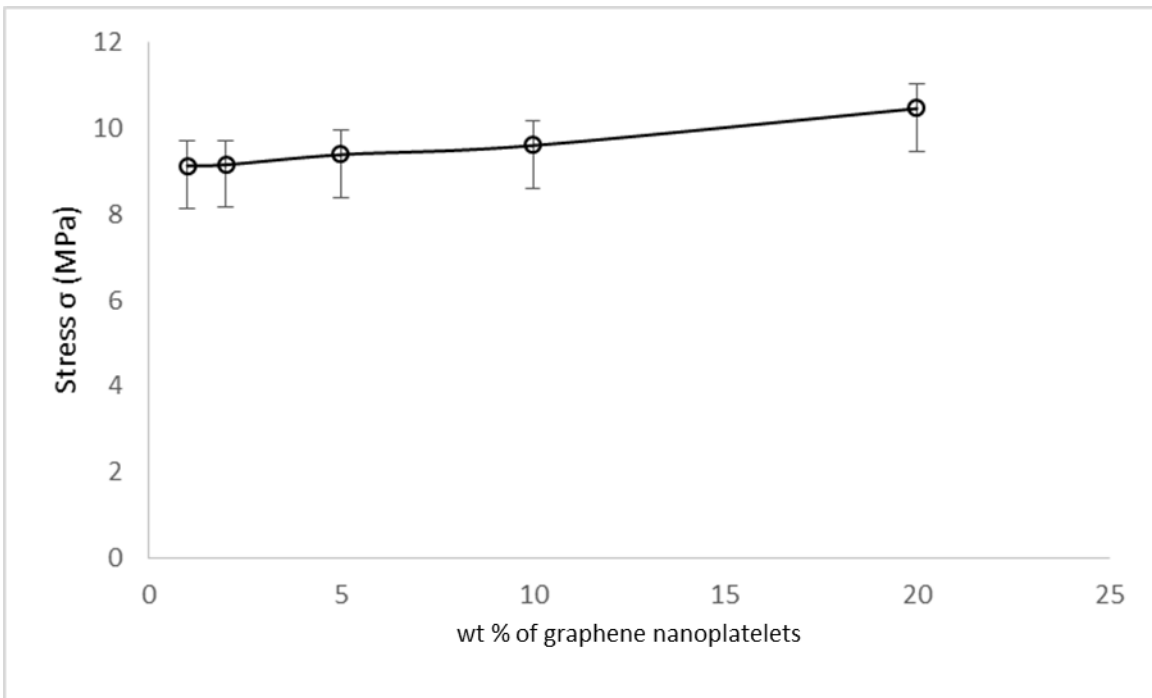
Figure 4.7 Tensile strength of fine graphene nanoplatelets based nanocomposites
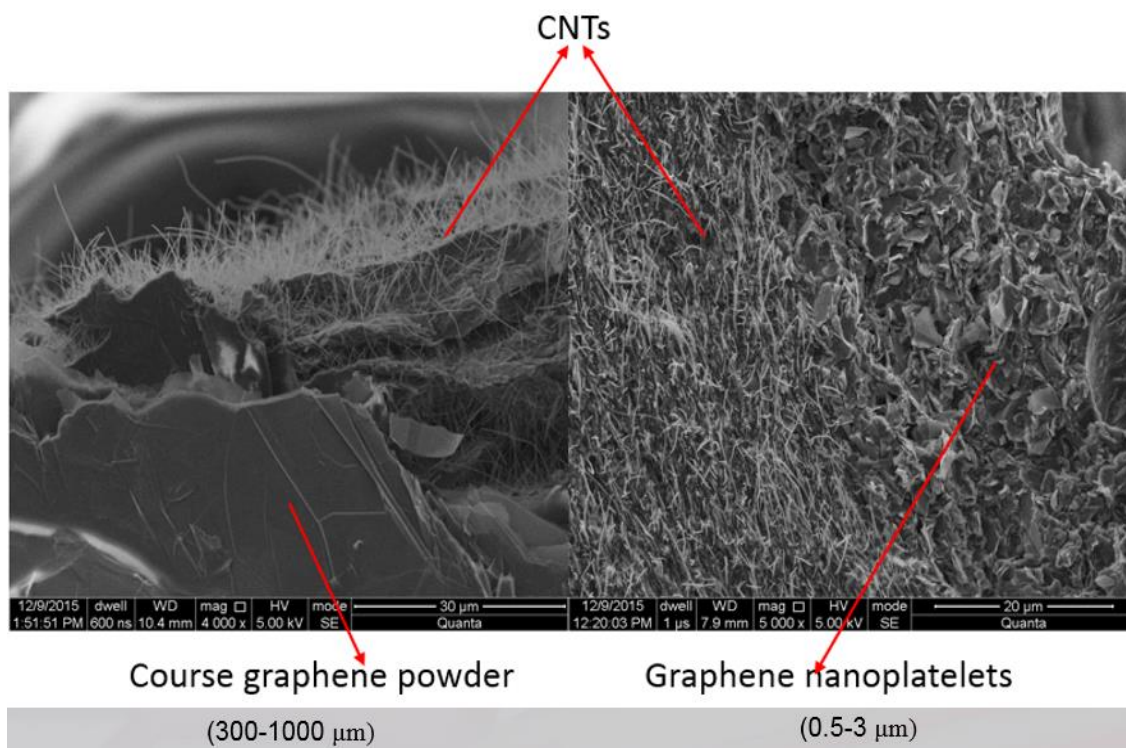
Figure 4.8 SEM micrograph of nanocomposites with additional fillers

5. **Electrical properties of hybrid nanocomposites**

Here results of electrical resistivity measurements of the hybrid nanocomposites are presented in this chapter.

5.1 Literature review of resistivity of buckypaper nanocomposites

CNTs are considered to be an attractive filler for fabricating highly electrically conductive nanocomposites because of its combination of a high intrinsic conductivity and high aspect ratio. Individual CNT have excellent conductivity of about $10^5 - 10^8$ S/m and reaches a high aspect ratio up to $100 - 1000$ (Laurent, Flahaut, Peigney, & Rousset, 1998). In addition, when mechanical deformation is applied on the nanocomposites, there is a corresponding variation of resistance. Researchers have used this electromechanical property for strain sensing (Y.-T. Huang et al., 2012). This nanocomposites strain sensor has advantages of (a) multi-direction sensing and (b) being easily embedded in composite structure to monitor strain variation or damage in the target area. Gauge factor is utilized to determine sensitivity to strain.

Despite excellent intrinsic electrical conductivity, CNTs reinforced nanocomposites show much higher resistance (Liang & Tjong, 2006). Unlike conductivity of single CNT, electrical conductivity in CNTs nanocomposites depends on the filler loading, as also described by percolation theory (Kasteleyn & Fortuin, 1969) (Sykes & Essam, 1964) (McLachlan et al., 2005b). When low quantity of fillers are present in the nanocomposites, the fillers form small clusters or individually stands. Since the average distance between the particles exceeds filler size, the nanocomposites exhibit similar resistivity as the polymer matrix. When sufficient loading of fillers occurs in the

nanocomposites, a continuous electricity conducting network forms. This threshold

content is called percolation threshold. At this critical filler concentration, the

conductivity of the nanocomposites rapidly increase. Based on geometrical

considerations, the loading value of the fillers to form percolation threshold is highly

influenced by the aspect ratio (length to diameter ratio) of the particles.

There is abundant literature on conductive of CNT/polymer nanocomposites but a

striking variation in the value of percolation threshold is reported. These published

percolation threshold ranges from 0.0025 wt. % to several wt. % (Moriarty, Whittemore,

Sun, Rawlins, & Grunlan, 2011). There are several possible reasons to explain these

disparities. Firstly, the nanostructure of the CNTs and thus the resulting characteristics

and properties are strongly dependent on the synthesis method. CNTs with different

characteristics and properties are produced even when the parameters during CNT

synthesis remain the same (Song & Youn, 2005). Secondly, impurities cause decrease of

conductivity in nanocomposites (Ambrosi & Pumera, 2010). Amorphous carbon, catalyst

particles and defects resulted from manufacturing process can cause these impurities.

Further, treatments such as purification, sonication etc. can significantly affect the

properties of CNTs (H.-Z. Geng et al., 2007). Thirdly, despite low contact resistance

between CNTs, insulating matrix polymer at CNT-CNT junction prevent direct contact.

As a result, phonon transaction though insulating polymer increases resistance of the

nanocomposites (Souier, Santos, Al Ghaferi, Stefancich, & Chiesa, 2012). Electrical

conductivity of pure CNTs networks are as high as 10^4-10^5 S/m, whereas reported

CNT/polymer nanocomposites have a conductivity ranging 10 to 100 S/m. Furthermore,

when dispersed in insulating polymers, the state of the CNTs as well as the category and

the strength of CNT-matrix interactions, are highly affected by the nanocomposite fabricating process. These factors eventually affect the electrical properties of the nanocomposites. Several reported results of resistivity of CNT/polymer nanocomposites are listed in Table 5.1.

Table 5.1. Resistivity of buckpaper composites from literature

Reference	Material	Resistivity (10^{-5} Ω·m)
(S. Wang, 2015)	Magnetic aligned MWCNT buckypaper	1.13
(Chapartegui et al., 2012)	Neat buckypaper	22.7
(Chang et al., 2013a)	Neat buckypaper	20.8
(S. Wang, 2015)	MWCNT buckypaper/Epon862	39.2
(Chapartegui et al., 2012)	MWCNT buckypaper / Benzoxazine	34.5
(Chang et al., 2013a)	MWCNT buckypaper /Parmax	10
(Zhang et al., 2007)	Aligned MWCNT buckypaper/pCBT	1.9

5.2 Experimental results of resistivity

The electrical resistivity of the nanocomposites strips is obtained as:

$$\rho = R(w \times t)/l \tag{5.1}$$

Where R is the calculated resistance by Ohm's Law, w and l are the width and thickness of composite strips. L is the length of the composite strip.

The thickness of the samples are obtained using SEM micrographs of cross sections as shown in Figure 5.1. An average thickness of 100 µm is used in the resistivity calculation.
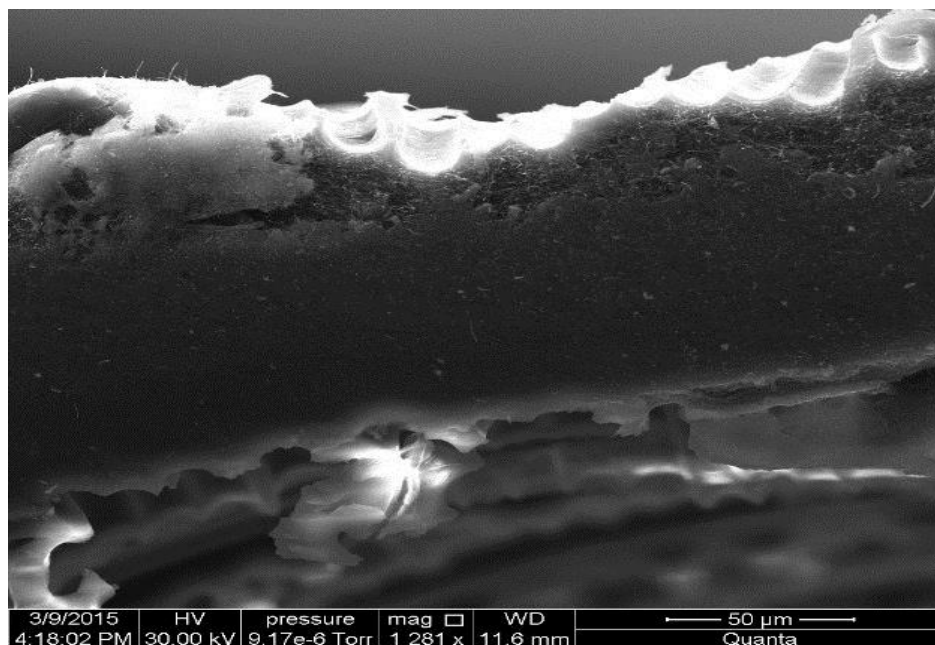
Figure 5.1 SEM micrograph of nanocomposites for cross section

Figure 5.2 shows the resistivity of the clean buckypaper nanocomposite and buckypaper composite with different quantities of coarse graphene platelets. The values reported are averaged from tests on three identical samples. Table 5.1 compares the resistivity values for neat buckypaper composite obtained in current investigation with those from literature. The resistivity of composites is comparable, particularly there is a good correlation between values obtained in this study and that by Wang and Chapartegui with Epon862 and benzoxazine matrix materials (Chapartegui et al., 2012). The resistivity of the neat CNT sheet without any matrix and that with aligned nanotubes is understandably lower than that of the composite in the current study.

When the second conductive filler is added to the nanocomposite system the resistivity decreases. When the second phase filler is coarse graphene platelets there is a significant decrease from 34.7 Ω·m to 13.4 Ω·m using the 5 wt. % coarse graphene platelets - epoxy as the matrix. This further decreases as the content of filler is increased

to 10 wt. % and 15 wt. %. The plot seems to indicate that continuous network of

graphene-CNT fillers is achieved at 5 wt % graphene filler therefore further addition does

not change the conductivity significantly.
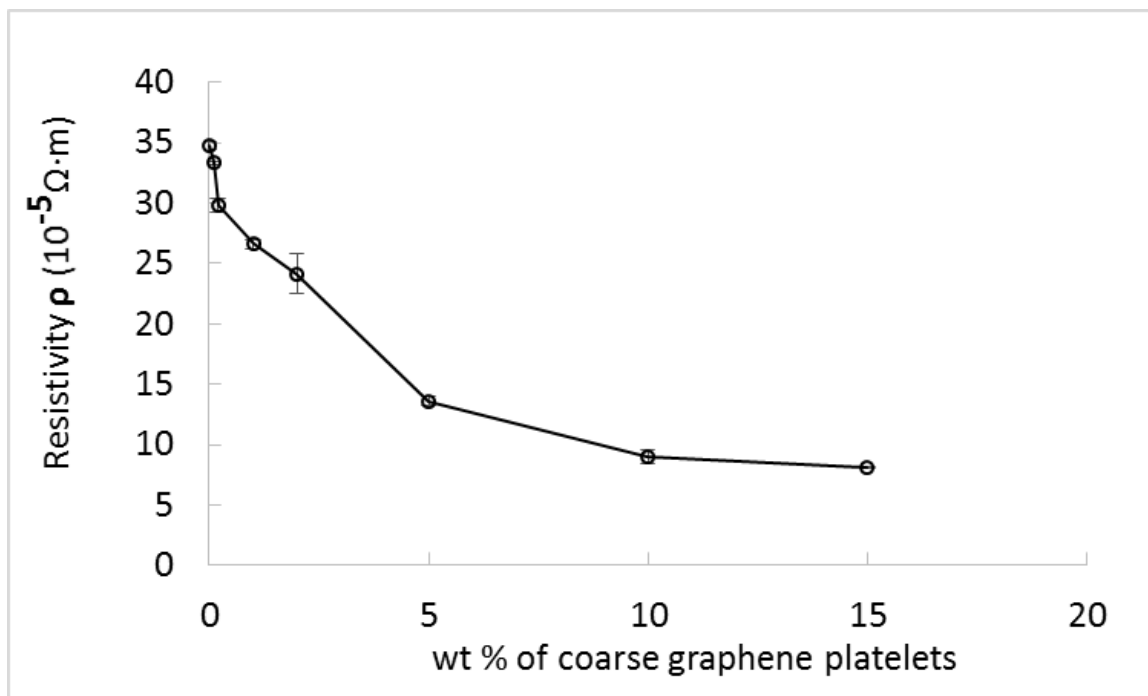
Figure 5.2 Resistivity of coarse graphene platelets based nanocomposites

However, there is no such pronounced change in resistivity when the filler is fine

graphene nanoplatelets as shown in Figure 5.3. The decrease in resistivity is an order of

magnitude lower when the filler is smaller sized fine graphene nanoplatelets. Resistivity

of fine graphene nanoplatelets reinforced nanocomposites decrease from 33.9 $\Omega \cdot$m to

29.8 $\Omega \cdot$m, when fine graphene nanoplatelets concentration eventually increase to 20 wt.

%. Agglomeration of fine graphene nanoplatelets could be an explanation for these

observations.
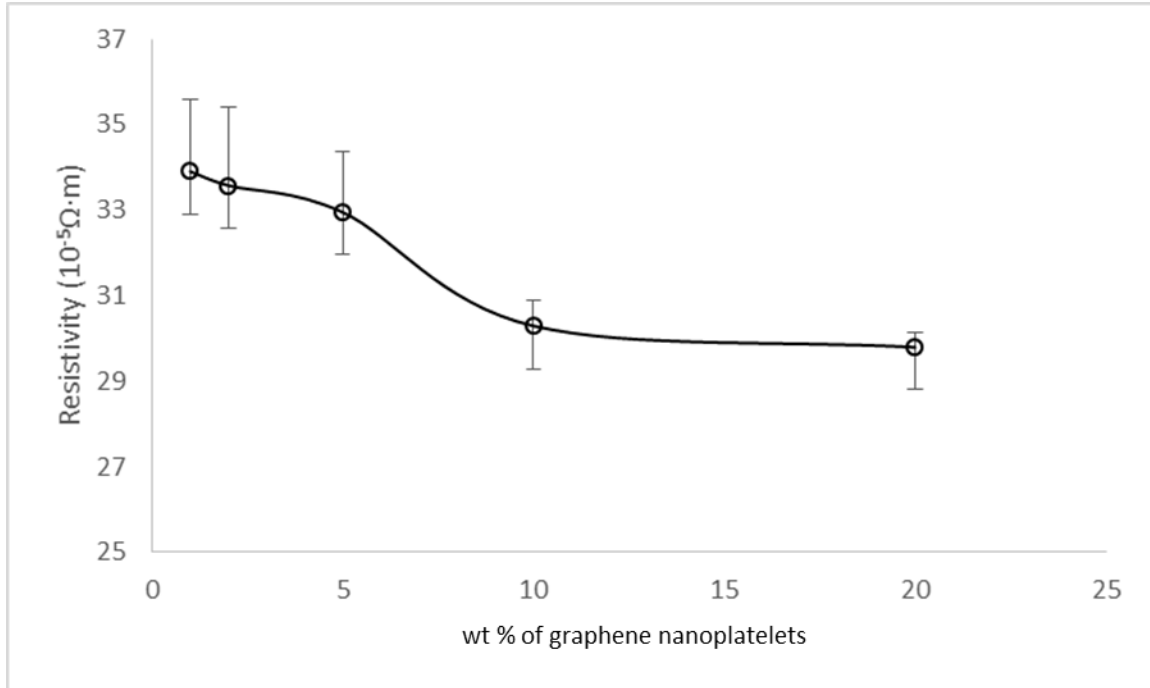
Figure 5.3 Resistivity of fine graphene nanoplatelets based nanocomposites

There are several theoretical models by Kirkpatrick (Kirkpatrick, 1973b),
McLachlan (McLachlan, Blaszkiewicz, & Newnham, 1990b), Mamunya (Mamunya,
Davidenko, & Lebedev, 1996) that have been proposed to explain the resistivity (or
conductivity) of composites with conductive fillers like CNTs. Kirkpatrick's model is
based on contact between filler particles in a matrix and is given by

$$\sigma_m = \frac{1}{\rho_m} = A(\phi - V_{bc})^b \qquad (5.2)$$

Where σ_m is the conductivity and ρ_m is the resistivity of the composite, A is the
conductivity of the fillers, ϕ is the volume fraction of the fillers, V_{bc} is the percolation
threshold of filler, and b is an experimentally determined constant exponent and depends
on the particle shape. This phenomological model has successfully explained

conductivity of many particulate and fiber composites including carbon nanotube –

polymer composites (Seidel & Lagoudas, 2009). There is a significant increase in

conductivity when the volume fraction of the filler particles is higher than the percolation

threshold (V_{bc}) which represents the minimum quantity of filler to form a continuous

network. The percolation threshold as well as the critical exponent have been known to

vary depending on particle size (Moriarty et al., 2011). Larger particle typically lower the

percolation threshold as smaller quantity of filler particles can result in a continuous

network.

In the current study, neat CNT sheet is a connected network therefore has low

resistivity. Infiltrating the nonconductive epoxy into the CNT sheet results in reduced

connectivity, therefore increases the resistivity of the composite. Addition, of second

conductive filler can reduce the resistivity by (a) increasing the volume fraction of

conductive fillers ϕ and (b) reducing the percolation threshold V_{bc} . With the addition of a

second conductive filler, there is an increase in the content of conductive fillers which

happens with both coarse graphene platelets and fine graphene nanoplatelets. In the case

of bigger coarse graphene platelets there is significant decrease in resistivity, potentially

because the percolation threshold for the composite is also reduced. It is known that

percolation threshold is lower when the filler particles are larger (Jing, Zhao, & Lan,

2000). The larger size of coarse graphene platelets (300 -1000 μm) modifies the

percolation threshold in these hybrid composites while this effect is not present for the

composite with fine graphene nanoplatelets (1-3 μm). Results indicate that the coarse

graphene platelets bridges CNT network more effectively than the fine graphene

nanoplatelets. Agglomeration of fine graphene platelets can be another reason for the

reduced effectiveness of these fillers.

6. **Electro-mechanical behavior of hybrid nanocomposites**

Here this chapter is presenting the results and discussion of experimental observations of electro-mechanical behavior of the hybrid nanocomposites. The experiments measure the electrical resistivity of the nanocomposites as they are subject to mechanical deformation. Results indicate a tenfold increase in gauge factor with the addition of coarse graphene platelet filler. An analytical model is developed to explain the experimental observations. Results of the analytical model match the pattern observed in experiments.

6.1 Introduction

Due to the extraordinary electrical, mechanical, and thermal properties, CNTs have immense potential for sensing applications. Particularly, SWNT have been reported to have outstanding piezo-resistive response (Randal, 2005). This behavior can be quantified using gauge factor. Gauge factor is defined as the ratio of fractional change in electrical resistance to the fractional change in length which is strain see equation below.

$$Gague\ Factor\ =\ \frac{1}{R} \times \frac{\Delta R}{\varepsilon} \qquad (6.1)$$

Previous investigations show that the gauge factor of SWCNTs ranges from 400 to 2900 (Stampfer C, 2006). This is much than most of the conventional materials including semi-conductors and metals. This extremely high gauge factor for individual SWCNTs has been employed to develop novel nano-electromechanical sensing devices (Stampfer C, 2006).

However, it is challenging to apply such superior piezo-resistivity to industrial

applications. Firstly, structural and electronic inhomogeneities and variations remain in SWCNTs synthesized under identical conditions (Biercuk, Ilani, Marcus, & McEuen, 2008). Secondly, it is extremely difficult to precisely control the position and alignment of an individual nanotube. To overcome the issues, CNTs are used in ensembles like CNT thin films for practical applications. The random assembly of a large number of individual tubes can be treated homogenous. Thus, the structure and electronic properties of CNT sheets can be considered to be uniform. In addition, the problems associated with tube positioning and orientation can be mitigated. Researchers have attempted to obtain single-walled and multi-walled carbon nanotubes thin film sensor for various applications, such as structure health monitoring (SHM), human health monitoring (I. Kang, Schulz, Kim, Shanov, & Shi, 2006b), finger-sensing device (Hwang et al., 2011), micro-electromechanical systems (Luo & Liu, 2013). Despite of their advantages, the disadvantage of CNT thin film sensor is their relatively low sensitivity compared to individual nanotube.

Gauge factor for CNT ensemble based sensors varies in a range from 0.5 to 22.4 (H. Zhao et al., 2010) which is relatively low compared to single CNT sensors. Compared to conventional metal-foil strain sensors with a gauge factor around 2, most of the results are much higher. Several reported values of gauge factors from publications are shown in Table 6.1. Usually, MWCNTs nanocomposites are more effective, responding to strain and stress change than SWCNTs nanocomposites. In the subsequent section it presents our experimental results of evaluating electro-mechanical response of these composites.

Table 6.1. Gauge factor of various CNT thin-film nanocomposites

Nanocomposites	Gauge factor	Reference
MWCNT/polycarbonate	7	(Zhang, 2006)
MWCNT (1.44 vol. %) / polyethylene oxide (PEO)	1.6 ~50	(Park, M., 2008)
MWCNT (1 wt. %)/ poly(methyl methacrylate) (PMMA)	15	(Z. Wang et al., 2004)
SWCNT (1 wt. %) / polyelectrolyte (PE)	16	(Kenneth J. Loh, Lynch, Shim, & Kotov, 2007)
MWCNT (0.1 wt. %)/ epoxy	3.4~4.3	(Wichmann et al., 2009)
MWCNT (17 wt. %)	7.98	(Kanoun, 2010)
MWCNT (36.6 wt. %)	1.57	
MWCNT (0.5 vol. %)/ poly(propylene) (PP)	2	(Paleo et al., 2010)
MWCNT (1 wt. %) /	22.4 (tension) 7 (compression)	(Hu et al., 2010)

6.2 Electromechanical behavior of neat buckypaper nanocomposites.

Neat buckypaper nanocomposites exhibit change in resistance when subject to mechanical deformation. Figure 6.1 shows the resistivity strain response of these composites. There is an increase in resistivity from 35.2 to 36.1 with the application of deformation. The results obtain a gauge factor of 0.49 for these composites.
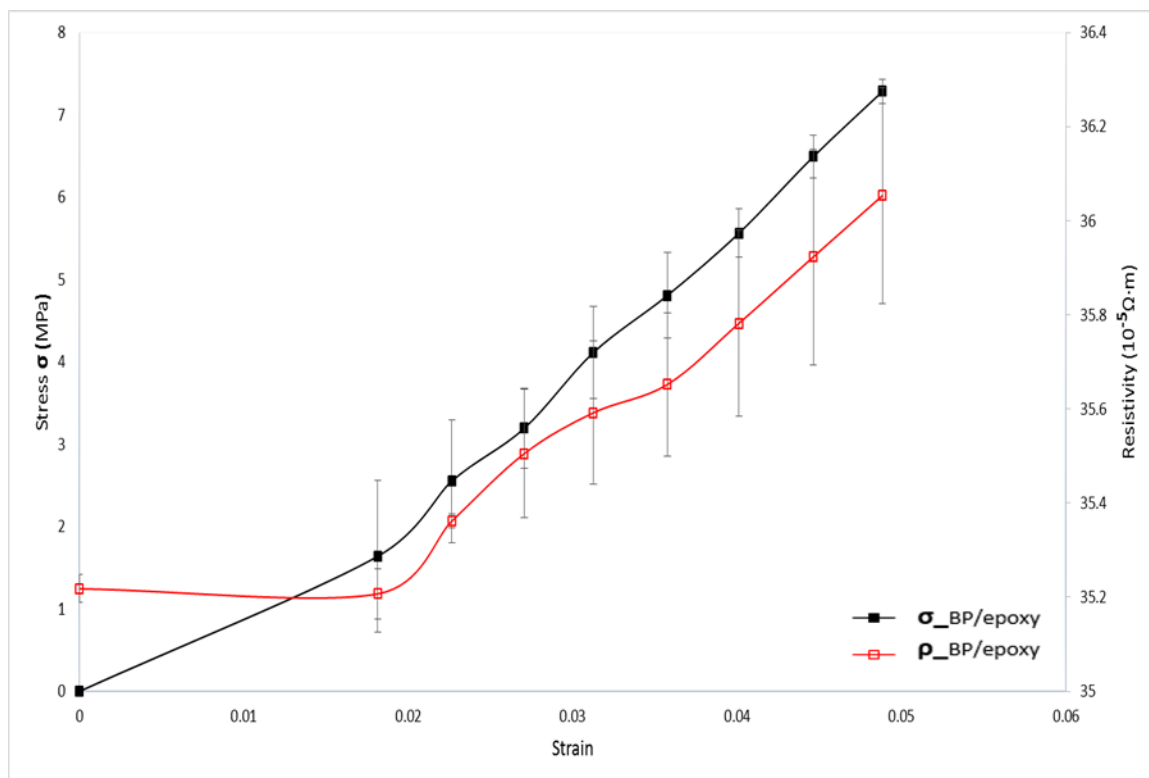
Figure 6.1 Stress-strain and resistivity-strain response of neat buckypaper nanocomposites

6.3 Electromechanical behavior of hybrid nanocomposites with coarse graphene platelet fillers

Figure 6.2 show the resistivity-strain and stress-strain response of nanotube sheet-epoxy composite modified with 5wt. % of coarse fine graphene nanoplatelets. The resistivity of the composites decreases as the load application increases. There is a clear increase in electrical resistivity in neat CNT sheet-resin composites from $35.2 \times 10^{-5} \Omega \cdot m$ to $36.03 \times 10^{-5} \Omega \cdot m$ (The device accuracy is less than 1% as mentioned in Chapter 3). This effect is increased by an order of magnitude when epoxy resin is modified by 5wt. % coarse graphene platelets adding. The resistivity increases dramatically and linearly from $18.1 \times 10^{-5} \Omega \cdot m$ to $26.8 \times 10^{-5} \Omega \cdot m$.
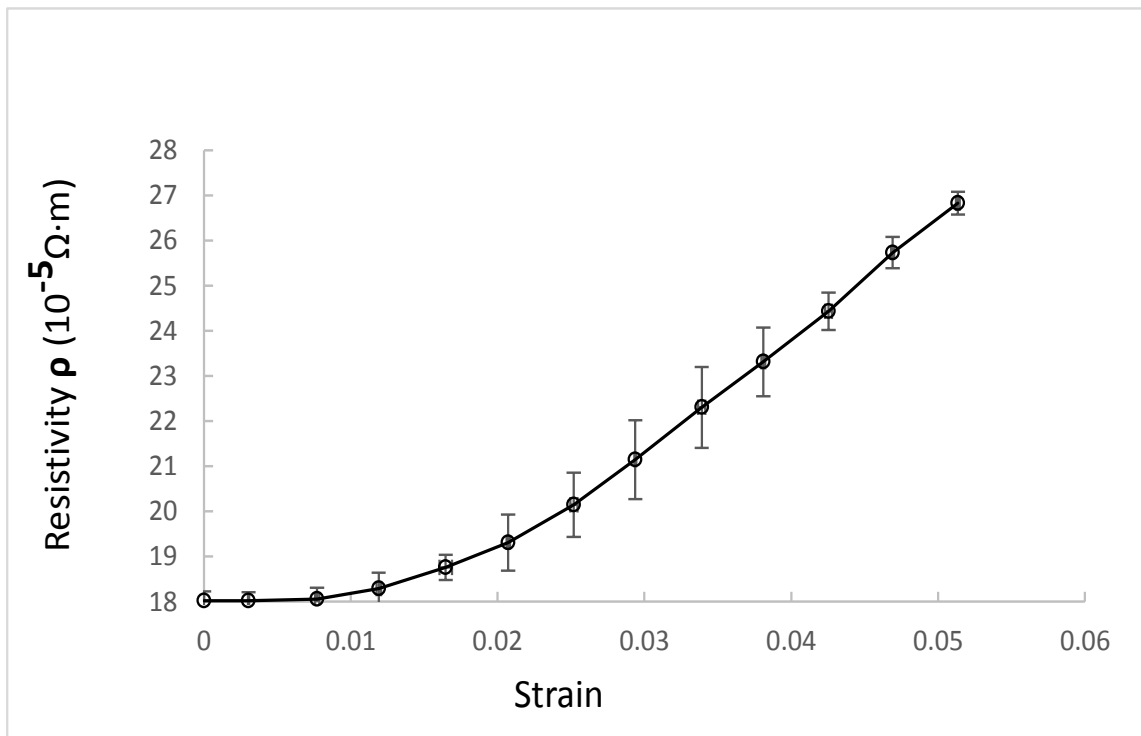
Figure 6.2 Resistivity change with applied strain for coarse graphene platelets (5 wt. %) based nanocomposites

Each dataset corresponds to an average of three samples as shown in Figure 6.3 for 5 % coarse graphene platelets reinforced epoxy- buckypaper composite. The neat CNT sheet-epoxy composite shows a linear stress strain response followed by clean fracture at 5 % strain. Addition of coarse graphene platelets to epoxy and CNT sheet increases the stiffness and strength of the composites. More results are shown in Figure 6.4. To clearly see trend of each curve, although error bars are not added for both Figure 6.4 and Figure 6.5, they can be found in similar plots. The improvement in stiffness reduces as the coarse graphene platelets content is increased. Also the strain at failure is lower (4.1 %) when the coarse graphene platelets content is increased to 10 and 15 wt. %.

There is a corresponding increase in tensile strength to 161.2 kPa from 72.8 kPa for neat CNT sheet composite for 15 wt. % coarse graphene platelets modification. Even with a 5 wt. % modification of epoxy matrix the tensile strength increases to 102.8 kPa.
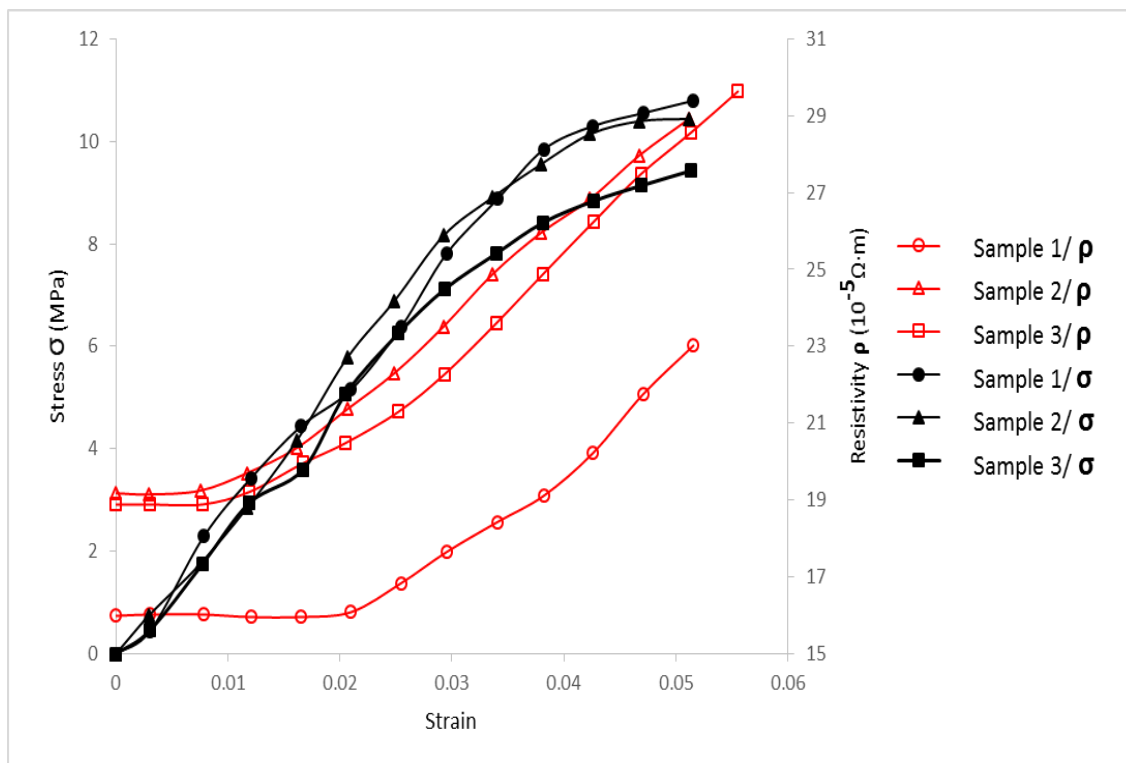
Figure 6.3 Stress-strain and resistivity-strain response of 5 wt. % coarse graphene platelets based nanocomposites

The Gauge factor of these nanocomposites is shown as in Figure 6.6. The gauge factor increases from a relatively low 0.49 to an order of magnitude higher 9.52, when the content of the coarse filler increases from 0 to 5 wt. %. The gauge facture drops to 4.84 when the content of coarse particles is increased further to 15 wt. %. The drop in gauge factor with high graphene platelet content may be because of the formation of continuous network which is not easily disrupted under load application.
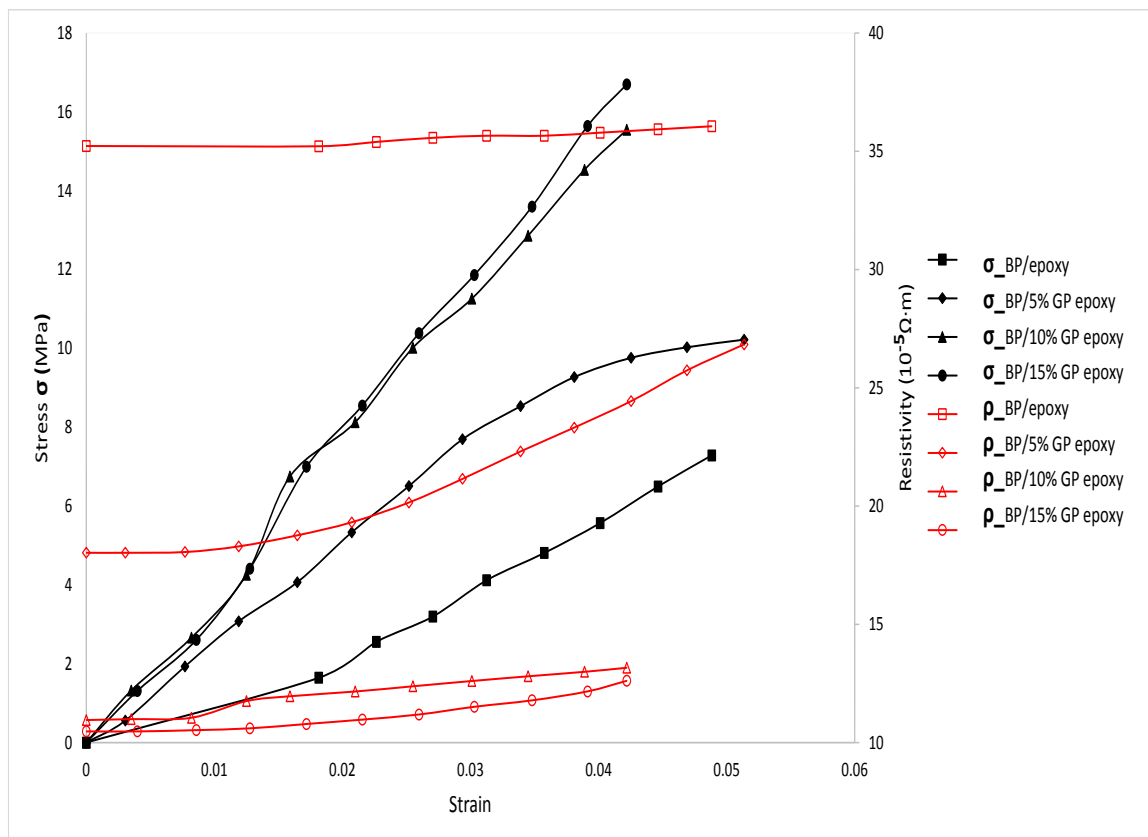
Figure 6.4 Stress-strain & resistivity-strain plot for various content of coarse graphene platelets based buckypaper

6.4 Electromechanical behavior of hybrid nanocomposites with graphene nanoplatelet fillers

Figure 6.5 shows the stress-strain and resistivity-strain response of nanotube sheet –epoxy resin composite modified with fine graphene nanoplatelets. There is a small increase in stiffness with the addition of fine graphene nanoplatelets but not as big an increase as that observed with coarse graphene platelets. The strain to failure decreases from 5 wt. % to 4.6 wt. %. Unlike with coarse graphene platelets there is no appreciable increase in tensile strength, in fact tensile strength decreases marginally from 72.8 kPa to 65.9 kPa and 64.04 kPa with 5 wt. % and 10 wt. % fine graphene nanoplatelets modifies

resin mixtures.

There is an increase in electro-mechanical response with fine graphene nanoplatelets addition, for example with 5 wt. % addition of fine graphene nanoplatelets in resin, the resistivity changes from 32.9×10^{-3} $\Omega \cdot$m to 34.16×10^{-3} $\Omega \cdot$m. The comparable numbers for neat CNT sheet composite are 35.2×10^{-3} $\Omega \cdot$m to 36.03×10^{-3} $\Omega \cdot$m. Though there is a marginal increase, this is not of the same scale as that observed for coarse graphene platelets. Problems with agglomeration of fine graphene nanoplatelets may be the main reason for not observing a significant increase.
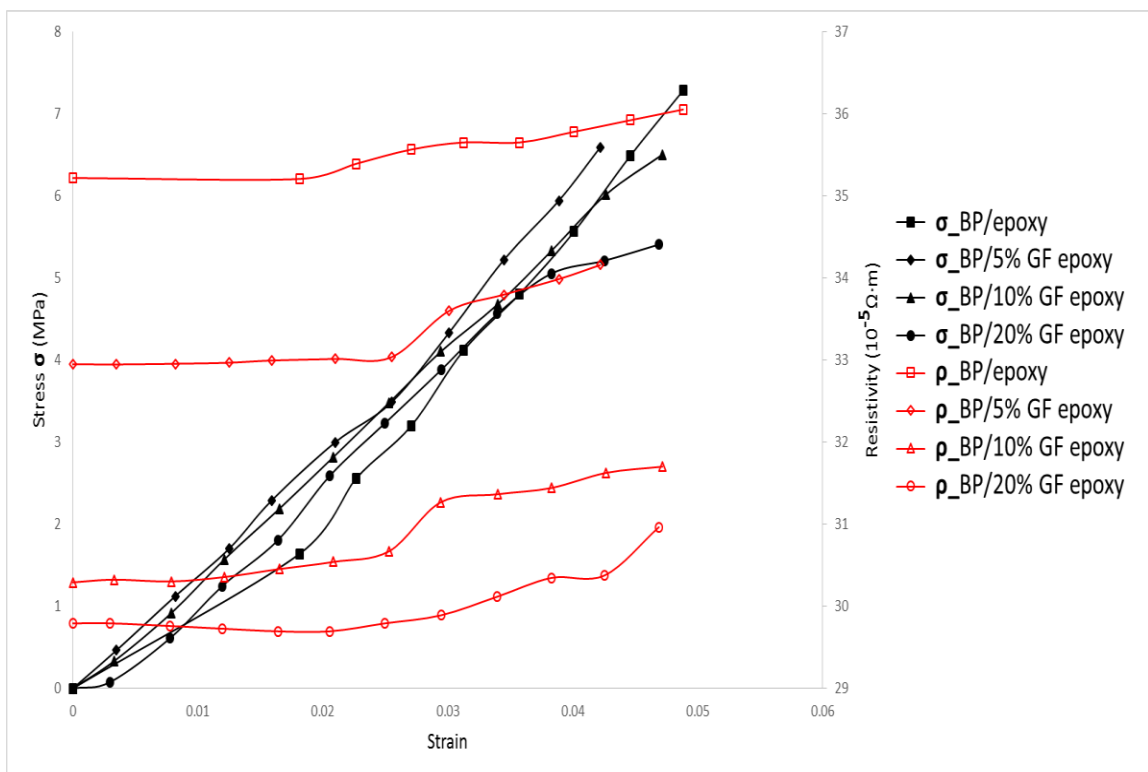
Figure 6.5 Stress-strain & resistivity-strain for various content of fine graphene nanoplatelets based buckypaper

Figure 6.7 shows the gauge factor corresponding to fine graphene nanoplatelets epoxy reinforced Buckypaper. Similar pattern to coarse filler modified nanocomposites

is observed, but the magnitude of increase is not significant. As explained earlier agglomeration of fine graphene nanoplatelets may be the reason for observing smaller increase in gauge factors.
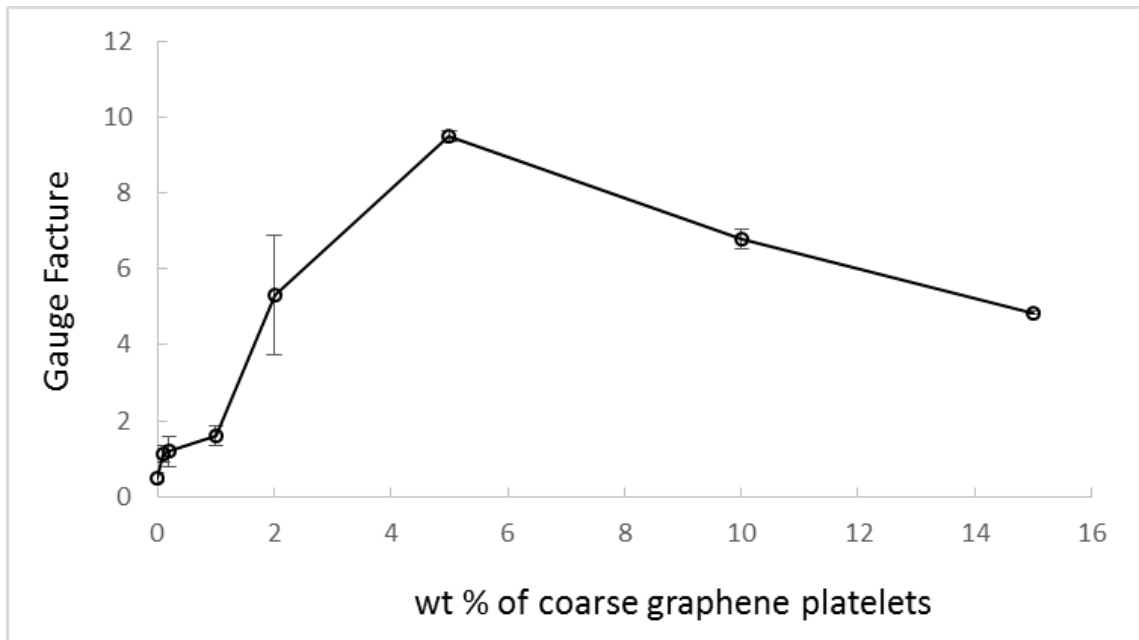
Figure 6.6 Gauge factor of nanocomposites with coarse graphene platelets
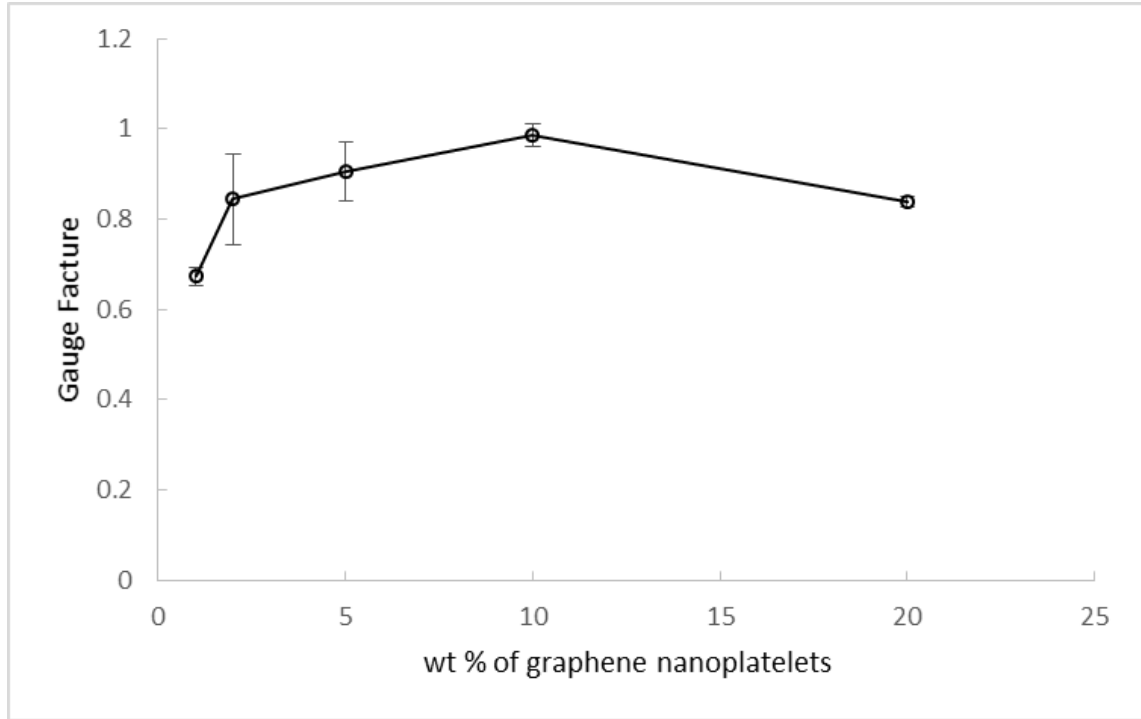
Figure 6.7 Gauge factor of nanocomposites with fine graphene nanoplatelets

6.5 Analytical model for electro-mechanical behavior of hybrid nanocomposites

An analytical model is developed to theoretically explain the experimental observations of electro-mechanical behavior. An equation for resistivity change is developed in terms of geometric features, volume fractions of the two fillers and applied strain. The predictions of the model qualitatively match the experimental observations.

6.5.1 Literature review of resistivity change under deformation

A few publications have attempted to model the change in resistance of nanotube composites with mechanical deformation. Carmona [50] developed a function to show how the local volume fraction varies with respect to compressibility of the matrix and filler phases due to external pressure. Due to applied loading, the local filler loading will

be altered, which will cause a change in the composite's resistivity according to the resistivity-concentration shape function. This model for the resistivity change, $\Delta\rho/\rho$ in terms of applied pressure difference, (*P-P0*) is defined as:

$$\frac{\Delta\rho}{\rho} = \left(\frac{\emptyset}{\emptyset+(1-\emptyset)\exp(-a(P-P_o))} - \emptyset\right)^{-t}(\emptyset - \emptyset_c)^{-t} - 1 \qquad (6.2)$$

Where, $\emptyset_c$ and t are the percolation threshold and critical exponent. A is a fit constant to describe sensitivity of the resistivity change.

Another model was suggested by Zhang et al (J. H. Kang et al., 2009) to predict the piezo-resistive behavior of polyurethane/ MCNTs nanocomposites. Despite of intrinsic piezo-resistivity of the CNTs, the piezo-resistivity in the polymer/CNTs nanocomposites is believed to be contributed by the tunneling effect. This model comprises of constants that includes tunneling width (inter-particle distance) and the potential barrier height between the matrix and filler. The model is given by equation

$$\frac{d(\ln(\rho))}{ds} = c + \frac{1.48T_1}{T+T_0} - \frac{0.02T_1T_0}{(T+T_0)^2} \qquad (6.3)$$

Where, c, is a modifying constant term, T, is the temperature and T_1 is a parameter including information about the tunneling gap. Parameters can be found by fitting the 0-strain temperature dependence of conductivity.

6.5.2 Analytical model of nanocomposites with single filler

There are three possible reasons for the change in resistivity of nanocomposites under deformation. Firstly, the resistivity of individual CNT will change due to strain. Secondly, mechanical deformation causes breakup of contact network at CNT-CNT and

CNT-graphene fillers, hence results of change in resistance. Thirdly, tunneling effect

depends on distance between conducting fillers. Tunneling resistance changes when there

is a change happen to distance between adjacent conducting fillers. The model focusses

on tunneling resistance because this could be the primary contributing factor to the

change in resistance.

This model starts with nanocomposites with only one filler which is CNTs. It is

assumed that the resistance of the polymer matrix is uniform and constant everywhere.

The resistance of paths perpendicular to the current flow is negligible, thus, the number

of conducting particles and the number of conducting paths between electrodes become

factors in this relationship. As shown in Figure 6.8, CNts are represented by circles with

diameter D and s is the average distance between CNTs.
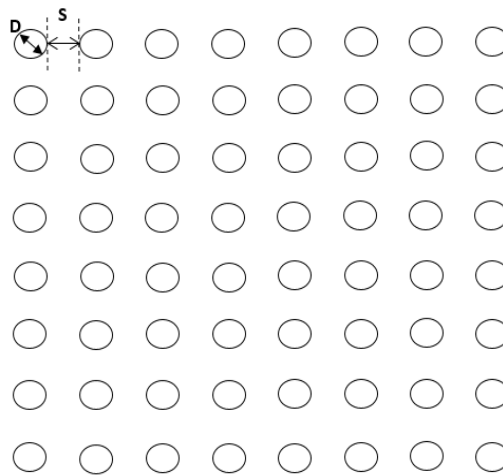
Figure 6.8 Schematic geometry

The total resistance can be expressed by (Ruschau, Yoshikawa, & Newnham,

1992)

$$R = \frac{(L-1)R_m + LR_c}{S} \approx \frac{L(R_m + R_c)}{S} \qquad (6.4)$$

Where R is the total resistance of the nanocomposites, L the number of fillers to form one conducting path, S the number of conducting networks, and R_m and R_c are the resistance of matrix (between 2 fillers) and a single filler particle, respectively. When there is a big gap between particles in the nanocomposites, no current flows though the gap. But, when the inter-particle separation is small, and the tunneling effect occurs. The tunneling current at low applied voltage is described in the equation below (Simmons, 1963) ,(Simmons, 1963b),(Simmons & Unterkofler, 1963).

$$J = \frac{3\sqrt{2m\varphi}}{2s} \left(\frac{e}{h}\right)^2 V exp(-\frac{4\pi s}{h}\sqrt{2m\varphi}) \tag{6.5}$$

Where J is the tunneling current through inter-particle gap, m and e are the mass and charge of electron, separately, h Plank's constant, V is the applied low voltage, s is the thickness of the insulating distance between conducting fillers, and ϕ the height of the potential barrier for the insulating area i.e. the energy required to transact on electron between adjacent particles.

Assuming that A is the effective tunneling area, where the tunneling effect happens, the tunneling resistance R_m is given by,

$$R = \frac{V}{AJ}[\frac{8\pi h s}{3a^2\gamma e^2}\exp(\gamma s)] \tag{6.6}$$

Where

$$\gamma = \frac{4\pi}{h}\sqrt{2m\varphi} \tag{6.7}$$

As the resistance of the filler is smaller compared to the polymer matrix, the intrinsic resistance of the fillers can be neglected. The total resistance for the nanocomposites is then calculated as

$$R = \frac{L}{S}\left[\frac{8\pi hs}{3a^2\gamma e^2}\exp(\gamma s)\right] \tag{6.8}$$

If a mechanical strain is applied to the nanocomposites, the resistance will be altered due to the change of tunneling resistance, resulting from the change of the distance between adjacent conducting particles. Assuming that the inter-particle separation is altered to be s from s_0, the resistivity change (R/R_o) can then be theoretically calculated as

$$\frac{R}{R_O} = \frac{s}{s_O}exp[-\gamma(s_O - s)] \tag{6.9}$$

Where R_o and s_o are the original resistance and distance between particles, respectively.

As the Young's modulus of the polymer is much lower than that of conducting particles, the deformation of conducting fillers under mechanical strain can be neglected. The Young's modulus of CNT reaches up to around 1 TPa, while the Young's modulus of employed epoxy is less than 10 GPa. As a result, the change of the inter-particle distance along the conducting path is only due to the deformation of the epoxy matrix. Thus, under uniaxial tension, the separation s resulted applied stress can be given by

$$s = (1 + \varepsilon)s_o \tag{6.10}$$

Where ε is the strain of the polymer matrix equaling to the strain of the nanocomposites.

To calculate the average distance between the CNT fillers, CNTs are assumed to be of the same size, and arranged evenly in the 2-D model shown in Figure 6.8. Then, the interparticle separation s_o is given by

$$s_o = \frac{1}{2}D\left(\left(\frac{\pi}{\theta}\right)^{\frac{1}{2}} - 2\right)$$
(6.11)

Where D is the diameter of the CNTs, θ is the CNT filler volume fraction. This equation is similar to average distance in a cubic lattice (S. Wu, 1985)

$$s = D\left[\left(\frac{\pi}{6}\right)^{\frac{1}{3}}\theta^{-\frac{1}{3}} - 1\right]$$
(6.12)

Then the equation of resistivity change can be achieved as

$$\frac{R}{R_o} = (1 + \varepsilon)exp\left[-\varepsilon\gamma * \frac{1}{2}D\left(\left(\frac{\pi}{\theta}\right)^{\frac{1}{2}} - 2\right)\right]$$
(6.13)

6.5.3 Analytical model for hybrid nanocomposites with additional fillers

In our situation, an additional filler is incorporated with epoxy, and thus incorporated with final nanocomposites. The second filler is modeled to be square

platelet as shown in Figure 6.9
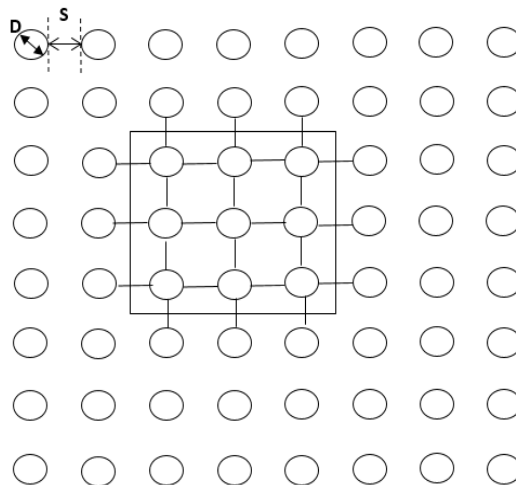
Figure 6.9 Schematic geometry of hybrid nanocomposites with additional filler

In our previous model, tunneling resistance mainly depends on the average

distance between conducting fillers which are CNTs. Due to the additional fillers, some

of the CNTs are covered by graphene platelets. This results in a reduction of average

distance s_o. The number of interparticle separations in this surface lattice is given by

$$n \approx 2 \frac{A}{(D+s_o)^2} \qquad (6.14)$$

Here A is surface area of the entire nanocomposite in consideration.

Then, the number of separations covered by additional fillers is given by

$$n' = \frac{\theta' A}{d^2} \left\{ 2 \left(\frac{d}{D+s_o} \right)^2 - 0.5 \left[4 \left(\frac{d}{D+s_o} \right) - 8 \right] \right\} \qquad (6.15)$$

Where θ' is the volume fraction and d is the length of additional fillers.

The average distance is proportional to the number of inter-particle separations.

Because of the reduction of inter-particle separations, the average distance can be

modified as

$$s'_o = (1 - \frac{n'}{n})s_o = (1 - \frac{n'}{n})\frac{1}{2}D[(\frac{\pi}{\theta})^{\frac{1}{2}} - 2] \qquad (6.16)$$

Then, applying mechanical strain to the sample, there is a change in tunneling

distance due to the deformation of low stiffness epoxy, assuming that same strain change

occurs to distances between adjacent particles along axial direction. The inter-particle

separation will then contribute to the average distance of tunneling distance. The average

distance can be calculated as

$$s' = (1 + \varepsilon)s'_o + \frac{\varepsilon A\theta'}{(\frac{2\varepsilon A\theta'}{(D+s_o)^2}+(n-n'))} \qquad (6.17)$$

Where the second term of the equation is from contribution of released inter-

particle separations caused by mechanical deformation of epoxy.

Thus, the resistivity change can be finally modified as

$$\frac{R}{R_o} = \frac{s'}{s'_o}exp[-\gamma(s'_o - s')] = f(\theta, D, \varepsilon, \theta', d) \qquad (6.18)$$

Where this function is in terms of volume fractions of CNTs and additional fillers,

diameters of CNTs and additional fillers, and mechanical deformation.

6.5.4 Results of analytical model
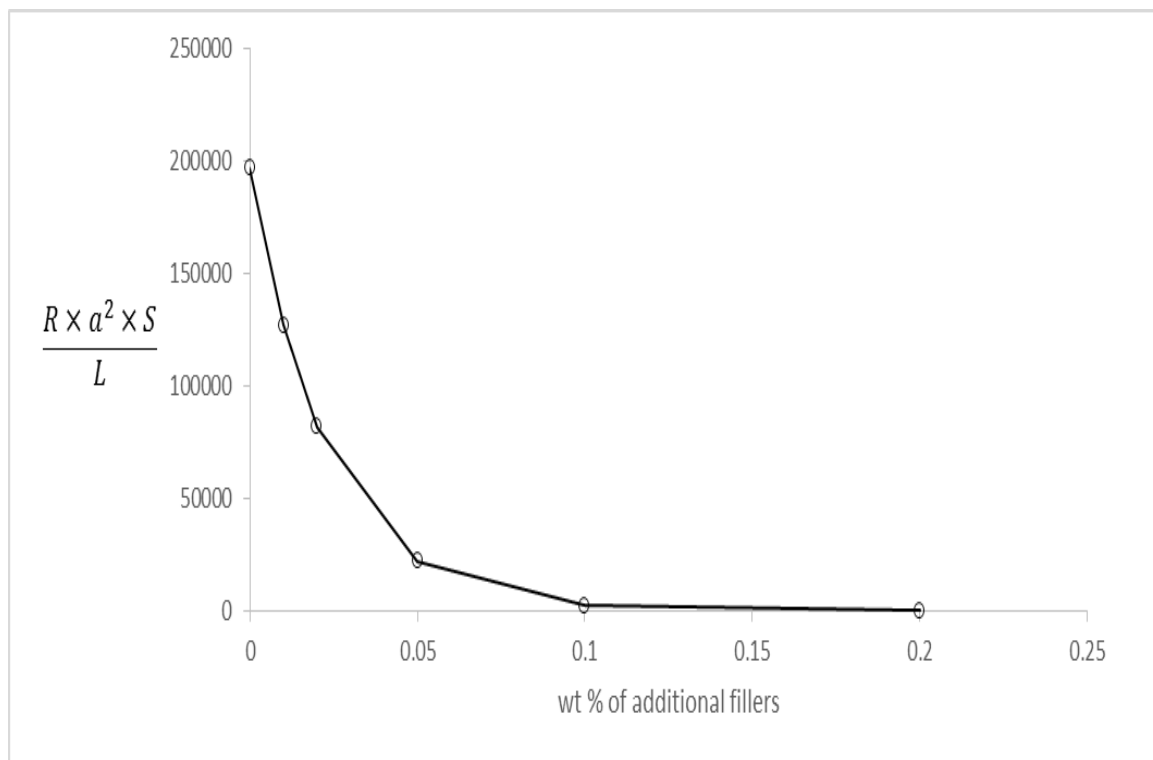
Figure 6.10 Resistivity vs content of additional fillers

Results of resistance varying with content of additional fillers are shown in Figure 6.10. *S*, *L*, and a^2 are constants which are mentioned in previous section. Resistivity rapidly decreases when additional fillers at low loading, and then the trend gradually converges with increase of additional filler concentration. This is because of formation of continuous electrical conducting network. This matches what are observed in experiments, even though exact numbers are not achieved because there is some ambiguity in the numerical values of some constants. Also this resistivity description only accounts for tunneling effect.

Both results for neat buckypaper nanocomposites and additional fillers reinforced

nanocomposites are as shown in Figure 6.11. Apparently form the graph, nanocomposites with additional fillers demonstrate higher sensitivity, responding to strain, though neat buckypaper/epoxy nanocomposites still show resistivity change with respect to strain. This trend also matches our experimental results.
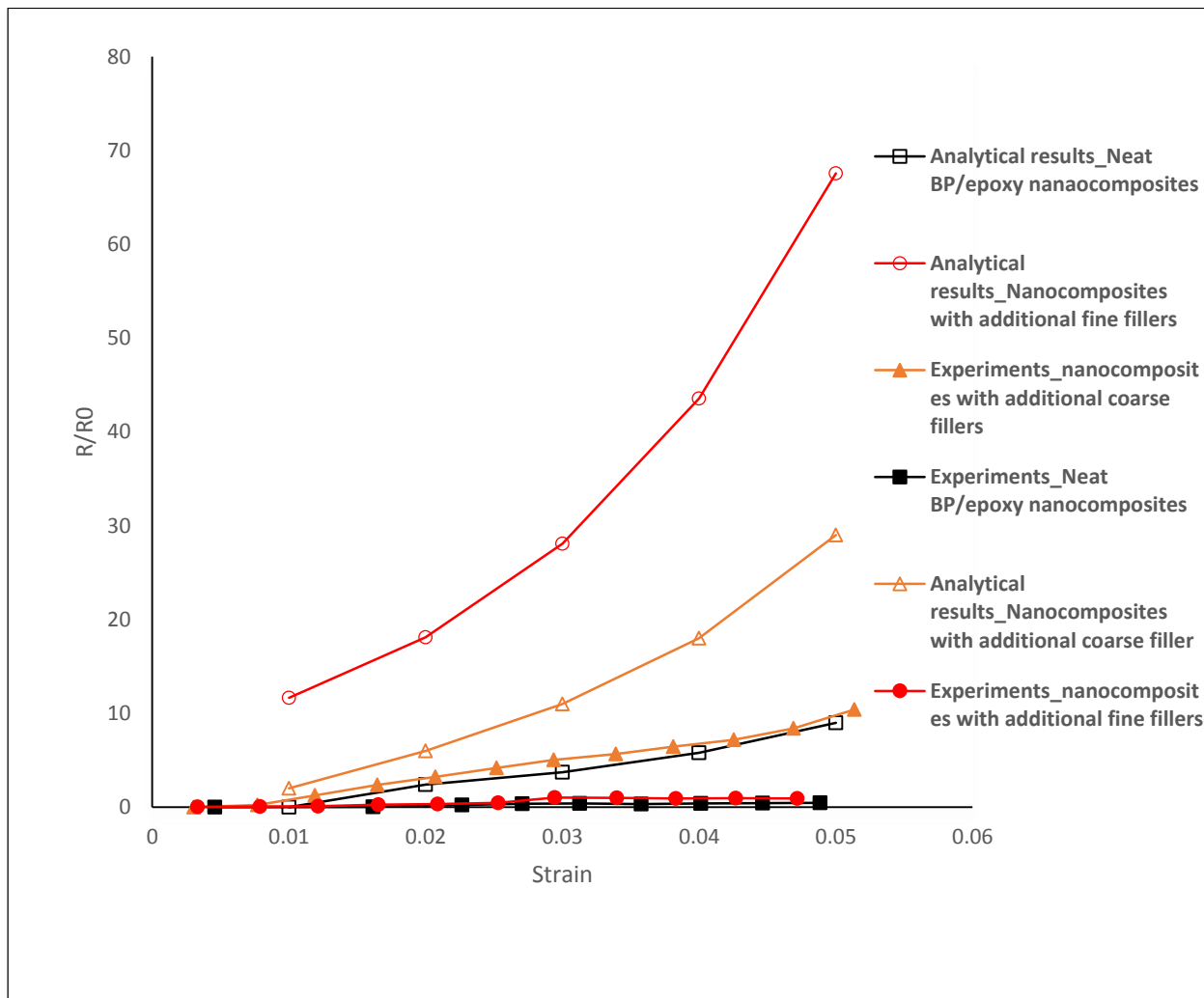
Figure 6.11 Resistivity change of neat bukypaper/epoxy nanocomposites and hybrid nanocomposites (5 wt. %)

However, analytical results of nanocomposites with additional small fillers show most electro-mechanical behavior compared to nanocomposites with additional big fillers

and neat BP/epoxy nanocomposites. This doesn't match what are achieved during experiments, in which the resistance change of nanocomposites with additional small filler is slightly larger than that of neat BP/epoxy nanocomposites but much less than that of nanocomposites with additional big filler. Again, the reason that causes such dismatch is because of agglomeration of graphene nanoplatelets.
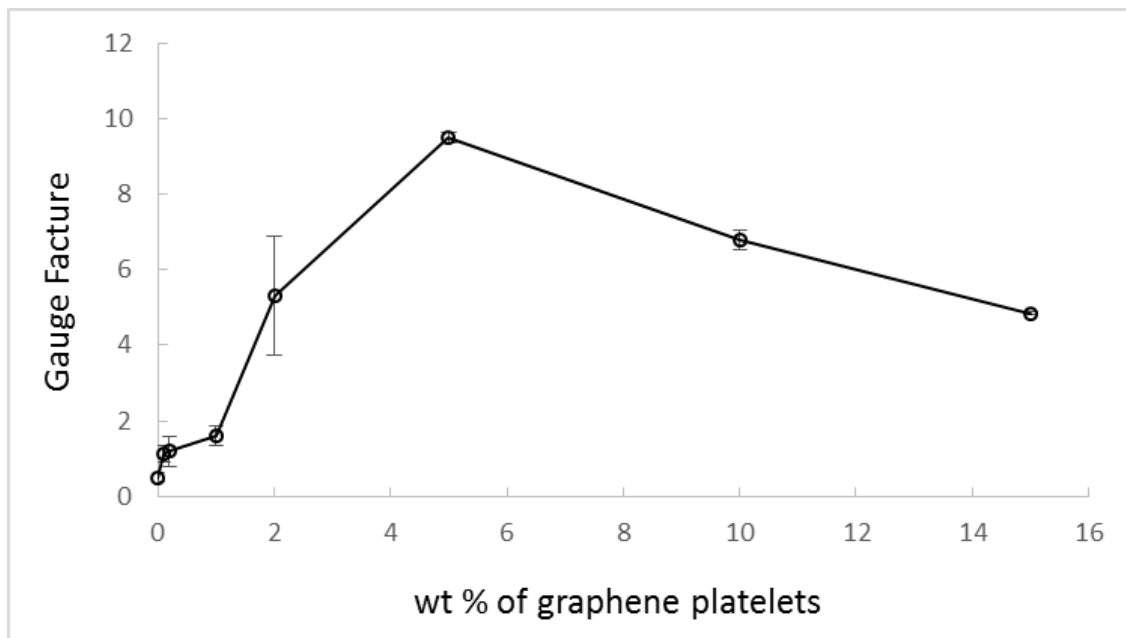
Figure 6.12 Gauge factor of nanocomposites with coarse graphene platelets
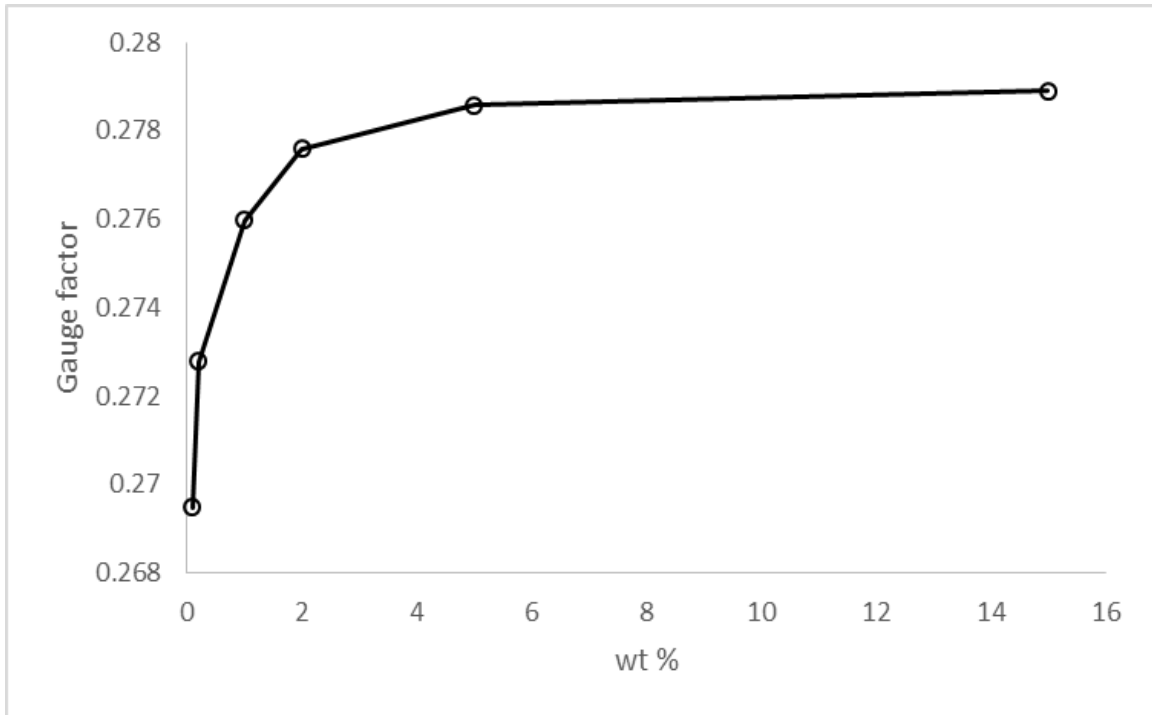
Figure 6.13 Gauge factor vs volume fraction of second fillers

Figure 6.13 shows results of gauge factor change, with respect to additional fillers volume fraction. Gauge factor increases with increasing volume fraction of additional fillers. However, this model can only explain until formation of continuous conducting network. At high contents, there is less change of interparticle separations at CNT-CNT and CNT-graphene interfaces. This is the reason for reduction in gauge factor in composites with high filler content.

Summary and recommendations

7.1 Summary

In this work, nanocomposites are fabricated by vacuum assisting process and cured in room temperature. Several kinds of epoxy mixture, with various weight percentages of fine graphene nanoplatelets and coarse graphene platelets, are employed to infiltrate through buckypaper. Resistance of these hybrid nanocomposites is measured using the four-point-probe-testing method under applied tensile loading.

Nanocomposites are subject to electrical current and a LabVIEW code in Figure 3.12 is used to monitor the voltage drop of the nanocomposites. The resistance can then be calculated by Ohm's Law. During the voltage monitoring process, mechanical deformation is supplied by tension machine. The resistance of the nanocomposites changes due to the mechanical strain and is measured through these experiments.

A reinforcement of mechanical properties occurs to both coarse graphene platelets prepared hybrid nanocomposites and fine graphene nanoplatelets based nanocomposites. Compared to Young's Modulus of pure buckypaper/polymer nanocomposites which is 149.15 MPa, the Young's Modulus of hybrid nanocomposites increases to 395.58 MPa. A similar reinforcement is observed for failure strength. It increases from 7.28 MPa to 16.12 MPa. The reinforcement in coarse graphene platelets based nanocomposites is higher than nanocomposites with graphene nano platelet fillers.

There is significant decrease of resistivity for nanocomposites, when additional coarse graphene platelets is mixed with liquid epoxy to infiltrate buckypaper. The resistivity decreases from 34.7 $\Omega \cdot$m to 13.4 $\Omega \cdot$m using the 5 wt. % coarse graphene platelets epoxy as the matrix, and it further decreases as the content of filler is increased

to 10 wt. % and 15 wt. %. Because it reaches the percolation threshold, the resistivity decreases slowly when the content is further increased.

The resistivity change with mechanical deformation is observed in these nanocomposites. The resistivity-strain of nanocomposites whose matrix is modified with 5 wt. % of coarse graphene platelets achieve the best resistivity-strain behavior. There is a clear increase in electrical resistivity in neat CNT sheet-resin composites from $35.2 \times 10^{-5} \Omega \cdot m$ to $36.03 \times 10^{-5} \Omega \cdot m$, while the strain reaches almost 5 %. However, this effect is much higher for 5 wt. % coarse graphene platelets modification with a gauge factor of 9.5 as shown in Figure 6.6. Further increase in filler content reduces the gauge factor. This is because of the formation of a continuous network.

A less effective reinforcement of electrical properties, mechanical properties, and electro-mechanical properties is observed in fine graphene nanoplatelets prepared nanocomposites. This is because fine graphene nanoplatelets agglomerate during fabricating process, which results of less change of surface contact. Thus, fine graphene nanoplatelets can't effectively aligned on surface of nanocomposites, and further reinforce properties of hybrid nanocomposites.

A model is developed to analytically model the experimental observations. This resistivity model incorporates the effect of mechanical deformation on the resistivity of neat CNT composites. This model is then modified to include the effect of additional fillers. With application of the model, similar trends are obtained in the effect of filler content on resistivity and gauge factor compared to experimental results.

7.2 Recommendations for future work

1. During the tension test, it is observed resistance of nanocomposites drops immediately after the current is applied. It takes around 3-4 minutes to stabilize as shown in Figure 0.1. This is observed both for neat buckypaper nanocomposites and hybrid nanocomposites. Our experimental results are based on stable samples, however, the reasons for this phenomenon need to be explained.
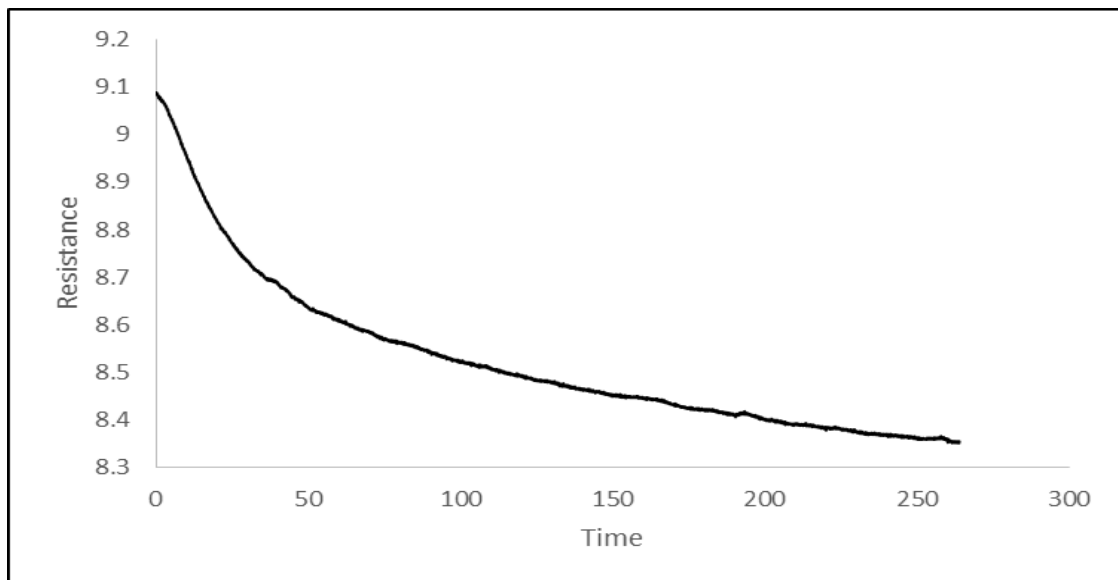
Figure 0.1 Resistance variation at the beginning of the test

2. Ideal circles are employed to model CNTs during analytical modeling process. More suitable geometry model should be developed to improve built model. The contact resistance is supposed to change rapidly, once CNT-CNT and CNT-second filler are separated due to mechanical deformation. This will also affect resistivity-strain behavior. These factors need to be incorporated into the analytical model.

3. Ultrasonication should be employed to mix fine graphene nanoplatelets modified epoxy matrix to avoid agglomeration. Thus, better results may be obtained for mechanical properties, electrical properties, and electro-mechanical properties.

4. Hybrid nanocomposites fabricated in this research can be employed to detect strain on delaminated composites and composites repair patch. Future work along these lines will advance the concepts developed here.

REFERENCES

Ahmadalinezhad, A., Wu, G., & Chen, A. (2011). Mediator-free electrochemical biosensor based on buckypaper with enhanced stability and sensitivity for glucose detection. Biosensors and Bioelectronics, 30(1), 287–293. http://doi.org/10.1016/j.bios.2011.09.030

Aldalbahi, A., & Panhuis, M. in het. (2012). Electrical and mechanical characteristics of buckypapers and evaporative cast films prepared using single and multi-walled carbon nanotubes and the biopolymer carrageenan. Carbon, 50(3), 1197 – 1208. http://doi.org/http://dx.doi.org/10.1016/j.carbon.2011.10.034

Al-Haik, M., Dai, J., Garcia, D., Chavez, J., Taha, M. R., Luhrs, C., & Phillips, J. (2009). Novel growth of multiscale carbon nanofilaments on carbon and glass fibers. Nanoscience and Nanotechnology Letters, 1(2), 122–127.

Al-Haik, M., Luhrs, C., Reda Taha, M., Roy, A., Dai, L., Phillips, J., & Doorn, S. (2010). Hybrid carbon fibers/carbon nanotubes structures for next generation polymeric composites. Journal of Nanotechnology, 2010.

Ambrosi, A., & Pumera, M. (2010). Nanographite impurities dominate electrochemistry of carbon nanotubes. Chemistry–A European Journal, 16(36), 10946–10949.

Bahr, J. L., Yang, J., Kosynkin, D. V., Bronikowski, M. J., Smalley, R. E., & Tour, J. M. (2001). Functionalization of carbon nanotubes by electrochemical reduction of aryl diazonium salts: a bucky paper electrode. Journal of the American Chemical Society, 123(27), 6536–6542.

Barrett, B. (1995). Regression Analysis: Concepts and Applications. Technometrics, 37(2), 229–229.

Baughman, R. H., Cui, C., Zakhidov, A. A., Iqbal, Z., Barisci, J. N., Spinks, G. M., … Kertesz, M. (1999). Carbon Nanotube Actuators. Science, 284(5418), 1340–1344. http://doi.org/10.1126/science.284.5418.1340

Baughman, R. H., Zakhidov, A. A., & de Heer, W. A. (2002). Carbon nanotubes--the route toward applications. Science, 297(5582), 787–92.

Behabtu, N., Young, C. C., Tsentalovich, D. E., Kleinerman, O., Wang, X., Ma, A. W. K., … Pasquali, M. (2013). Strong, Light, Multifunctional Fibers of Carbon Nanotubes with Ultrahigh Conductivity. Science, 339(6116), 182–186.

Berber, S., Kwon, Y.-K., & Tománek, D. (2000). Unusually high thermal conductivity of carbon nanotubes. Physical Review Letters, 84(20), 4613.

Bethune, D. S., Klang, C. H., de Vries, M. S., Gorman, G., Savoy, R., Vazquez, J., & Beyers, R. (1993). Cobalt-catalysed growth of carbon nanotubes with single-

atomic-layer walls. Nature, 363(6430), 605–607. http://doi.org/10.1038/363605a0

Biercuk, M., Ilani, S., Marcus, C., & McEuen, P. (2008). Carbon Nanotubes (Topics in Applied Physics vol 111).

Bin, Y., Kitanaka, M., Zhu, D., & Matsuo, M. (2003). Development of Highly Oriented Polyethylene Filled with Aligned Carbon Nanotubes by Gelation/Crystallization from Solutions. Macromolecules, 36(16), 6213–6219. http://doi.org/10.1021/ma0301956

Böger, L., Wichmann, M. H. G., Meyer, L. O., & Schulte, K. (2008). Load and health monitoring in glass fibre reinforced composites with an electrically conductive nanocomposite epoxy matrix. Composites Science and Technology, 68(7-8), 1886–1894. http://doi.org/10.1016/j.compscitech.2008.01.001

Chang, C.-Y., Phillips, E. M., Liang, R., Tozer, S. W., Wang, B., Zhang, C., & Chiu, H.-T. (2013a). Alignment and properties of carbon nanotube buckypaper/liquid crystalline polymer composites. Journal of Applied Polymer Science, 128(3), 1360–1368. http://doi.org/10.1002/app.38209

Chapartegui, M., Barcena, J., Irastorza, X., Elizetxea, C., Fernandez, M., & Santamaria, A. (2012). Analysis of the conditions to manufacture a MWCNT buckypaper/benzoxazine nanocomposite. Composites Science and Technology, 72(4), 489–497. http://doi.org/10.1016/j.compscitech.2011.12.001

Chapartegui, M., Barcena, J., Irastorza, X., Elizetxea, C., Fiamegkou, E., Kostopoulos, V., & Santamaria, A. (2013). Manufacturing, characterization and thermal conductivity of epoxy and benzoxazine multi-walled carbon nanotube buckypaper composites. Journal of Composite Materials, 47(14), 1705–1715.

Cheng, Q., Bao, J., Park, J., Liang, Z., Zhang, C., & Wang, B. (2009). High Mechanical Performance Composite Conductor: Multi-Walled Carbon Nanotube Sheet/Bismaleimide Nanocomposites. Advanced Functional Materials, 19(20), 3219–3225. http://doi.org/10.1002/adfm.200900663

Chen, X., Saito, T., Yamada, H., & Matsushige, K. (2001). Aligning single-wall carbon nanotubes with an alternating-current electric field. Applied Physics Letters, 78(23), 3714–3716.

Choi, E. S., Brooks, J. S., Eaton, D. L., Al-Haik, M. S., Hussaini, M. Y., Garmestani, H., … Dahmen, K. (2003). Enhancement of thermal and electrical properties of carbon nanotube polymer composites by magnetic field processing. Journal of Applied Physics, 94(9), 6034–6039. http://doi.org/http://dx.doi.org/10.1063/1.1616638

Coleman, J. N., Blau, W. J., Dalton, A. B., Muñoz, E., Collins, S., Kim, B. G., …

Baughman, R. H. (2003). Improving the mechanical properties of single-walled carbon nanotube sheets by intercalation of polymeric adhesives. Applied Physics Letters, 82(11), 1682–1684. http://doi.org/http://dx.doi.org/10.1063/1.1559421

Correa-Duarte, M. A., Grzelczak, M., Salgueirino-Maceira, V., Giersig, M., Liz-Marzan, L. M., Farle, M., … Diaz, R. (2005). Alignment of carbon nanotubes under low magnetic fields through attachment of magnetic nanoparticles. The Journal of Physical Chemistry B, 109(41), 19060–19063.

Cottinet, P.-J., Souders, C., Tsai, S.-Y., Liang, R., Wang, B., & Zhang, C. (2012). Electromechanical actuation of buckypaper actuator: Material properties and performance relationships. Physics Letters A, 376(12–13), 1132–1136. http://doi.org/10.1016/j.physleta.2012.02.011

Díez-Pascual, A. M., Guan, J., Simard, B., & Gómez-Fatou, M. A. (2012a). Poly(phenylene sulphide) and poly(ether ether ketone) composites reinforced with single-walled carbon nanotube buckypaper: II – Mechanical properties, electrical and thermal conductivity. Composites Part A: Applied Science and Manufacturing, 43(6), 1007–1015. http://doi.org/10.1016/j.compositesa.2011.11.003

Erik T Thostenson and Tsu-Wei Chou. (2003). On the elastic properties of carbon nanotube-based composites: modelling and characterization. Journal of Physics D: Applied Physics, 36(5), 573.

Fan, Z., & Advani, S. G. (2005). Characterization of orientation state of carbon nanotubes in shear flow. Polymer, 46(14), 5232–5240.

F. L. De Volder, M., H. Tawfick, S., H. Baughman, R., & Hart, A. J. (2013). Carbon Nanotubes: Present and Future Commercial Applications. Science, 336(6119), 535–539.

Gendron, D., Ansaldo, A., Bubak, G., Ceseracciu, L., Vamvounis, G., & Ricci, D. (2015). Poly(ionic liquid)-carbon nanotubes self-supported, highly electroconductive composites and their application in electroactive devices. Composites Science and Technology, 117, 364–370. http://doi.org/10.1016/j.compscitech.2015.07.016

Geng, H.-Z., Kim, K. K., So, K. P., Lee, Y. S., Chang, Y., & Lee, Y. H. (2007). Effect of acid treatment on carbon nanotube-based flexible transparent conducting films. Journal of the American Chemical Society, 129(25), 7758–7759.

Geng, Y., Liu, M. Y., Li, J., Shi, X. M., & Kim, J. K. (2008). Effects of surfactant treatment on mechanical and electrical properties of CNT/epoxy nanocomposites. Composites Part A: Applied Science and Manufacturing, 39(12), 1876–1883.

Haggenmueller, R., Guthy, C., Lukes, J. R., Fischer, J. E., & Winey, K. I. (2007). Single

wall carbon nanotube/polyethylene nanocomposites: thermal and electrical conductivity. Macromolecules, 40(7), 2417–2421.

Hammel, E., Tang, X., Trampert, M., Schmitt, T., Mauthner, K., Eder, A., & Pötschke, P. (2004). Carbon nanofibers for composite applications. European Materials Research Society 2003, Symposium B: Advanced Multifunctional Nanocarbon Materials and Nanosystems, 42(5–6), 1153–1158. http://doi.org/10.1016/j.carbon.2003.12.043

Hoskin, B. C., & Baker, A. A. (1986). Composite materials for aircraft structures. American Institute of Aeronautics and Astronautics. Retrieved from https://books.google.com/books?id=THtTAAAAMAAJ

Huang, C., Chen, S., Reneker, D. H., Lai, C., & Hou, H. (2006). High-Strength Mats from Electrospun Poly (p-Phenylene Biphenyltetracarboximide) Nanofibers. Advanced Materials, 18(5), 668–671.

Huang, Y.-T., Huang, S.-C., Hsu, C.-C., Chao, R.-M., & Vu, T. K. (2012). Design and Fabrication of Single-Walled Carbon Nanonet Flexible Strain Sensors. Sensors, 12(3), 3269. http://doi.org/10.3390/s120303269

Hu, N., Karube, Y., Arai, M., Watanabe, T., Yan, C., Li, Y., … Fukunaga, H. (2010). Investigation on sensitivity of a polymer/carbon nanotube composite strain sensor. Carbon, 48(3), 680 – 687. http://doi.org/http://dx.doi.org/10.1016/j.carbon.2009.10.012

Hwang, J., Jang, J., Hong, K., Kim, K. N., Han, J. H., Shin, K., & Park, C. E. (2011). Poly (3-hexylthiophene) wrapped carbon nanotube/poly (dimethylsiloxane) composites for use in finger-sensing piezoresistive pressure sensors. Carbon, 49(1), 106–110.

IEEE Std1650-2005, IEEE Standard Test Methods for Measurement of Electrical Porperties of Carbon Nanotubes.

Iijima, S. (1991). Helical microtubules of graphitic carbon. Nature, 354(6348), 56–58. http://doi.org/10.1038/354056a0

Ismach, A., & Joselevich, E. (2006). Orthogonal Self-Assembly of Carbon Nanotube Crossbar Architectures by Simultaneous Graphoepitaxy and Field-Directed Growth. Nano Letters, 6(8), 1706–1710. http://doi.org/10.1021/nl0610026

Jamshidian, M., Tehrany, E. A., Imran, M., Jacquot, M., & Desobry, S. (2010). Poly-Lactic Acid: production, applications, nanocomposites, and release studies. Comprehensive Reviews in Food Science and Food Safety, 9(5), 552–571.

Jing, X., Zhao, W., & Lan, L. (2000). The effect of particle size on electric conducting

percolation threshold in polymer/conducting particle composites. Journal of Materials Science Letters, 19(5), 377–379.

Kang, I., Schulz, M. J., Kim, J. H., Shanov, V., & Shi, D. (2006a). A carbon nanotube strain sensor for structural health monitoring. Smart Materials and Structures, 15(3), 737.

Kang, J. H., Park, C., Scholl, J. A., Brazin, A. H., Holloway, N. M., High, J. W., … Harrison, J. S. (2009). Piezoresistive characteristics of single wall carbon nanotube/polyimide nanocomposites. Journal of Polymer Science Part B: Polymer Physics, 47(10), 994–1003.

Kanoun, O. (2010). Flexible strain sensors fabricated with carbon nano-tube and carbon nano-fiber composite thin films., (518), 7343–7347.

Kan, W. (2013). STATISTICS-ENHANCED MULTISTAGE PROCESS MODELS FOR INTEGRATED DESIGN & MANUFACTURING OF POLY (VINYL ALCOHOL) TREATED BUCKYPAPER. THE FLORIDA STATE UNIVERSITY COLLEGE OF ENGINEERING.

Kasteleyn, P., & Fortuin, C. (1969). Phase transitions in lattice systems with random local properties (Vol. 26, p. 11). Presented at the Physical Society of Japan Journal Supplement, Vol. 26. Proceedings of the International Conference on Statistical Mechanics held 9-14 September, 1968 in Koyto., p. 11.

Keith, J., King, J., & Johnson, B. (2008). Electrical conductivity modeling of carbon filled polypropylene based resins for fuel cell bipolar plate applications. Journal of New Materials for Electrochemical Systems, 11(4), 253–257.

Kirkpatrick, S. (1973b). Percolation and Conduction. Rev. Mod. Phys., 45(4), 574–588. http://doi.org/10.1103/RevModPhys.45.574

Knapp, W., Schleussner, D., & Wüest, M. (2008). Investigation of ionization gauges with carbon nanotube (CNT) field-emitter cathodes. Journal of Physics: Conference Series, 100(9), 092007.

Koratkar, N. A. (2013). Graphene in composite materials : synthesis, characterization and applications.

Kroto, H. W., Heath, J. R., O'Brien, S. C., Curl, R. F., & Smalley, R. E. (1985). C60: Buckminsterfullerene. Nature, 318(6042), 162–163. http://doi.org/10.1038/318162a0

Kumar, B., Castro, M., & Feller, J.-F. (2012). Tailoring the chemo-resistive response of self-assembled polysaccharide-CNT sensors by chain conformation at tunnel junctions. Carbon, 50(10), 3627. http://doi.org/10.1016/j.carbon.2012.03.034

Laurent, C., Flahaut, E., Peigney, A., & Rousset, A. (1998). Metal nanoparticles for the catalytic synthesis of carbon nanotubes. New J. Chem., 22(11), 1229–1237. http://doi.org/10.1039/A801991F

Lee, W., Lee, J. U., Jung, B. M., Byun, J.-H., Yi, J.-W., Lee, S.-B., & Kim, B.-S. (2013). Simultaneous enhancement of mechanical, electrical and thermal properties of graphene oxide paper by embedding dopamine. Carbon, 65, 296–304.

Liang, G., & Tjong, S. (2006). Electrical properties of low-density polyethylene/multiwalled carbon nanotube nanocomposites. Materials Chemistry and Physics, 100(1), 132–137.

Li, C., Thostenson, E. T., & Chou, T.-W. (2008). Sensors and actuators based on carbon nanotubes and their composites: A review. Composites Science and Technology, 68(6), 1227–1249. http://doi.org/10.1016/j.compscitech.2008.01.006

Liu, K., Sun, Y., Zhou, R., Zhu, H., Wang, J., Liu, L., … Jiang, K. (2010). Carbon nanotube yarns with high tensile strength made by a twisting and shrinking method. Nanotechnology, 21(4), 045708.

Li, Z., Downes, R., & Liang, Z. (2015). In Situ Polymerized pCBT Composites with Aligned Carbon Nanotube Buckypaper: Structure and Properties. Macromolecular Chemistry and Physics, 216(3), 292–300. http://doi.org/10.1002/macp.201400443

Loh, K. J., Kim, J., Lynch, J. P., Kam, N. W. S., & Kotov, N. A. (2007). Multifunctional layer-by-layer carbon nanotube–polyelectrolyte thin films for strain and corrosion sensing. Smart Materials and Structures, 16(2), 429.

Loh, K. J., Lynch, J. P., Shim, B. S., & Kotov, N. A. (2007). Tailoring Piezoresistive Sensitivity of Multilayer Carbon Nanotube Composite Strain Sensors. Journal of Intelligent Material Systems and Structures. http://doi.org/10.1177/1045389X07079872

Luo, S., & Liu, T. (2013). Structure–property–processing relationships of single-wall carbon nanotube thin film piezoresistive sensors. Carbon, 59, 315–324.

Mamunya, E. P., Davidenko, V. V., & Lebedev, E. V. (1996). Effect of polymer-filler interface interactions on percolation conductivity of thermoplastics filled with carbon black. Composite Interfaces, 4(4), 169–176. http://doi.org/10.1163/156855497X00145

Ma, P.-C., Siddiqui, N. A., Marom, G., & Kim, J.-K. (2010). Dispersion and functionalization of carbon nanotubes for polymer-based nanocomposites: A review. Composites Part A: Applied Science and Manufacturing, 41(10), 1345–1367. http://doi.org/10.1016/j.compositesa.2010.07.003

Maune, H., & Bockrath, M. (2006). Elastomeric carbon nanotube circuits for local strain sensing. Applied Physics Letters, 89(17), 173131.

McLachlan, D. S. (2000). Analytical Functions for the dc and ac Conductivity of Conductor-Insulator Composites. Journal of Electroceramics, 5(2), 93–110.

McLachlan, D. S., Blaszkiewicz, M., & Newnham, R. E. (1990a). Electrical resistivity of composites. Journal of the American Ceramic Society, 73(8), 2187–2203.

McLachlan, D. S., Blaszkiewicz, M., & Newnham, R. E. (1990b). Electrical Resistivity of Composites. Journal of the American Ceramic Society, 73(8), 2187–2203. http://doi.org/10.1111/j.1151-2916.1990.tb07576.x

McLachlan, D. S., Chiteme, C., Park, C., Wise, K. E., Lowther, S. E., Lillehei, P. T., … Harrison, J. S. (2005a). AC and DC percolative conductivity of single wall carbon nanotube polymer composites. Journal of Polymer Science Part B: Polymer Physics, 43(22), 3273–3287.

McLachlan, D. S., Chiteme, C., Park, C., Wise, K. E., Lowther, S. E., Lillehei, P. T., … Harrison, J. S. (2005b). AC and DC percolative conductivity of single wall carbon nanotube polymer composites. Journal of Polymer Science Part B: Polymer Physics, 43(22), 3273–3287. http://doi.org/10.1002/polb.20597

Mittal, V. (2011) Nanocomposites with Biodegradable Polymers: Synthesis, Properties, and Future Perspectives. OUP Oxford.

Mohiuddin, M., & Van Hoa, S. (2011). Electrical resistance of CNT-PEEK composites under compression at different temperatures. Nanoscale Research Letters, 6(1), 419–419. http://doi.org/10.1186/1556-276X-6-419

Moisala, A., Li, Q., Kinloch, I., & Windle, A. (2006). Thermal and electrical conductivity of single-and multi-walled carbon nanotube-epoxy composites. Composites Science and Technology, 66(10), 1285–1288.

Moriarty, G. P., Whittemore, J. H., Sun, K. A., Rawlins, J. W., & Grunlan, J. C. (2011). Influence of polymer particle size on the percolation threshold of electrically conductive latex-based composites. Journal of Polymer Science Part B: Polymer Physics, 49(21), 1547–1554. http://doi.org/10.1002/polb.22344

Mukai, K., Asaka, K., Sugino, T., Kiyohara, K., Takeuchi, I., Terasawa, N., … Aida, T. (2009). Highly Conductive Sheets from Millimeter-Long Single-Walled Carbon Nanotubes and Ionic Liquids: Application to Fast-Moving, Low-Voltage Electromechanical Actuators Operable in Air. Advanced Materials, 21(16), 1582–1585.

Namilae, S., & Chandra, N. (2005). Multiscale model to study the effect of interfaces in

carbon nanotube-based composites. Journal of Engineering Materials and Technology, 127(2), 222–232.

Paleo, A. J., Hattum, F. W. J. van, Pereira, J., Rocha, J. G., Silva, J., Sencadas, V., & Lanceros-Méndez, S. (2010). The piezoresistive effect in polypropylene—carbon nanofibre composites obtained by shear extrusion. Smart Materials and Structures, 19(6), 065013.

Papa, H., Gaillard, M., Gonzalez, L., & Chatterjee, J. (2014). Fabrication of functionalized carbon nanotube buckypaper electrodes for application in glucose biosensors. Biosensors, 4(4), 449–460.

Park, J.-M., Gu, G.-Y., Wang, Z.-J., Kwon, D.-J., & DeVries, K. L. (2013). Interfacial durability and electrical properties of CNT or ITO/PVDF nanocomposites for self-sensor and micro actuator applications. Applied Surface Science, 287, 75–83. http://doi.org/10.1016/j.apsusc.2013.09.069

Park, M. (2008). Strain-dependent electrical resistance of multi-walled carbon nanotube/polymer composite films., (19).

Pham, G. T., Park, Y.-B., Wang, S., Liang, Z., Wang, B., Zhang, C., … Leslie Kramer. (2008a). Mechanical and electrical properties of polycarbonate nanotube buckypaper composite sheets. Nanotechnology, 19(32), 325705.

Randal, J. G. (2005). Piezoresistance of carbon nanotubes on deformable thin-film membranes, (86), 93104–7.

Rawlings, J. O., Pantula, S. G., & Dickey, D. A. (1998). Applied regression analysis: a research tool. Springer Science & Business Media.

Rein, M. D., Breuer, O., & Wagner, H. D. (2011). Sensors and sensitivity: Carbon nanotube buckypaper films as strain sensing devices. Composites Science and Technology, 71(3), 373–381. http://doi.org/10.1016/j.compscitech.2010.12.008

Robert M., J. (1999). Mechanics of Composites materials (Second edition).

Ruschau, G., Yoshikawa, S., & Newnham, R. (1992). Resistivities of conductive composites. Journal of Applied Physics, 72(3), 953–959.

Sahini, M., & Sahimi, M. (1994). Applications of percolation theory. CRC Press.

Saito, R., Fujita, M., Dresselhaus, G., & Dresselhaus, M. S. (1992). Electronic structure of chiral graphene tubules. Applied Physics Letters, 60(18), 2204–2206. http://doi.org/http://dx.doi.org/10.1063/1.107080

Salvetat, J.-P., Bonard, J.-M., Thomson, N., Kulik, A., Forro, L., Benoit, W., & Zuppiroli, L. (1999). Mechanical properties of carbon nanotubes. Applied Physics

A, 69(3), 255–260.

Seidel, G. D., & Lagoudas, D. C. (2009). A micromechanics model for the electrical conductivity of nanotube-polymer nanocomposites. Journal of Composite Materials, 43(9), 917–941.

Simmons, J. G. (1963). Electric tunnel effect between dissimilar electrodes separated by a thin insulating film. Journal of Applied Physics, 34(9), 2581–2590.

Simmons, J. G., & Unterkofler, G. J. (1963). Potential barrier shape determination in tunnel junctions. Journal of Applied Physics, 34(6), 1828–1830.

Song, Y. S., & Youn, J. R. (2005). Influence of dispersion states of carbon nanotubes on physical properties of epoxy nanocomposites. Carbon, 43(7), 1378–1385.

Souier, T., Santos, S., Al Ghaferi, A., Stefancich, M., & Chiesa, M. (2012). Enhanced electrical properties of vertically aligned carbon nanotube-epoxy nanocomposites with high packing density. Nanoscale Research Letters, 7(1), 1–8.

Sreekumar, T., Liu, T., Kumar, S., Ericson, L. M., Hauge, R. H., & Smalley, R. E. (2003). Single-wall carbon nanotube films. Chemistry of Materials, 15(1), 175–178.

Stampfer C. (2006). Nano-electromechanical displacement sensing based on single-walled carbon nanotubes.

Standard Test Method for D-C Resistance or Conductance of Moderately Conductive Materials. (2004). ASTM.

Standard Test Methods for DC Resistance or Conductance of Insulating Materials. (2005). ASTM.

Sykes, M. F., & Essam, J. W. (1964). Exact critical percolation probabilities for site and bond problems in two dimensions. Journal of Mathematical Physics, 5(8), 1117–1127.

Thostenson, E. T., & Chou, T.-W. (2006). Carbon nanotube networks: Sensing of distributed strain and damage for life prediction and self healing. Advanced Materials, 18(21), 2837–2841. http://doi.org/10.1002/adma.200600977

Tibbetts, G. G., Lake, M. L., Strong, K. L., & Rice, B. P. (2007). A review of the fabrication and properties of vapor-grown carbon nanofiber/polymer composites. Composites Science and Technology, 67(7), 1709–1718.

Tombler, T. W., Zhou, C., Alexseyev, L., Kong, J., Dai, H., Liu, L., … Wu, S.-Y. (2000). Reversible electromechanical characteristics of carbon nanotubes under local-probe manipulation. Nature, 405(6788), 769–772.

http://doi.org/10.1038/35015519

Treacy, M. M. J., Ebbesen, T. W., & Gibson, J. M. (1996). Exceptionally high Young's modulus observed for individual carbon nanotubes. Nature, 381(6584), 678–680. http://doi.org/10.1038/381678a0

Vargas-Bernal, R., Herrera-Pérez, G., Calixto-Olalde, M. E., & Tecpoyotl-Torres, M. (2013a). Analysis of DC electrical conductivity models of carbon nanotube-polymer composites with potential application to nanometric electronic devices. Journal of Electrical and Computer Engineering, 2013.

Vargas-Bernal, R., Herrera-Pérez, G., Calixto-Olalde, M. E., & Tecpoyotl-Torres, M. (2013b). Analysis of DC Electrical Conductivity Models of Carbon Nanotube-Polymer Composites with Potential Application to Nanometric Electronic Devices. Retrieved from https://nanohub.org/resources/17265

Vohrer, U., Kolaric, I., Haque, M. ., Roth, S., & Detlaff-Weglikowska, U. (2004). Carbon nanotube sheets for the use as artificial muscles. European Materials Research Society 2003, Symposium B: Advanced Multifunctional Nanocarbon Materials and Nanosystems, 42(5–6), 1159–1164. http://doi.org/10.1016/j.carbon.2003.12.044

Wang, S. (2015). Characterization and Analysis of Electrical Conductivity Properties of Nanotube Composites. Florida State University.

Wang, X., Yong, Z. Z., Li, Q. W., Bradford, P. D., Liu, W., Tucker, D. S., ... & Zhu, Y. T. (2013). Ultrastrong, stiff and multifunctional carbon nanotube composites. *Materials Research Letters*, *1*(1), 19-25.

Wang, Z., Liang, Z., Wang, B., Zhang, C., & Kramer, L. (2004). Processing and property investigation of single-walled carbon nanotube (SWNT) buckypaper/epoxy resin matrix nanocomposites. Composites Part A: Applied Science and Manufacturing, 35(10), 1225–1232. http://doi.org/10.1016/j.compositesa.2003.09.029

Wichmann, M. H. G., Buschhorn, S. T., Gehrmann, J., & Schulte, K. (2009). Piezoresistive response of epoxy composites with carbon nanoparticles under tensile load. Phys. Rev. B, 80(24), 245437. http://doi.org/10.1103/PhysRevB.80.245437

Wong, E. W., Sheehan, P. E., & Lieber, C. M. (1997). Nanobeam Mechanics: Elasticity, Strength, and Toughness of Nanorods and Nanotubes. Science, 277(5334), 1971–1975.

Wu, Q., Zhang, C., Liang, R., & Wang, B. (2008). Fire retardancy of a buckypaper membrane. Elsevier, 1164–1165.

Wu, S. (1985). Phase structure and adhesion in polymer blends: a criterion for rubber toughening. Polymer, 26(12), 1855–1863.

Xin, H., & Woolley, A. T. (2004). Directional Orientation of Carbon Nanotubes on Surfaces Using a Gas Flow Cell. Nano Letters, 4(8), 1481–1484. http://doi.org/10.1021/nl049192c

Xu, J.-Z., Chen, T., Yang, C.-L., Li, Z.-M., Mao, Y.-M., Zeng, B.-Q., & Hsiao, B. S. (2010). Isothermal crystallization of poly (l-lactide) induced by graphene nanosheets and carbon nanotubes: a comparative study. Macromolecules, 43(11), 5000–5008.

Yeh, C. S. (2007). A Study of Nanostructure and Properties of Mixed Nanotube Buckypaper Materials: Fabrication, Process Modeling, Characterization and Property Modeling.

Yin, G., Hu, N., Karube, Y., Liu, Y., Li, Y., & Fukunaga, H. (2011). A carbon nanotube/polymer strain sensor with linear and anti-symmetric piezoresistivity. Journal of Composite Materials, 0021998310393296.

Zallen, R. (2008). The physics of amorphous solids. John Wiley & Sons.

Zhang, W. (2006). Carbon nanotube/polycarbonate composites as multifunctional strain sensors. J. Nanosci. Nanotechnol., 6, 960–964.

Zhang, W., Sakalkar, V., & Koratkar, N. (2007). In situ health monitoring and repair in composites using carbon nanotube additives. Applied Physics Letters, 91(13), -. http://doi.org/http://dx.doi.org/10.1063/1.2783970

Zhao, H., Zhang, Y., Bradford, P. D., Zhou, Q., Jia, Q., Yuan, F.-G., & Zhu, Y. (2010). Carbon nanotube yarn strain sensors. Nanotechnology, 21(30), 305502.

Zhao, X., Koos, A. A., Chu, B. T., Johnston, C., Grobert, N., & Grant, P. S. (2009). Spray deposited fluoropolymer/multi-walled carbon nanotube composite films with high dielectric permittivity at low percolation threshold. Carbon, 47(3), 561–569.